

THE ICELAND MICROCONTINENT AND A CONTINENTAL GREENLAND-ICELAND-FAROE RIDGE

Gillian R. Foulger¹, Tony Doré², C. Henry Emeleus^{1,§}, Dieter Franke³, Laurent Geoffroy⁴, Laurent Gernigon⁵, Richard Hey⁶, Robert E. Holdsworth¹, Malcolm Hole⁷, Ármann Höskuldsson⁸, Bruce Julian¹, Nick Kuszniir⁹, Fernando Martinez¹⁰, Ken J.W. McCaffrey¹, James H. Natland¹¹, Alex Peace¹², Kenni Petersen¹³, Christian Schiffer¹, Randell Stephenson¹⁴ & Martyn Stoker¹⁵.

¹ Department of Earth Sciences, Durham University, Science Laboratories, South Rd. DH1 3LE, UK

² Statoil UK Ltd., Statoil House, 11a Regent Street, London SW1Y 4ST, UK

³ Bundesanstalt für Geowissenschaften und Rohstoffe (Federal Institute for Geosciences and Natural Resources), Germany

⁴ Université de Bretagne Occidentale, Brest, 29238 Brest, CNRS, UMR 6538, Laboratoire Domaines Océaniques, 29280 Plouzané, France

⁵ Norges Geologiske Undersøkelse (NGU), Geological Survey of Norway, Leiv Erikssons vei 39, N-7491 Trondheim, Norway

⁶ Hawaii Institute of Geophysics and Planetology, School of Ocean and Earth Science and Technology, University of Hawaii, Honolulu, HI 96822 USA

⁷ Department of Geology & Petroleum Geology, University of Aberdeen, Aberdeen AB243UE, UK.

⁸ Háskóli Íslands (University of Iceland), Sturlugötu 7, 101 Reykjavík, Iceland

⁹ School of Environmental Sciences, University of Liverpool, Jane Herdman Building, Liverpool L69 3GP, UK

¹⁰ Hawaii Institute of Geophysics and Planetology, School of Ocean and Earth Science and Technology, University of Hawaii, Honolulu, HI 96822 USA

¹¹ Rosenstiel School of Marine and Atmospheric Science, University of Miami, Miami FL 33149, USA

¹² Department of Earth Sciences, Memorial University of Newfoundland, St. Johns, Newfoundland, Canada, A1B 3X5; currently at School of Geography and Earth Sciences, McMaster University, 1280 Main Street West, Hamilton, Ontario, Canada L8S 4K1

¹³ Department of Geoscience, Aarhus University, Høegh-Guldbergs Gade 2, DK-8000 Aarhus C., Denmark

¹⁴ School of Geosciences, Geology and Petroleum Geology, Meston Building, King's College, University of Aberdeen, Aberdeen AB24 3UE, UK

¹⁵ Australian School of Petroleum, University of Adelaide, Adelaide, South Australia 5005 Australia

§ deceased

1 *Abstract*

2 The breakup of Laurasia to form the Northeast Atlantic Realm disintegrated an inhomogeneous
3 collage of cratons sutured by cross-cutting orogens. Volcanic rifted margins formed that are underlain
4 by magma-inflated, extended continental crust. North of the Greenland-Iceland-Faroe Ridge a new
5 rift—the Aegir Ridge—propagated south along the Caledonian suture. South of the Greenland-Iceland-
6 Faroe Ridge the proto-Reykjanes Ridge propagated north through the North Atlantic Craton along an
7 axis displaced ~150 km to the west of the rift to the north. Both propagators stalled where the
8 confluence of the Nagssugtoqidian and Caledonian orogens formed an ~300-km-wide transverse
9 barrier. Thereafter, the ~150 x 300-km block of continental crust between the rift tips—the Iceland
10 Microcontinent—extended in a distributed, unstable manner along multiple axes of extension. These
11 axes repeatedly migrated or jumped laterally with shearing occurring between them in diffuse transfer
12 zones. This style of deformation continues to the present day in Iceland. It is the surface expression of
13 underlying magma-assisted stretching of ductile continental crust that has flowed from the Iceland
14 Microplate and flanking continental areas to form the lower crust of the Greenland-Iceland-Faroe
15 Ridge. Icelandic-type crust which underlies the Greenland-Iceland-Faroe Ridge is thus not
16 anomalously thick oceanic crust as is often assumed. Upper Icelandic-type crust comprises magma
17 flows and dykes. Lower Icelandic-type crust comprises magma-inflated continental mid- and lower
18 crust. Contemporary magma production in Iceland, equivalent to oceanic layers 2-3, corresponds to
19 Icelandic-type upper crust plus intrusions in the lower crust, and has a total thickness of only 10-15
20 km. This is much less than the total maximum thickness of 42 km for Icelandic-type crust measured
21 seismically in Iceland. The feasibility of the structure we propose is confirmed by numerical modeling
22 that shows extension of the continental crust can continue for many tens of millions of years by
23 lower-crustal ductile flow. A composition of Icelandic-type lower crust that is largely continental can
24 account for multiple seismic observations along with gravity, bathymetric, topographic, petrological
25 and geochemical data that are inconsistent with a gabbroic composition for Icelandic-type lower crust.
26 It also offers a solution to difficulties in numerical models for melt-production by downward-revising
27 the amount of melt needed. Unstable tectonics on the Greenland-Iceland-Faroe Ridge can account for
28 long-term tectonic disequilibrium on the adjacent rifted margins, the southerly migrating rift
29 propagators that build diachronous chevron ridges of thick crust about the Reykjanes Ridge, and the
30 tectonic decoupling of the oceans to the north and south. A model of complex, discontinuous
31 continental breakup influenced by crustal inhomogeneity that distributes continental material in
32 growing oceans fits other regions including the Davis Strait, the South Atlantic and the West Indian
33 Ocean.

34 1 Introduction 4
35 2 Continental breakup forming the Northeast Atlantic Realm..... 5
36 2.1 High-velocity lower crust 7
37 2.2 Seafloor spreading north and south of the Greenland-Iceland-Faroe Ridge 9
38 2.2.1 North of the Greenland-Iceland-Faroe Ridge 9
39 2.2.2 South of the Greenland-Iceland-Faroe Ridge 10
40 3 The Greenland-Iceland-Faroe Ridge..... 10
41 3.1 Crustal structure..... 11
42 3.2 The Faroe-Shetland basin—a bellwether of GIFR tectonic instability 13
43 4 A new model for the Greenland-Iceland-Faroe Ridge 14
44 4.1 Mass balance..... 15
45 4.2 Problems and paradoxes solved..... 16
46 5 Thermo-mechanical modeling..... 18
47 6 Geochemistry 21

48	6.1	Composition of the melt source.....	21
49	6.2	Temperature of the melt source.....	22
50	6.3	$^3\text{He}/^4\text{He}$	23
51	7	Discussion.....	23
52	7.1	The Greenland-Iceland-Faroe Ridge.....	23
53	7.2	Crustal flow.....	24
54	7.3	Magmatism.....	25
55	7.3.1	The concept of the North Atlantic Igneous Province.....	25
56	7.3.2	Magma volume.....	25
57	7.3.3	The chevron ridges.....	26
58	7.3.4	The North Atlantic geoid high.....	27
59	7.3.5	Regions analogous to the GIFR.....	27
60	7.3.6	Regions analogous to the NE Atlantic Realm.....	27
61	8	Conclusions.....	28
62			

63 List of acronyms. See also Table 2.

64

65	GIFR	-	Greenland-Iceland-Faroe Ridge
66	JMMC	-	Jan Mayen Microplate Complex
67	SDR	-	Seaward-dipping reflector
68	NVZ	-	Northern Volcanic Zone
69	EVZ	-	Eastern Volcanic Zone
70	WVZ	-	Western Volcanic Zone
71	HVLC	-	High-velocity lower crust
72	T_P	-	potential temperature
73	V_P	-	compressional (P -) wave velocity
74	REE	-	rare-Earth element
75	SCLM	-	sub-continental lithospheric mantle

76

77 Keywords: Atlantic; Iceland; continental breakup; tectonics; Icelandic-type crust; SDRs;
78 geochemistry; geophysics.

79

80

81 1 Introduction

82 The NE Atlantic Realm, the region north of the Charlie Gibbs Fracture Zone, including the seas and
83 seaboards west of Greenland, has persistently resisted attempts to account for many of its features in
84 terms of conventional plate tectonics. Although the region figured prominently in the development of
85 the spectacularly successful continental drift and plate tectonic theories, *e.g.*, with the discovery of
86 symmetrical magnetic anomalies across the Reykjanes Ridge, it has also defied predictions made by
87 this theory that are successful in most other areas. This is particularly true along the Greenland-
88 Iceland-Faroe Ridge (GIFR) where the crust is typically 30 km thick and the bathymetry a full
89 kilometer shallower than is expected by cooling and subsidence models for oceanic-crust [Detrick *et*
90 *al.*, 1977]. These observations cannot be satisfactorily explained simply as conventional sea-floor-
91 spreading with a larger-than-typical magmatic rate at Iceland (Figure 1).

92 It is ironic that, despite the GIFR region not fitting the simple plate tectonic theory, it played an
93 important role in development of that theory. In the early 20th century Iceland attracted the attention
94 of Alfred Wegener who, as part of his theory of continental drift [Wegener, 1915], predicted that
95 Greenland and Scandinavia were separating at 2.5 m/a. Although his estimate of rate was two orders
96 of magnitude too large, his general theory was correct. Wegener was influenced by arguments that a
97 land bridge, postulated on biogeographical grounds to have connected Europe and America, was
98 inconsistent with isostasy. At the time, such land bridges were widely invoked to explain the
99 similarity, at some times in geological history, between biota on opposite sides of wide oceans.
100 Wegener recognized that biogeographical observations worldwide could be explained by continental
101 drift without land bridges.

102 Following acceptance of continental drift, the land bridge theory was essentially dropped. Ironically,
103 the NE Atlantic is perhaps the only place in the world where a long, ocean-spanning land bridge did
104 actually exist [Ellis & Stoker, 2014] (Section 3). The reason why such a bridge existed, even when the
105 ocean had attained a width of over 1000 km, is one feature of many of the NE Atlantic that has, to
106 date, not been satisfactorily explained.

107 A model for development of the NE Atlantic Realm that can account for these and all other
 108 observations in a holistic way is required. Models that involve simple palinspastic reconstructions of
 109 Laurasian super-continent breakup, and assume a bimodal crustal composition (continental or
 110 oceanic) with sharp boundaries, are insufficient [Barnett-Moore *et al.*, 2018; Nirrengarten *et al.*,
 111 2018]. Models that explain the quantity, distribution and petrology of igneous rocks in an *ad hoc*
 112 fashion are not forward-predictive and cannot account for observations such as the close juxtaposition
 113 of volcanic and non-volcanic margins, high-velocity lower crust (HVLC), frequent ridge jumps, and
 114 southward-propagating rifts on the Reykjanes Ridge [Hey *et al.*, 2010; Peron-Pinvidic & Manatschal,
 115 2010]. Nor can such models, a century after Wegener's work, explain why a land bridge spanned the
 116 NE Atlantic Ocean until it had attained a width of ~1,000 km, and why 40% of its length remains
 117 subaerial to the present day as the island of Iceland.

118 In this paper we develop such a model. We propose that the currently ~1,200 km wide Greenland-
 119 Iceland-Faroe Ridge (GIFR) formed by magma-assisted continental extension facilitated by ductile
 120 crustal flow, in a similar fashion to magmatic passive margins. The extraordinary width of the GIFR
 121 was enabled by the inclusion of a ~45,000 km² block of continental crust which we term the Iceland
 122 Microcontinent. The lower part of the ~30 km thick GIFR crust is magma-dilated continental mid-
 123 and lower crust. Surface extension has been taken up on the GIFR by distributed, migrating rifts with
 124 shear between them accommodated diffusely. Continental material is dispersed throughout the GIFR
 125 and sea-floor spreading has not yet been established on a single, stable rift. Complete continental
 126 breakup has thus still not fully occurred at this latitude.

127 Our paper is structured in the following way. First, we describe the unusual setting and complex
 128 history of breakup of the NE Atlantic Realm that predicated the subsequent complexities (Section 2).
 129 We then summarize structural and tectonic observations from the GIFR and the adjacent Faroe-
 130 Shetland basin (Section 3). In Section 4 we present our new model for the structure and evolution of
 131 the GIFR. Section 5 presents a numerical thermo-mechanical simulation that illustrates the model is
 132 physically viable given reasonable geological assumptions and Section 6 shows that it is consistent
 133 with the petrology, geochemistry and source potential temperatures of NE Atlantic igneous rocks.
 134 Finally, in Section 7, we discuss wider implications and analogous regions elsewhere in the oceans.

135 **2 Continental breakup forming the Northeast Atlantic Realm**

136 Opening of the NE Atlantic Realm in the early Cenozoic was not a simple, abrupt, isolated event. It
 137 was the latest event in a >300 Myr period of episodic rifting and cooling that lasted from the Late
 138 Palaeozoic through the Mesozoic. It affected a region extending some half the circumference of the
 139 Earth and disassembled a heterogeneous patchwork of cratonic blocks and orogens [Bingen & Viola,
 140 2018; Gasser, 2014; Gee *et al.*, 2008b; Peace *et al.*, this volume; Wilkinson *et al.*, 2017].

141 Final breakup occurred by magma-assisted continental extension [Gernigon *et al.*, this volume;
 142 Lundin & Doré, 2005; Peace *et al.*, this volume; Roberts, 2003; Roberts *et al.*, 1999; Skogseid *et al.*,
 143 2000; Soper *et al.*, 1992]. The crust extended by tens or hundreds of kilometers from the Rockall
 144 Trough to the Barents Sea [Funck *et al.*, 2017; Gaina *et al.*, 2017; Skogseid *et al.*, 2000; Stoker *et al.*,
 145 2017]. Pre-breakup magmatism occurred throughout the region including in Britain, the Rockall
 146 Trough, East Greenland, the Faroe Islands and small-volume, small-fraction, scattered fields found in
 147 west Greenland and Newfoundland [Larsen *et al.*, 2009; Peace *et al.*, 2016; Wilkinson *et al.*, 2017].
 148 Final development of the axes of breakup in the NE Atlantic was influenced by both the direction of
 149 extensional stress, pre-existing structure, and magmatism [Peace *et al.*, 2018; Peace *et al.*, submitted;
 150 Schiffer *et al.*, this volume].

151 Greenland is cross-cut by several orogens that continue across formerly adjacent landmasses. Easterly
 152 orientated orogens include the Inglefield mobile belt in the north (Paleoproterozoic—ca. 1.96 - 1.91
 153 Ga), the central Greenland Nagssugtoqidian orogen bounded to the north by the Disko Bugt suture
 154 and to the south by the Nagssugtoqidian front (Paleoproterozoic—ca. 1.86 - 1.84 Ga), and the south

155 Greenland Ketilidian orogen (Paleoproterozoic—ca. 1.89 - 1.80 Ga) (Figure 2) [Garde *et al.*, 2002;
 156 van Gool *et al.*, 2002]. On the Eurasian continent the Nagssugtoqidian orogen is represented in
 157 Scotland as the Lewisian gneiss (Laxfordian) and the Ketilidian orogen is represented in NW Ireland
 158 as the Rhinns Complex (Figure 3).

159 The much younger Caledonian suture formed in the Ordovician-Devonian and closed the Tornquist
 160 Sea and Iapetus Ocean to unite Laurentia, Baltica and Avalonia [Pharaoh, 1999; Schiffer *et al.*, this
 161 volume; Soper *et al.*, 1992]. The Scottish Caledonides lie orthogonal to the eastward continuation of
 162 the Nagssugtoqidian and Ketilidian orogens [Holdsworth *et al.*, 2018]. The western frontal thrust of
 163 this suture runs down east Greenland ~100 - 300 km from the coast [Gee *et al.*, 2008a; Haller, 1971;
 164 Henriksen, 1999; Henriksen & Higgins, 1976]. A dipping feature imaged seismically using receiver
 165 functions at ~40 - 100 km beneath east Greenland is interpreted as a subducted slab, trapped in the
 166 continental lithosphere, when the Caledonian suture finally closed (Figure 4) [Schiffer *et al.*, 2014].
 167 Residual Caledonian slabs beneath the region were predicted earlier by plate models for the
 168 geochemistry of Icelandic volcanics [Foulger & Anderson, 2005; Foulger *et al.*, 2005]. A congruent
 169 structure—the Flannan reflector—has been imaged seismically beneath north Scotland [Schiffer *et al.*,
 170 *et al.*, 2015; Smythe *et al.*, 1982].

171 The breakup phases that formed the oceans west and east of Greenland are described in detail by
 172 Peace *et al.* [this volume], Gernigon *et al.* [this volume] and Martinez and Hey [this volume]. It is
 173 summarized here and a brief chronology of the most significant events is given in Table 1. The north-
 174 propagating mid-Atlantic Ridge reached the latitude of the future Charlie Gibbs Fracture Zone in the
 175 Late Cretaceous (~86.3 - 83.6 Ma) and the Rockall Trough formed (Figure 1). The rift then
 176 propagated west of present-day Greenland at ~63 Ma forming magma-poor margins and opening the
 177 Labrador Sea [Abdelmalak *et al.*, 2018; Keen *et al.*, 2018; Nirrengarten *et al.*, 2018; Oakey &
 178 Chalmers, 2012; Roest & Srivastava, 1989].

179 Propagation proceeded unhindered across the Grenville and Ketilidian orogens and the North Atlantic
 180 craton but stalled at the junction of the Nagssugtoqidian and Rinkian orogens [Connelly *et al.*, 2006;
 181 Grocott & McCaffrey, 2017; Peace *et al.*, 2018; Peace *et al.*, submitted]. There, the crust was locally
 182 thick [Clarke & Beutel, 2019; Funck *et al.*, 2007; Funck *et al.*, 2012; Peace *et al.*, 2017; St-Onge *et al.*,
 183 2009] and pre-existing subducted slabs may also have been preserved in the lithosphere [Heron *et al.*,
 184 2019]. Rift propagation stalled and the Davis Strait NNE-SSW sinistral, right-stepping
 185 transtensional accommodation zone formed. This subsequently opened by magma-assisted continental
 186 transtension and transpression. Further north Baffin Bay opened by a combination of continental
 187 extension and possibly some subsidiary sea-floor spreading [Chalmers & Laursen, 1995; Chauvet *et al.*,
 188 2019; Oakey & Chalmers, 2012; Suckro *et al.*, 2012; Welford *et al.*, 2018]. The Davis Strait today
 189 is a 550-km wide shallow ridge of extended, magma-inflated, continental crust that spans the ocean
 190 from Baffin Island to West Greenland [Dalhoff *et al.*, 2006; Heron *et al.*, 2019; Schiffer *et al.*, 2017].

191 At ~56 - 52 Ma rifting began to propagate east of Greenland forming the proto-Reykjanes Ridge and a
 192 ridge-ridge-ridge triple junction at the location of the current Bight fracture zone (Figure 1). Shortly
 193 thereafter, at ~50 - 48 Ma, the pole of rotation for Labrador Sea/Baffin Bay opening migrated south
 194 by ~1000 km resulting in clockwise rotation of ~30 - 40° of the direction of motion of Greenland
 195 relative to Laurentia [Oakey & Chalmers, 2012; Srivastava, 1978]. As a consequence the Labrador
 196 Sea/Baffin Bay plate boundary west of Greenland became less favorable to extension [Gaina *et al.*,
 197 2017] and motion was progressively transferred to the axis east of Greenland. From ~36 Ma, opening
 198 was taken up entirely in the NE Atlantic [Chalmers & Pulvertaft, 2001; Gaina *et al.*, 2017].

199 As was the case for breakup west of Greenland, development of the mid-Atlantic Ridge in the NE
 200 Atlantic was strongly influenced by pre-existing structure [Schiffer *et al.*, this volume]. The classic
 201 “Wilson Cycle” model suggests that continental breakup occurs along older sutures [Ady &
 202 Whittaker, 2018; Buitter & Torsvik, 2014; Chenin *et al.*, 2015; Krabbendam, 2001; Petersen &

203 Schiffer, 2016; Vauchez *et al.*, 1997]. The collage of cratons and cross-cutting orogens that comprised
 204 the disintegrating Laurasian supercontinent had several sutures that influenced breakup.

205 Development of the oceanic regions north and south of the GIFR described in more detail in Sections
 206 2.2.1 and 2.2.2 is summarized here. North of the present GIFR, the axis of extension opened by
 207 southerly propagation within the Caledonian orogen. That orogen consists of overthrust stacks of
 208 nappes and sinistral shear zones including the Møre-Trøndelag Fault Zone (Norway) and the Walls
 209 Boundary-Great Glen Fault and Highland Boundary Fault (Scotland). These features may have
 210 controlled the structures that opened [Dewey & Strachan, 2003; Doré *et al.*, 1997; Fossen, 2010; Peace
 211 *et al.*, this volume]. The new mid-Atlantic Ridge formed obliquely along the orogen, however, so the
 212 propagating rift tip eventually intersected its edge at the Caledonian Western Frontal Thrust [Schiffer
 213 *et al.*, this volume]. There, it stalled.

214 South of the present GIFR the proto-Reykjanes Ridge propagated north from the Bight Fracture Zone,
 215 cut unhindered across the Ketilidian orogen as did the Labrador Sea rift, and split the North Atlantic
 216 craton. It arrived at the confluence of the transverse Nagsugtoqidian and Caledonian orogens at ~C21
 217 (50 - 48 Ma) [Elliott & Parson, 2008] and stopped at a location ~300 km to the south and ~150 km to
 218 the west of the stalled, south-propagating ridge tip to the north. It was between and around these two
 219 stalled ridge tips that the GIFR formed, by magma-assisted deformation of the continental region
 220 between them.

221 2.1 High-velocity lower crust

222 High velocity lower crust (HVLC) is widespread beneath the margins of the NE Atlantic and has very
 223 similar geophysical properties to the lower part of the Icelandic-type crust that underlies the GIFR
 224 [Bott, 1974; Foulger *et al.*, 2003]. Because of this, understanding the origin and composition of
 225 HVLC is key to unraveling the development and current structure of the NE Atlantic. In this section,
 226 we discuss in detail its geophysical characteristics and possible origins.

227 Before oceanic crust began to form in the NE Atlantic Realm, wide rifted margins of stretched
 228 continental crust developed and in some areas were blanketed by thick sequences of seaward-dipping
 229 basalt flows (seaward-dipping reflectors—SDRs) [Á Horni *et al.*, 2016; Talwani & Eldholm, 1977].
 230 Lithospheric necking occurred by normal faulting in the upper crust and distributed magma inflation
 231 and ductile flow in the mid- and lower crust (Figure 5). Multiple changes in extension direction
 232 complicated the final structure [Barnett-Moore *et al.*, 2018].

233 The volcanic rifted margins may be divided into Inner-SDR and Outer-SDR regions [Planke *et al.*,
 234 2000]. The Inner-SDRs comprise lavas up to 5 - 10 km thick that blanket heavily dyke-injected
 235 continental upper crust formed during the continental extensional necking phase [*e.g.*, Benson, 2003;
 236 Geoffroy, 2005; Geoffroy *et al.*, 2015]. Beneath this the sill-injected lower crust exhibits high seismic
 237 velocities. Outer-SDRs sometimes lie seaward of these and directly overlie thinner HVLC, with
 238 seismic properties identical to the HVLC beneath the necked continental crust [Geoffroy *et al.*, 2015].
 239 HVLC may also extend for up to 100 km beneath both the adjacent oceanic and continental domains
 240 [Funck *et al.*, 2016 and references therein; Rudnick & Fountain, 1995; Thybo & Artemieva, 2013].

241 HVLC typically has seismic velocities intermediate between those expected for crust and mantle.
 242 Constraints on its density are poor because the densities of the SDRs and underlying lower crust are
 243 not well known. Geoffroy *et al.* [2015] define two kinds of HVLC – LC1 and LC2. Typical working
 244 values for velocity and density are, for LC1 $V_p \sim 7.2 - 7.3$ km/s and density 3000 - 3100 kg/m³, and for
 245 LC2 $V_p \sim 7.6$ to 7.8 km/s and density 3200 - 3300 kg/m³ (Figure 5) [Bauer *et al.*, 2000; Geoffroy *et al.*
 246 *et al.*, 2015; Schiffer *et al.*, 2016].

247 These geophysical properties are ambiguous regarding the composition, origin, and tectonic
 248 significance of HVLC. Possible lithologies include:

- 249 • Ultra-high-pressure granulite/eclogite crystalline basement representing exhumed continental
 250 mid- and lower crust [Abdelmalak *et al.*, 2017; Ebbing *et al.*, 2006; Gernigon *et al.*, 2004;
 251 Gernigon *et al.*, this volume; Mjelde *et al.*, 2013]. Such material can have both high V_p (7.2 -
 252 8.5 km/s) and high density [2.8-3.6 g/cm³; Fountain *et al.*, 1994]. It outcrops in the
 253 Norwegian Western Gneiss Region which continues beneath the North Sea and the platform
 254 east of the Møre basin. Its top surface may comprise old suture accommodation zones that
 255 controlled deformation prior to breakup;
- 256 • Syn-extension sill-intruded mid-to-lower continental crust. In wide-angle seismic lines most
 257 HVLC beneath Inner-SDRs present high-amplitude, folded reflectors disconnected from the
 258 deepest layered lower crust [Clerc *et al.*, 2015; Geoffroy, 2005; Geoffroy *et al.*, 2015]. Such
 259 deformation fits with seaward ductile flow of this layer;
- 260 • Exhumed and syn-rift serpentinitized mantle. The HVLC beneath the mid-Norwegian early
 261 Cretaceous basins, the Labrador Sea, Baffin Bay, Rockall Trough and the Porcupine basin
 262 may be partially syn-rift serpentinitized mantle exhumed beneath the axes of maximum
 263 extension [Keen *et al.*, 2018; Lundin & Doré, 2011; O'Reilly *et al.*, 1996; Peron-Pinvidic *et al.*,
 264 2013; Reston *et al.*, 2001; Reynisson *et al.*, 2011]. It is directly observed at amagmatic
 265 margins, *e.g.*, the Iberian margin, where the serpentinitization is thought to be caused by
 266 seawater infiltrating down crustal faults and reacting with exhumed mantle at shallow depths.
 267 The HVLC beneath the NE Atlantic SDRs lies under several kilometers of sediments and
 268 crust and it is unlikely that seawater can penetrate sufficiently deep to cause pervasive
 269 serpentinitization beneath the basalt [Abdelmalak *et al.*, 2017; Gernigon *et al.*, 2004;
 270 Zastrozhnov *et al.*, 2018];
- 271 • Inherited serpentinitized material. Water could have been sourced from inherited Caledonian or
 272 Sveconorwegian-Grenvillian mantle wedge material [Fichler *et al.*, 2011; Petersen & Schiffer,
 273 2016; Schiffer *et al.*, 2016; Slagstad *et al.*, 2017]. The source of NE Atlantic basalts is known
 274 to be wet [Jamtveit *et al.*, 2001; Nichols *et al.*, 2002]. Pressure conditions corresponding to
 275 deep crust/shallow upper mantle depths and temperatures of 500 - 700°C should not be
 276 exceeded for serpentinite to exist [*e.g.*, Petersen & Schiffer, 2016; Ulmer & Trommsdorff,
 277 1995]. Numerical modeling confirms that such material can be preserved in rifted margins
 278 [Petersen & Schiffer, 2016] and that its strength would be less than half that of dry peridotite
 279 [Escartin *et al.*, 2001];
- 280 • Mantle infiltrated with gabbroic melt. Such material has been observed at magma-poor
 281 margins [Lundin & Doré, 2018; Müntener *et al.*, 2010] and would have an average seismic
 282 velocity midway between that of mantle and gabbro ($V_p \sim 7$ km/s);
- 283 • Hybrid material comprising a mixture of some or all of the above on various scales. For
 284 example, Schiffer *et al.* [2015] interpret HVLC bodies beneath east Greenland as Caledonian
 285 subduction material including eclogitized mafic crust. What appears geophysically to be a
 286 continuous layer might also vary laterally in composition—a classic example of geophysical
 287 ambiguity [Mjelde *et al.*, 2002].
 288
- 289 An interpretation of HVLC as underplated material, *i.e.*, high-temperature melt that accumulated
 290 during initial opening of the NE Atlantic [Eldholm & Grue, 1994b; Mjelde *et al.*, 1997; Mjelde *et al.*,
 291 2002; Mjelde *et al.*, 1998; Thybo & Artemieva, 2013] is challenged by key geophysical and structural
 292 observations from the outer Vøring basin. There, Cretaceous deformation was partly controlled by the
 293 top of a HVLC dome before the main magmatic event in the Late Paleocene-Early Eocene, suggesting
 294 that the dome may predate breakup magmatism by at least 15 - 25 Myr [Abdelmalak *et al.*, 2017;
 295 Gernigon *et al.*, 2004; Gernigon *et al.*, 2006].
- 296 In summary, the provenance of the HVLC underlying the Outer SDRs is ambiguous but it likely
 297 includes a large proportion of continental crust. As a consequence the exact locations of the outer
 298 limits of continuous offshore continental material (the continent-ocean boundary) is poorly known in
 299 some areas [Bronner *et al.*, 2011; Eagles *et al.*, 2015; Gernigon *et al.*, 2015; Lundin & Doré, 2018;

300 Schiffer *et al.*, 2018]. Continental crust may grade into thick oceanic crust via a magmatic transition
 301 zone tens of kilometers wide of stretched, intruded continental crust—the continent-ocean transition
 302 [Eagles *et al.*, 2015; Eldholm *et al.*, 1989; Gernigon *et al.*, this volume; Meyer *et al.*, 2009]. The
 303 width of the continent-ocean transition may be partly controlled by the degree of stretching with
 304 narrow extensional zones forming where new rifts follow pre-existing fabric, and wide zones where
 305 rifts cross-cut tectonic fabric [Buck, 1991; Dunbar & Sawyer, 1988; Harry *et al.*, 1993; Schiffer *et al.*,
 306 this volume].

307 Full rupture of the crust leading to region-wide sea-floor spreading may be discontinuous,
 308 diachronous and segmented [Elliott & Parson, 2008; Guan *et al.*, 2019; Manton *et al.*, 2018; Schiffer
 309 *et al.*, this volume; Theissen-Krah *et al.*, 2017]. Continental fragments trapped between pairs of
 310 volcanic rifted margins and transported into the new ocean to form “C-blocks” may be widespread
 311 (Figure 5; Section 4) [Geoffroy *et al.*, 2015; Geoffroy *et al.*, submitted]. Continental crust may also be
 312 distributed by igneous mullioning as seen in the southern Jan Mayen Microplate Complex (JMMC;
 313 Section 2.2.1), and by small-scale lateral rift migrations [Bonatti, 1985; Gernigon *et al.*, 2012; Gillard
 314 *et al.*, 2017]. Continental fragments may range in size from the 100-km scale down. Geophysical
 315 ambiguity and blanketing of microcontinents with lavas hinder mapping the full distribution of
 316 continental crust in the oceans. The eastern margin of the JMMC, for example, is overlain by SDRs
 317 and the subaerial part of the GIFR (i.e. Iceland) is blanketed with lavas younger than ~17 Ma [Breivik
 318 *et al.*, 2012; Gudlaugsson *et al.*, 1988]. Geochemistry can be used to complement geophysics by
 319 testing the viability of proposed HVLC petrologies (Section 6).

320 2.2 *Seafloor spreading north and south of the Greenland-Iceland-Faroe Ridge*

321 Clear, well-mapped, linear magnetic anomalies reveal the contrasting histories of ocean opening north
 322 and south of the GIFR (Figure 6). Breakup did not occur simultaneously along the entire seaboard, as
 323 often assumed, but involved several isolated propagators and intermediate continental blocks [Elliott
 324 & Parson, 2008; Gernigon *et al.*, this volume].

325 2.2.1 North of the Greenland-Iceland-Faroe Ridge

326 The earliest anomalies are likely associated with magma injection into extended continental crust.
 327 True sea-floor spreading on the Aegir Ridge began at ~54 Ma (C24r). It started at its northern end and
 328 propagated south to reach its full extent by ~52 Ma (Chron C23). Tectonic reorganization and fan-
 329 shaped spreading occurred about this ridge C22-C21 (~48 Ma) with spreading slower in the south
 330 than in the north (Table 1) [Gernigon *et al.*, 2015].

331 Much if not all of the southern extension deficit was accommodated by diffuse, dyke-assisted crustal
 332 dilation in the continental crust immediately to the west. This region later became the southern JMMC
 333 [Brandsdóttir *et al.*, 2015]. Crustal extension of up to 500% occurred forming mullioned crust
 334 [Gernigon *et al.*, 2015; Schiffer *et al.*, 2018]. Extension ultimately concentrated on the most westerly
 335 axis of dilation which developed into the Kolbeinsey Ridge. The first unambiguous magnetic anomaly
 336 formed there at ~24 Ma [C6/7; Blischke *et al.*, 2017; Vogt *et al.*, 1980].

337 The Aegir Ridge dwindled and became extinct a little after ~31 - 28 Ma [C12-C10; Gernigon *et al.*,
 338 2015] after which all spreading north of the GIFR was taken up on the proto-Kolbeinsey Ridge. This
 339 migration of the locus of extension likely occurred as a result of a tectonic reorganization that rotated
 340 the local direction of motion counter-clockwise [Gaina *et al.*, 2017]. This would have rendered the
 341 southern part of the Aegir Ridge less favorable for spreading and encouraged extension on the proto-
 342 Kolbeinsey Ridge. That extension progressively detached the continental block and adjacent
 343 mullioned crust between the proto-Kolbeinsey Ridge and the Aegir Ridge to form the JMMC
 344 [Schiffer *et al.*, 2018]. Opening of the Atlantic north of the GIFR (e.g. the Norwegian-Greenland Sea)
 345 thus occurred on a series of unconnected, sub-parallel, migrating, propagating rifts.

346 The northern part of the JMMC is a coherent microcontinent on the 100-km scale [Peron-Pinvidic *et al.*, 2012]. SDRs formed on its eastern margin [Kodaira *et al.*, 1998]. The crust that makes up its
 347 southern part is severely intruded continental crust with clear rift zones [Brandsdóttir *et al.*, 2015].
 348 The nature of its transition into Iceland is, however, unknown.
 349

350 Despite developing in the highly magmatically productive environment of the early NE Atlantic the
 351 late Aegir Ridge was magma-starved and formed oceanic crust only 4 - 7 km thick [Breivik *et al.*,
 352 2006; Greenhalgh & Kuszniir, 2007]. This contrasts with both the Kolbeinsey Ridge and the
 353 Reykjanes Ridge which are underlain by oceanic crust ~10 km thick. Extreme variations in magmatic
 354 rate over short distances are inconsistent with mechanisms of melt production that envisage extensive,
 355 coherent regions of influence and suggest, instead, local dependency on melt productivity [Lundin *et al.*, 2018; Simon *et al.*, 2009].
 356

357 2.2.2 South of the Greenland-Iceland-Faroe Ridge

358 South of the GIFR, on the European side, poorly constrained, complicated magnetic anomalies SW of
 359 the Faroe Islands suggest early disaggregated sea-floor spreading. The first unambiguous and
 360 continuous spreading anomaly south of the Faroe Plateau formed at ~47 Ma (C21) [Elliott & Parson,
 361 2008; Ellis & Stoker, 2014; Stoker *et al.*, 2012]. On the Greenland side, the oldest linear magnetic
 362 anomalies produced by the proto-Reykjanes Ridge date from C24-22 (56 - 52 Ma), but they may
 363 represent rift-related basalt extrusion in the Outer-SDR region and not true oceanic spreading. Linear
 364 magnetic anomalies terminate along the SE Greenland margin, unlike the European side where they
 365 are continuous along the margin. This is consistent with early westward migration of the spreading
 366 axis. It finally stabilized along a zone ~150 km west of the Aegir Ridge.

367 Extension proceeded normal to the strike of the Reykjanes Ridge and the continental edges until ~37 -
 368 38 Ma (C17) when an abrupt counter-clockwise rotation of the direction of plate motion occurred.
 369 Spreading in the Labrador Sea then rapidly ceased (Table 1) [Gaina *et al.*, 2017; Jones, 2003;
 370 Martinez & Hey, this volume]. The Bight ridge-ridge-ridge triple junction ceased to exist and the
 371 linear Reykjanes Ridge reconfigured to a right-stepping ridge-transform array such that the new ridge
 372 segments were normal to the new direction of plate motion.

373 Subsequently, and up to the present day, the Reykjanes Ridge has been slowly migrated east by a
 374 series of small-offset, right-stepping propagators within the plate boundary zone that have eliminated
 375 the transforms [Benediktsdóttir *et al.*, 2012; Hey *et al.*, 2010; Martinez & Hey, this volume]. They
 376 originate at the GIFR and migrate south at rates of 10 - 25 cm/a, each slicing a few kilometers off the
 377 Eurasian plate and transferring it to the North American plate [Hey *et al.*, 2016]. At least five and
 378 possibly as many as seven propagators [Jones *et al.*, 2002] have now transferred a swathe of the
 379 Eurasian plate ~30 km wide to the North American plate between the GIFR and the Bight Fracture
 380 Zone [Benediktsdóttir *et al.*, 2012].

381 Progression of each propagator tip is associated with transient changes in thickness of $\sim 2 \pm 1$ km in
 382 the oceanic crust formed. This has the curious consequence that the Reykjanes Ridge is flanked by
 383 diachronous “chevrons” (also called “V-shaped ridges”) of alternating thick and thin crust that are
 384 most clearly seen in the gravity field (Figure 7) [Vogt, 1971].

385 **3 The Greenland-Iceland-Faroe Ridge**

386 The GIFR comprises a ~1,200-km-long, shallow, trans-oceanic aseismic ridge up to 450 km wide in
 387 the northerly direction (Figure 1). At present, 40% of it is exposed above sea level in Iceland. It is
 388 shallower than 600 m and 500 m deep offshore west and east Iceland respectively, ~1000 m shallower
 389 than the ocean basins to the north and south (Figure 8).

390 The GIFR was subaerial along its entire length for most of the history of the NE Atlantic.
 391 Biogeographical evidence for plant and animal dispersal [Denk *et al.*, 2011] and dating of the onset of
 392 overflow of intermediate- and deep waters between the Norway and Iceland basins [Ellis & Stoker,
 393 2014; Stoker *et al.*, 2005b] suggest that it formed a largely intact, trans-Atlantic land bridge (the
 394 Thulean land bridge) until ~10 - 15 Ma and that much survived above sea level longer than this. This
 395 leads to the surprising conclusion that the Thulean land bridge survived intact until the NE Atlantic
 396 Ocean had attained a width of ~1000 km.

397 Magnetic anomalies on the GIFR are poorly defined, broader than classical oceanic spreading
 398 anomalies, and resemble more closely anomalies on the outer SDRs (Figure 6) [*e.g.*, Gaina *et al.*,
 399 2017]. Very few can be clearly traced across the GIFR so the detailed history of breakup in this region
 400 cannot be deduced reliably. Previous interpretations have relied largely on extrapolation of anomalies
 401 to the north and south that are clear, assuming simple oceanic crustal accretion in the region between.

402 Prior explanations for the poorly developed magnetic anomalies include repeated dyke intrusion into
 403 the same zone during more than one magnetic chron, re-magnetization by later intrusions, weathering,
 404 lateral migration of spreading centers and magmatism at multiple spreading centers [Bott, 1974].
 405 Unclear anomalies are also expected because basalt extrusion was subaerial and flooded older lavas,
 406 and because the legacy magnetic data available are poor quality, limited, and poorly levelled.

407 We concur with these suggestions but go further and propose that distinct, oceanic-type linear
 408 magnetic anomalies do not exist on the GIFR because it does not comprise oceanic crust formed by
 409 classical sea-floor spreading. Instead, much of it may consist of magma-dilated, ductile continental
 410 crust. Upper Icelandic-type crust [Bott, 1974 ; Foulger *et al.*, 2003] corresponds to current basaltic
 411 production. Lower Icelandic-type crust corresponds to magma-inflated mid- and lower continental
 412 crust, the most likely lithology for the HVLC that is widespread beneath the NE Atlantic passive
 413 margins (Section 2.1).

414 3.1 Crustal structure

415 The GIFR has been the target of numerous refraction, wide-angle reflection, and passive seismic
 416 experiments [Foulger *et al.*, 2003] as well as gravity, magnetic and magnetotelluric work [Beblo &
 417 Bjornsson, 1978; 1980; Beblo *et al.*, 1983; Eysteinnsson & Hermance, 1985; Hermance & Grillot,
 418 1974; Thorbergsson *et al.*, 1990]. It was the anomalous seismic nature of its crust that led to it being
 419 termed “Icelandic-type” [Bott, 1974; Foulger *et al.*, 2003]. It features an upper crust with a thickness
 420 of ~3 - 10 km with high vertical velocity gradients, and a lower crust ~10 - 30 km thick with low
 421 vertical velocity gradients (Figure 9 and Figure 10) [Darbyshire *et al.*, 1998a; Foulger *et al.*, 2003;
 422 Holbrook *et al.*, 2001; Hopper *et al.*, 2003]. The lower crust has a V_P of 7.0 - 7.3 km/s. Icelandic-type
 423 crust has, in recent years, usually been assumed to be anomalously thick oceanic crust with the lower
 424 crust equivalent to oceanic layer 3. That model became the default assumption after Bjarnason *et al.*
 425 [1993] reported a deep reflecting horizon at ~20 - 24 km depth beneath SW Iceland. It replaced an
 426 earlier model that interpreted the layer beneath the upper crust as anomalously hot mantle
 427 [Angenheister *et al.*, 1980; Gebrande *et al.*, 1980; Palmason, 1971; Tryggvason, 1962].

428 The model that Icelandic-type lower crust is oceanic is inconsistent with other observations. Isostatic
 429 studies reveal the density of the lower crust to be ~3150 kg/m³, which is too high for it to be oceanic
 430 [Gudmundsson, 2003; Menke, 1999]. At the same time, its seismic velocity is too low for normal
 431 mantle peridotite. Models involving partial melt are ruled out by the low attenuation of seismic shear
 432 waves which suggests that Icelandic-type lower crust is no hotter than 800 - 900°C if it is peridotite
 433 [Sato *et al.*, 1989] and 875 - 950°C if it is gabbroic [Menke & Levin, 1994; Menke *et al.*, 1995].

434 The theory that Icelandic lower crust is oceanic is largely based on interpreting deep seismic
 435 reflections as the Moho. However, such reflections can also be interpreted as sills intruded into
 436 continental lower crust. Refracted head waves are almost never observed in Iceland and the large
 437 amplitudes of reflections expected from a Moho are not observed in receiver functions [Du &

438 Foulger, 1999; Du *et al.*, 2002; Du & Foulger, 2001]. These properties are similar to those of HVLC
 439 beneath the Inner- and Outer SDRs of the continental margins [Mjelde *et al.*, 2001]. The possible
 440 compositions and provenances of that material, discussed in Section 2.1, thus provide candidates for
 441 Icelandic-type lower crust.

442 A serpentinized mantle origin for Icelandic-type lower crust is unlikely. If it were serpentinized
 443 mantle, ~20% of serpentinization of peridotite at ~1 GPa (~30 km depth) is required [Christensen,
 444 2004]. Serpentinization in a rifting environment occurs from the top down and water is unlikely to be
 445 able to reach the mantle at the active rift zones of Iceland. If it did, it would only be stable at
 446 temperatures < 700 °C or possibly < 500 °C [Tuttle & Bowen, 1958] and the Icelandic lower crust is
 447 hotter than this [Menke & Levin, 1994; Menke *et al.*, 1995; Sato *et al.*, 1989]. The only other possible
 448 way of serpentinizing the mantle is via fluxing from beneath. In the NE Atlantic such serpentinization
 449 could have occurred in the Caledonian suture [Fichler *et al.*, 2011] and water is present in the source
 450 of basalts erupted in Iceland [Jamtveit *et al.*, 2001; Nichols *et al.*, 2002]. However, no peridotite
 451 xenoliths have been found in Iceland despite a century of extensive geological mapping and drilling,
 452 suggesting that, whereas serpentinite may exist beneath some rifted margins, it probably does not
 453 comprise lower Icelandic-type crust or HVLC beneath the adjacent volcanic margins.

454 Transitional crust comprising massively dyke- and sill-intruded, hyper-extended mid- and lower
 455 continental crust is the most likely composition for Icelandic-type lower crust, as it is for much of the
 456 HVLC beneath the volcanic margins. There is considerable support for this:

- 457 • The seismic velocity and density of continental lower crust match those of Icelandic-type
 458 lower crust. Continental lower crust is thought to comprise predominately mafic garnet-
 459 bearing granulites which have $V_p \sim 7.1 - 7.3$ km/s and densities of 3000 - 3150 kg/m³
 460 [Rudnick & Fountain, 1995]. It may also contain minor components of metapelite,
 461 intermediate and felsic granulites and mafic melts that would reduce V_p and density.
- 462 • The thickness of the brittle surface layer in Iceland and the viscosity of the underlying
 463 material have been constrained by geodetic studies of post-diking stress relaxation [Foulger *et al.*,
 464 1992; Heki *et al.*, 1993; Hofton & Foulger, 1996a; b; Pollitz & Sacks, 1996] and post-
 465 glacial rebound [Sigmundsson, 1991]. The brittle surface layer is ~10 km thick, a value that is
 466 consistent with the maximum depth of earthquakes [Einarsson, 1991] and corresponds
 467 roughly to the upper crust from explosion seismology and receiver functions (Figure 9). The
 468 lower crust beneath has a viscosity of ~10¹⁹ Pa s and is thus ductile.
- 469 • The Faroe Islands are underlain by continental crust topped by > 6 km of basalt [Bott *et al.*,
 470 1974; Ólavsdóttir *et al.*, 2017]. Seismic data from the eastern part of the Iceland-Faroe Ridge
 471 detect stretched continental crust similar to that underlying the Rockall Bank where HVLC
 472 has been interpreted as inherited continental crust of Palaeo-European affinity [Bohnhoff &
 473 Makris, 2004].
- 474 • Palinspastic reconstructions of Iceland require up to 150 km of crust older than the surface
 475 lavas to underlie the island—the extreme westerly and easterly ~15-Ma palaeo-rift products
 476 are separated by ~450 km whereas only ~300 km of widening could have occurred at the
 477 ambient rate of 1.8 cm/a. Reassembly of the NE Atlantic Ocean also requires up to 150 km of
 478 continental crust (original unstretched width) to lie in the ocean [Blischke *et al.*, 2017; Bott,
 479 1985; Foulger, 2006; Gaina *et al.*, 2009; Gaina *et al.*, 2017; Gernigon *et al.*, 2015]. A similar
 480 width is required by the original lateral offset of the tips of the Aegir Ridge and proto-
 481 Reykjanes Ridge. A southerly continuation of the JMMC beneath the GIFR would be a
 482 simple source of this material [Bott, 1985; Foulger & Anderson, 2005; Schiffer *et al.*, 2018].
 483 Icelandic-type crust also underlies the transitional region between the NE Icelandic shelf and
 484 the JMMC [Brandsdóttir *et al.*, 2015].

- 485 • Magma-assisted extension at the far western and eastern ends of the proto-GIFR, outside of
 486 the axes of breakup, is predicted by stress modeling and may have fed additional continental
 487 crust into the developing GIFR.
- 488 • There are multiple lines of petrological and geochemical evidence for a component of
 489 continental crust in Icelandic lavas, including Proterozoic and Mesozoic zircons [Amundsen
 490 *et al.*, 2002; Foulger, 2006; Paquette *et al.*, 2006; Schaltegger *et al.*, 2002] elevated $^{87}\text{Sr}/^{86}\text{Sr}$
 491 and Pb isotope ratios [Prestvik *et al.*, 2001] and extensive silicic and intermediate rocks
 492 including rhyolite and icelandite—an Fe-rich form of andesite (Section 6).

493 3.2 The Faroe-Shetland basin—a bellwether of GIFR tectonic instability

494 The Faroe-Shetland basin comprises the eastern extension of the GIFR, is thus sensitive to tectonic
 495 activity in that zone, and has been unstable throughout the Palaeogene-early Neogene [Stoker *et al.*,
 496 2018; Stoker *et al.*, 2005b]. Key phases are summarized in Figure 11 and include the following.

- 497 • Paleocene (~63 - 56 Ma): The pre-breakup rifting phase (late Danian—Thanetian) was
 498 characterized by formation of a series of sag and fault-controlled sub-basins [Dean *et al.*,
 499 1999; Lamers & Carmichael, 1999], coeval borderland uplift events (rift pulses) [Ebdon
 500 *et al.*, 1995; Goodwin *et al.*, 2009; Mudge, 2015] and rifting and extension accompanied by
 501 volcanism [Mudge, 2015; Ólavsdóttir *et al.*, 2017].
- 502 • Latest Paleocene (~56 - 55 Ma): Uplift [Ebdon *et al.*, 1995] and extrusion of syn-breakup
 503 flood basalts and tuffs [Mudge, 2015] probably mark the onset of local, discontinuous sea-
 504 floor spreading [Passey & Jolley, 2009].
- 505 • Early-Mid-Eocene (~54 - 46 Ma): The syn-breakup rift-to-drift transition continued during
 506 the early/mid-Ypresian-early Lutetian [Stoker *et al.*, 2018]. Cyclical coastal plain, deltaic and
 507 shallow-marine deposits attest to tectonic instability linked to episodic uplift of the
 508 Munkagrinnur and Wyville Thomson ridges on the south flank of the basin [Ólavsdóttir *et al.*
 509 *et al.*, 2010; Ólavsdóttir *et al.*, 2013b; Stoker *et al.*, 2013]. Onset of continuous sea-floor
 510 spreading in the Norway basin (chron C21) was accompanied by uplift events, continued
 511 growth of the Wyville Thomson and Munkagrinnur ridges, and formation of inversion domes
 512 in the basin [Ólavsdóttir *et al.*, 2010; Ólavsdóttir *et al.*, 2013b; Ritchie *et al.*, 2008; Stoker *et al.*
 513 *et al.*, 2013; Stoker *et al.*, 2018].
- 514 • Late Paleogene-early Neogene (~35 - 15 Ma): The present-day basin physiography was
 515 initiated in the latest Eocene/Early Oligocene with sagging leading to basin-ward collapse of
 516 the margin west of Shetland [Stoker *et al.*, 2013]. Onlapping Oligocene and Lower Miocene
 517 basinal sequences were deformed by compressional stresses and widespread inversion and
 518 fold growth culminated in the early Mid-Miocene [Johnson *et al.*, 2005; Ritchie *et al.*, 2008;
 519 Stoker *et al.*, 2005c].
- 520 • Mid-Miocene—Pleistocene (16/15 Ma - present): Basinal sedimentation was dominated by
 521 deep-water deposits [Stoker *et al.*, 2005b] with Early Pliocene uplift and tilting of the West
 522 Shetland and East Faroe margins accompanied by basinal subsidence and reorganization of
 523 bottom current patterns [Andersen *et al.*, 2000; Ólavsdóttir *et al.*, 2013b; Stoker *et al.*, 2005a;
 524 Stoker *et al.*, 2005b]. Mid-and Late Pleistocene sedimentation was dominated by shelf-wide
 525 glaciations [Stoker *et al.*, 2005a].

526 In summary, the Faroe-Shetland basin has experienced persistent tectonic unrest from the Paleocene
 527 to the Early Miocene (~63 - 15 Ma). This is reflected onland in the Faroe Islands in Paleogene and
 528 younger faults and dykes that show progressive changes in the direction of extension prior to and
 529 following NE Atlantic break-up [Walker *et al.*, 2011]. This chronic unrest likely reflects both
 530 instability on the GIFR to the west and the protracted breakup of the wider NE Atlantic region.

531 4 A new model for the Greenland-Iceland-Faroe Ridge

532 In this section, we build on the background given above and propose a new working hypothesis for
 533 development of the GIFR and how this affected the rest of the NE Atlantic Realm. Numerical
 534 modeling of the processes we propose, and model fit with petrology and geochemistry, are discussed
 535 in Sections 5 and 6.

536 As described above, the NE Atlantic Realm formed in a disorderly way as a consequence of inherited
 537 strength anisotropy, coupled with frequent changes in the poles of rotation of sub-regions [Hansen *et*
 538 *al.*, 2009; Schiffer *et al.*, 2018]. North of the GIFR, the Aegir rift opened by southward propagation
 539 obliquely along the Caledonian orogen. It stalled at the western frontal thrust and hooked around to
 540 the west (Figure 1). The Reykjanes Ridge to the south stalled at the Nagssugtoqidian orogen, ~300 km
 541 south of the Caledonian frontal thrust and ~150 km west of the Aegir Ridge (Section 2.2). The
 542 Reykjanes Ridge and Aegir Ridge thus formed a pair of propagating, approaching, laterally offset
 543 rifts. The broad barrier formed by the Nagssugtoqidian and Caledonian orogens prevented them from
 544 propagating further and conceivably eventually forming a continuous, conventional oceanic plate
 545 boundary.

546 As a consequence, the continental region between their tips, the ~300 x 150 km Iceland
 547 Microcontinent, deformed by magma-assisted, distributed continental transtension and developed into
 548 the GIFR as the ocean widened (Figure 12). The crust beneath the Iceland Microcontinent and
 549 flanking areas thinned by ductile flow in its deeper parts. Extensive magmatism built SDRs of the
 550 kind observed on the eastern margin of the JMMC and the NE Atlantic rifted margins. Initially, the
 551 GIFR may have comprised an array of four passive margins—one on each of the east Greenland and
 552 west Faroe margins, and one on either side of the Iceland Microcontinent.

553 As the GIFR lengthened, and up to the present day, deformation persisted in a distributed style along
 554 a series of ephemeral extensional rifts and diffuse, intermediate, poorly developed shear transfer
 555 zones [Gerya, 2011]. The loci of extension repeatedly reorganized by migrating laterally to positions
 556 that were stress-optimal and likely also influenced by pre-existing structures in the underlying
 557 continental crust. Rifts that became extinct were transported laterally out of the actively extending,
 558 central part. As it formed the GIFR was blanketed by lavas in the style of volcanic-rifted-margins.
 559 Similar rift migrations also occurred in the eastern Norway basin where the oceanic crust is thickest
 560 [Gernigon *et al.*, 2012]. After ~48 Ma (C22) it seems that this style of extension persisted only on the
 561 GIFR. The permanent disconnect between the Aegir Ridge and the Reykjanes Ridge and the low
 562 spreading rate in the NE Atlantic (1 - 2 cm/a) would have further encouraged long-term diffuse
 563 deformation.

564 Figure 13 shows palinspastic reconstructions of the observed positions of active and extinct rifts in the
 565 NE Atlantic Realm at various times. Swathes of extinct, short, NE-orientated ridges similar to those
 566 that are currently active onland in Iceland are observed also in submarine parts of the GIFR
 567 [Hjartarson *et al.*, 2017]. There is insufficient observational data at present to fully reconstruct the
 568 sequence of deformation on the GIFR because of the blanketing lava flows and insufficient
 569 geophysical and geological research to date. Nevertheless, in Figure 14 we attempt such a
 570 reconstruction by extrapolating in time from known active and extinct rifts [Hjartarson *et al.*, 2017;
 571 Johannesson & Saemundsson, 1998].

572 A large block of crust older than the surface lavas is required by palinspastic reconstructions to lie
 573 beneath Iceland [Foulger, 2006]. Thus, much of the Iceland Microcontinent may still exist beneath
 574 Iceland and comprise a C-block [Geoffroy *et al.*, 2015; Geoffroy *et al.*, submitted]. C-blocks are
 575 expected to be flanked by Outer-SDRs and the geometry of some dykes and lava flows in Iceland
 576 resemble these [Bourgeois *et al.*, 2005; Hjartarson *et al.*, 2017]. It has long been speculated that the
 577 continental crust required by geochemistry to underlie Iceland (Section 6) comprises a southerly
 578 extension of the magma-dilated southern JMMC. Give the extent of continental crust that is required

579 to underlie the GIFR it may be more appropriate to view the JMMC as an offshore extension of the
580 Iceland Microcontinent.

581 Deformation on the GIFR cannot be described by traditional rigid plate tectonics and corresponding
582 reconstructions. It corresponds to the case of multiple overlapping ridges, the limit of an extensional
583 zone [Engeln *et al.*, 1988]. It may be likened to a lateral array of hyper-extended SDRs underlain by
584 HVLC comprising heavily intruded, stretched, ductile continental crust. Repeated rejuvenation of the
585 rift axes by lateral migration may have boosted volcanism. Westerly migrations may have induced
586 extension to the north to concentrate in the westernmost axis of extension in the southern JMMC,
587 leading to extinction of the Aegir Ridge and formation of the Kolbeinsey Ridge at ~24 Ma. That
588 migration switched the sense of the ridges north and south of the GIFR from right-stepping to left-
589 stepping.

590 Iceland is ~450 km wide in an EW direction and exposes ~40% of the GIFR (Figure 1). The oldest
591 rocks found there to date are 17 Ma. There is no evidence, or reason to think, that the tectonic style on
592 the GIFR was fundamentally different in the past from present-day Iceland. On the contrary, the
593 similarity of the submarine GIFR synclines to structure on land in Iceland suggests that it was the
594 same [Hjartarson *et al.*, 2017].

595 Onland in Iceland extension over the last ~15 Ma has occurred via multiple unstable, migrating,
596 overlapping spreading segments connected by complex, immature shear transfer zones that reorganize
597 every few Myr (Figure 15). These include the South Iceland Seismic Zone [Einarsson, 1988; 2008]
598 and the Tjörnes Fracture Zone [*e.g.*, Rognvaldsson *et al.*, 1998]. Both are broad, diffuse seismic zones
599 that deform in a bookshelf-faulting manner and have not developed the clear topographic expression
600 of faults that experience long-term repeated slip.

601 There is geological evidence in Iceland for at least 12 spreading zones (Table 2) of which seven are
602 currently active, two highly oblique to the direction of plate motion, one waning, one propagating,
603 two non-extensional and five extinct. At least five lateral rift jumps are known and a sixth is currently
604 underway via transfer of extension from the Western Volcanic Zone (WVZ) to the Eastern Volcanic
605 Zone (EVZ). Extension has always been concentrated in a small number of active, ephemeral rift
606 zones at any one time (Figure 15).

607 There is no evidence that mature sea-floor spreading has yet begun anywhere along the GIFR. If such
608 were the case it would be expected that all extension would be rapidly transferred to that zone and
609 normal-thickness oceanic crust (*i.e.*, ~6 - 7 km) would begin to form. Indeed, the fact that rift-zone
610 migrations are still ongoing in Iceland suggest that this is not the case. There may be some narrow
611 zones where embryonic sea-floor spreading began but was abandoned due to subsequent lateral rift
612 jumps, *e.g.*, immediately east of the east Icelandic shelf, and in the deep channel in the Denmark
613 Strait. Until this can be confirmed, however, it remains a possibility that full continental breakup has
614 not yet occurred in the latitude band of the GIFR. This fundamentally challenges the concept that
615 continental breakup has yet occurred in this part of the NE Atlantic.

616 4.1 Mass balance

617 The GIFR today is 1,200 km long with a lower crust generally ~20 km thick and maximally ~30 km
618 beneath central Iceland (Figure 9). If a substantial part of this is continental, a large volume thus
619 needs to be accounted for. Taking a present-day average breadth for the GIFR of ~200 km, the surface
620 area is ~0.24 x 10⁶ km². If an average thickness of 15 km of continental material lies beneath, a
621 volume of ~3.6 x 10⁶ km³ is required.

622 We propose that this material was sourced from the Iceland Microcontinent and flanking continental
623 regions by ductile flow of mid- and lower crust. Ductile flow can stretch such crust to many times its
624 original length (necking), draw in material from great distances, and maintain large crustal

625 thicknesses. Numerical thermo-mechanical modeling (Section 5) confirms that these processes can
 626 account for the lower-crustal thicknesses proposed and even increase crustal thickness as material
 627 rises to fill the void created by rupture of the upper crust.

628 Flow is enabled by the low viscosity of the lower crust beneath Iceland. This has been shown to be
 629 10^{18} - 10^{19} Pa s by GPS measurements of post-diking stress relaxation following a regional, 10-m-
 630 wide dyke injection episode in the Northern Volcanic Zone (NVZ) 1975 - 1995 [Bjornsson *et al.*,
 631 1979; Foulger *et al.*, 1992; Heki *et al.*, 1993; Hofton & Foulger, 1996a; b]. Numerical modeling of
 632 those data also showed that the surface, brittle layer was approximately 10 km thick. The low
 633 viscosity found for the lower crust was confirmed by measurements and modeling of the rapid
 634 isostatic rebound from retreat of the Weichselian ice cap in Iceland and melting of the Vatnajökull
 635 glacier in south Iceland [Sigmundsson, 1991]. [Sigmundsson, 1991].

636 As a prelude to numerical thermo-mechanical modeling we present here a simple mass-balance
 637 calculation. Inland in Greenland, receiver function studies indicate a Moho depth of ~40 km [Kumar
 638 *et al.*, 2007]. The Caledonian crust of east Greenland is currently up to ~50 km thick [Darbyshire *et*
 639 *al.*, 2018; Schiffer *et al.*, 2016; Schmidt-Aursch & Jokat, 2005; Steffen *et al.*, 2017]. A pre-breakup
 640 Caledonian crustal thickness of about 60 km and a post-breakup thickness of 30 km [Holbrook *et al.*,
 641 2001] is not unrealistic.

642 Beneath the Faroe-Shetland basin, crustal thinning left only a 10-km-thick crust while below the
 643 Faroe shelf and islands seismic data indicate basement modified by weathering, igneous intrusions
 644 and tuffs with a thickness of about 25 - 35 km [Richard *et al.*, 1999]. Beneath the banks to the SW of
 645 the Faroe Islands the thickness of the subvolcanic crust is up to 25 km but it is as little as 8 km
 646 beneath the channels between them [Funck *et al.*, 2008]. In the Faroe Bank Channel and the channel
 647 between George Bligh and Lousy Bank, in prolongation of the GIFR, the continental middle crust is
 648 almost completely gone and the lower crust is dramatically thinned. Initial and final thicknesses of 60
 649 km and 15 km are reasonable.

650 Thinning of the mid- and lower crust of 30 km (Greenland) and 45 km (Faroe region) extending ~200
 651 km along the margins and ~100 km inland could provide $\sim 1.5 \times 10^6$ km³ of material. Assuming
 652 original northerly and easterly dimensions for the Iceland Microcontinent of 300 km and 150 km
 653 respectively, and thinning from an original 60 km to 15 km, an additional $\sim 2 \times 10^6$ km³ of material is
 654 accounted for. Together, this totals $\sim 3.5 \times 10^6$ km³ of material, very close to the $\sim 3.6 \times 10^6$ km³
 655 required.

656 This mass balance calculation illustrates simply that our model is reasonable. It also shows that the
 657 Iceland Microcontinent can provide over half of the continental material required. This suggests that
 658 the formation of such an unusually large microcontinent was likely a key element in the development
 659 of this unique region.

660 4.2 Problems and paradoxes solved

661 The model we propose can account naturally for many hitherto unexplained observations from the
 662 GIFR and surrounding regions, and it is supported by multiple lines of evidence. In particular, it
 663 offers a solution to the decades-old problems of why the Thulean land bridge existed, and the nature
 664 of Icelandic-type crust. Thus:

- 665 • A composition of Icelandic-type crust comprising magma-inflated continental crust blanketed
 666 with lavas can explain the high topography and bathymetry of the GIFR and its prolonged
 667 persistence above sea level.
- 668 • The assumption that the full thickness of Icelandic-type crust corresponds to melt has been
 669 widely accepted ever since Bjarnason *et al.* [1993] reported a reflective horizon at ~20 - 24
 670 km depth beneath south Iceland which they interpreted as the Moho. That model cannot,

- 671 however, account for the absence of refracted seismic phases (Section 3.1) which is
 672 inconsistent with gabbroic crust overlying mantle with a step-like interface velocity increase.
 673 The lack of such refractions is, however, consistent with the reflective horizon being a sill-
 674 like structure within or near the base of magma-inflated continental crust.
- 675 • Icelandic-type lower crust has a seismic velocity V_p of 7.0 - 7.3 km/s and a density of ~ 3150
 676 kg/m^3 . No reasonable basaltic petrology is consistent with this [Gudmundsson, 2003; Menke,
 677 1999], but these values fit a composition of magma-inflated continental crust.
 - 678 • A lower crust containing significant continental material solves the paradox of magmatic
 679 production on the GIFR. Icelandic-type lower crust cannot be gabbroic because a melt layer
 680 up to 40 km thick cannot be explained with any reasonable petrology and temperatures
 681 (Section 6) [Hole & Natland, this volume]. If the melt layer corresponds only to Icelandic-
 682 type upper crust plus magma inflating the lower crust—possibly a total thickness of up to ~ 15
 683 km—much less melt needs to be explained.
 - 684 • A substantial volume of continental material in the lower crust can explain why the
 685 thicknesses of the upper and lower crustal layers on the GIFR are de-correlated (Figure 9)
 686 [Foulger *et al.*, 2003; Korenaga *et al.*, 2002]. In particular, the lower crust is thick throughout
 687 a NW-SE swathe across central Iceland where the upper crust is of average thickness. In the
 688 far south, the upper crust has its maximum thickness but the lower crust is unusually thin
 689 (Figure 9).
 - 690 • MORB melt formed in the mantle below the crust passes through the latter, melting fusible
 691 components to a high degree, boosting melt volume, and acquiring the continental signature
 692 observed in Icelandic rocks including the geochemistry, Proterozoic and Mesozoic zircons,
 693 and voluminous felsic and intermediate petrologies (Section 6).
 - 694 • The numerous, northerly trending synclines detected by seismology throughout submarine
 695 parts of the GIFR are readily explained as volcanically active extensional zones that were
 696 abandoned by lateral jumps and subsequently became extinct [Hjartarson *et al.*, 2017] (Figure
 697 8).
 - 698 • If the JMMC is a northerly extension of the Iceland Microcontinent, the former may have
 699 shared the tectonic instability of the GIFR, providing an explanation for why the JMMC
 700 broke off east Greenland.

701 Our new model for the GIFR can account for the many unusual extensional, transtensional and shear
 702 tectonic elements in the region. These include the curious distributed, bookshelf mode in which shear
 703 deformation is taken up in Iceland in the South Iceland Seismic Zone and the Tjörnes Fracture Zone
 704 [Bergerat & Angelier, 2000; Einarsson, 1988; Taylor *et al.*, 1994].

705 It can also account for the widespread hook-like tectonic morphology that resembles the tips of
 706 overlapping propagating cracks (Figure 16). These suggest that short extensional elements are
 707 abundant. The southernmost Aegir Ridge is hooked westward, mirroring the shape of the Blosseville
 708 coast of Greenland and curving into the transverse Caledonian frontal thrust [Brooks, 2011]. The
 709 extensional NVZ of Iceland curves westward at its northern end where it links with the Kolbeinsey
 710 Ridge via the Tjörnes Fracture Zone. At its north end, the Reykjanes Ridge hooks to the east where it
 711 runs onshore to form the Reykjanes Peninsula extensional transform zone [Taylor *et al.*, 1994]. The
 712 direction of extension in the EVZ is rotated $\sim 35^\circ$ clockwise compared with the NVZ as shown by both
 713 the strike of dyke- and fissure swarms and current measurements of surface deformation made using
 714 GPS [*e.g.*, Perlt *et al.*, 2008]. The southernmost tip of this propagating rift, the Vestmannaeyjar
 715 archipelago, hooks to the west, complementing the east-hooking northern Reykjanes Ridge and
 716 Reykjanes Peninsula Zone (Figure 16).

717 The contrasting tectonic morphology and behavior north and south of the GIFR are naturally
 718 explained by tectonic decoupling by the GIFR that separates them. North of the GIFR the boundary is
 719 dominated by spreading ridges orthogonal to the direction of extension, separated by classic transform

720 faults. To the south, the Reykjanes Ridge as a whole is oblique to the spreading direction and devoid
 721 of transform faults. Numerous tectonic events occurred north or south of the GIFR but not in both
 722 regions simultaneously [Gernigon *et al.*, this volume; Martinez & Hey, this volume]. In Iceland,
 723 tectonic decoupling can explain the north-south contrast in geometry, morphology and history of the
 724 rift zones and the north-south asymmetry in geochemistry [*e.g.*, Shorttle *et al.*, 2013]. The latter may
 725 be important in mapping the distribution of continental material beneath Iceland.

726 Unstable tectonics on the GIFR can further explain the diachronous chevrons of alternating thick and
 727 thin crust that form at the tips of propagators within the Reykjanes Ridge plate boundary zone (Figure
 728 7; Sections 2.2.2 and 7.3.3). The onset times of several of the most recent of these propagators at the
 729 GIFR coincide with major ridge jumps in Iceland (Table 1). These observations are consistent with
 730 the propagators being triggered by major tectonic reorganizations on the GIFR. Several similar ridges
 731 are observed in the oceanic crust east of the Kolbeinsey Ridge [Jones *et al.*, 2002]. The chronic
 732 instability of the mid-Norwegian shelf and the adjacent Faroe-Shetland basin throughout the
 733 Palaeogene-earliest Neogene is also accounted for [Ellis & Stoker, 2014; Gernigon *et al.*, 2012;
 734 Stoker *et al.*, 2018] (Figure 11) (Section 3.2).

735 **5 Thermo-mechanical modeling**

736 We tested the plausibility of unusually prolonged survival of intact continental crust beneath the GIFR
 737 by modeling numerically the behavior under extension of structures characteristic of an ancient
 738 orogen such as the Caledonian and surrounding regions. The crust is required to have stretched to
 739 over twice its original width, retained a typical thickness of ~20 km, and persistently extended along
 740 more than one axis even up to the present day *i.e.* it underwent long-term, diffuse extension.

741 We used a two-dimensional thermo-mechanical modeling approach [Petersen & Schiffer, 2016] to
 742 calculate the visco-elastic-plastic response of an ancient orogen under simple extension. Full details of
 743 our methodological approach along with petrologic, thermodynamic, rheological, thermal
 744 conductivity, radiogenic heat productivity, initial model state, boundary conditions and melt
 745 productivity are described in detail by Petersen *et al.* [2018]. The initial state for the model we use
 746 here differs from that used by Petersen *et al.* [2018] only in that a) a uniform adiabatic temperature
 747 with potential temperature $T_p = 1325^\circ\text{C}$ is assumed for the entire mantle, and b) there is no MORB
 748 layer at the upper/lower mantle boundary.

749 Prior to continental breakup, crustal thickness and structure likely varied throughout the region, but
 750 precise details of the pre-rift conditions are not well known. Insights may be gained from well-
 751 studied, currently intact orogens. The Himalaya orogen, a heterogeneous stack of multiple terranes,
 752 entrained subduction zones, and continental material, is underlain by one or more fossil slabs trapped
 753 in the lithosphere. These locally thicken the crust and their lower parts are in the dense eclogite facies
 754 (Figure 17) [Tapponnier *et al.*, 2001]. The Palaeozoic Ural Mountains preserve a crustal thickness of
 755 50 - 55 km [Berzin *et al.*, 1996]. The Caledonian crust is up to ~50 km thick under east Greenland
 756 [Darbyshire *et al.*, 2018; Schiffer *et al.*, 2016; Schmidt-Aursch & Jokat, 2005; Steffen *et al.*, 2017]
 757 and ~45 km thick beneath Scandinavia [Artemieva & Thybo, 2013; Ebbing *et al.*, 2012].

758 The pre-breakup crust in the region of the future NE Atlantic comprised the south-dipping Ketilidian
 759 and Nagssugtoqidian orogens and the bivergent Caledonian orogen with east-dipping subduction of
 760 Laurentia (Greenland) and west-dipping subduction of Baltica (Scandinavia) (Figure 4). The GIFR
 761 thus formed over fossil forearc/volcanic front lithosphere that may initially have had a structure
 762 similar to that of the Zangbo Suture of the Himalaya orogen (Figure 17). North of the GIFR the
 763 supercontinent broke up longitudinally along the Caledonian suture where the crust was thinner.

764 We modeled the Caledonian frontal thrust as an orogenic belt where the lithosphere contrasts with
 765 that of the flanking Greenland and Scandinavia areas in a) increased crustal thickness, and b) eclogite
 766 from fossil subducted slabs embedded in the lithospheric mantle (Figure 4) [Schiffer *et al.*, 2014]. The

767 eclogite is relatively dense, potentially driving delamination, but is rheologically similar to dry
 768 peridotite [Petersen & Schiffer, 2016 and references therein]. Additional weakening of the hydrated
 769 mantle wedge preserved under the suture would enhance the model behavior we describe below
 770 [Petersen & Schiffer, 2016]. For the mantle, we assume a pyrolite composition that is subject to melt
 771 depletion during model evolution.

772 Figure 18 shows our initial, simplified model setup [Petersen *et al.*, 2018]. Pre-rift continental crustal
 773 thickness is 40 km for the lithosphere adjacent to the orogen. The crust beneath the 200-km-wide
 774 orogen is 50 km thick and underlain by an additional 20-km-thick slab of HVLC with an assumed
 775 mafic composition. Phase transitions and density are self-consistently calculated from
 776 pressure/temperature conditions throughout the model such that the topmost part of the body is above
 777 eclogite facies and the lower part is in the eclogite facies and thus negatively buoyant.

778 Densities and entropy changes are pressure- and temperature-dependent and calculated using
 779 Perple_X-generated lookup tables [Connolly, 2005] based on the database of Stixrude and Lithgow-
 780 Bertelloni [2011]. We use a wide box (2000 km x 1000 km) to enable simulation of considerable
 781 extension distributed over a broad region, a grid resolution of 2 km, and a run time of 100 Myr at a
 782 full extension rate of 1 cm/a. Rifting of the lithosphere is kinematically forced by imposing plate
 783 separation at a rate of 0.5 cm/a via outwards perpendicular velocities at both left and right boundaries
 784 throughout the depth range of 0 - 240 km.

785 A multigrid approach is employed to solve the coupled equations for conservation of mass, energy
 786 and momentum as described by Petersen *et al.* [2015; 2018]. For the continental crust, we assume
 787 plagioclase-like viscous behavior [Ranalli, 1995]. The HVLC is assumed to follow an eclogite flow
 788 law [Zhang & Green, 2007]. The upper mantle is assumed to follow a combined diffusion/dislocation
 789 creep flow law [Karato & Wu, 1993]. The lower mantle, here defined as the region where the
 790 pressure/temperature-dependent density exceeds 4300 kg/m³, approximately corresponding to
 791 Ringwoodite-out conditions, is assumed to follow the linear flow law inferred by Čížková *et al.*
 792 [2012].

793 As the structure extends, rifting develops in the broad region where the crust is thickest. The Moho
 794 temperature is highest there (i.e. ~800°C; Figure 18 central panels) due to greater burial and
 795 radiogenic heat production. During the first 10 Myr of widening, extensional strain within the crust is
 796 laterally distributed due to the delocalizing effect of flow in the lower crust [*e.g.*, Buck, 1991].
 797 Thinning of the mantle lithosphere is not counteracted by this effect and within 10 Myr it has been
 798 thinned by a factor of up ~2. This results in onset of decompression melting after ~12 Myr. At this
 799 point, the crust in the stretched orogen retains a large thickness of 30 - 40 km. This contrasts with the
 800 sequence of events where the crust is thin and brittle under which conditions decompression melting
 801 only onsets after breakup i.e. when complete thinning of the continental crust occurs [Petersen *et al.*,
 802 2018].

803 Thinning of the mantle lithosphere leads to lateral density gradients between the asthenosphere and
 804 displaced colder lithospheric mantle that destabilize the lithospheric mantle [Buck, 1986; Keen &
 805 Boutelier, 1995; Meissner, 1999]. Consequently, the mantle lithosphere, including the already
 806 negatively buoyant HVLC, starts to delaminate at ~12 Myr (Figure 18). As a result, asthenosphere at
 807 a potential temperature (T_p) of ~1325°C and crust at an initial temperature of ~600 - 800°C are rapidly
 808 juxtaposed. This leads to increased heat flow into the crust which therefore remains ductile enough to
 809 flow and continues to extend in the delocalized, “wide rift mode” of Buck [1991]. The loci of
 810 extension repeatedly migrate laterally and this mode of deformation continues as long as lower crust
 811 is available. The loci of extension only stabilize after ~70 Myr.

812 Figure 18 shows the predicted structure after 51 Myr, approximately the present day, and a
 813 magnification of the 51-Myr lithology panel is shown in Fig. 19. The continental crust is still intact
 814 across the now 1,200-km-wide ocean and extending diffusely. Decompression melting is occurring

815 beneath two zones. The HVLC body has disintegrated and the largest pair of fragments are 200 - 300
816 km in diameter. These, along with carapaces of lithospheric mantle, have subsided to a depth near the
817 base of the transition zone. Between them, a narrow arm of mantle upwells and flattens at the base of
818 the crust to form a broad sill-like body ~200 km thick that underlies the entire ocean. Upwelling
819 includes some material from just below the transition zone as a consequence of the sinking HVLC
820 displacing uppermost lower-mantle material.

821 Full lithosphere breakup has not occurred by 51 Myr. It is imminent at 71 Myr (Figure 18). The lower
822 crust beneath distal areas flows into the thinning extending zone and only when the supply of ductile
823 lower crust is depleted does extension localize, leading to full lithosphere rupture and sea-floor
824 spreading. This may take several tens of millions of years. In the case where the crust is thinner and/or
825 HVLC is lacking modeling predicts transition to sea-floor spreading after only a few million years.

826 The generic model presented here shows that it is possible for extending lithosphere to remain for as
827 long as 70 Myr in a delocalized 'wide' stretching mode [sensu Buck, 1991] with lower crust from
828 distal areas flowing into the extending zone. Since the delamination, the mantle lithosphere has
829 effectively been removed and decompression melting occurs where the mantle wells up beneath the
830 rift system. Together, these interdependent processes provide a physical mechanism for how
831 continental crust could be preserved beneath the GIFR despite more than 50 Myr of extension (Figure
832 20). At the same time, the model accounts for the magmatism observed on the GIFR in that it predicts
833 decompression melting in the mantle. These melts rise, intrude and erupt, covering the continental
834 crust as it stretches, and would produce crust similar to the "embryonic" crust proposed to occur in the
835 Norway Basin [Geoffroy, 2005; Gernigon *et al.*, 2012].

836 The predictions of our model for present-day structure compare well with seismic tomography images
837 (Figure 21). For example, a cross section through the full-waveform inversion tomographic model of
838 Rickers *et al.* [2013] shows several features that are in close correspondence to those we predict.
839 These include the flanking high-wave-speed bodies at the bottom of the transition zone, a narrow,
840 weak, vertical, low-wave-speed body between them and a broader, stronger, low-wave-speed body in
841 the top ~200 km underlying the entire ocean. The high-wave-speed bodies correspond to the
842 delaminated lithospheric mantle and the low-wave-speed anomalies correspond to the temperature
843 anomalies predicted by the modeling (Figure 19). A mantle temperature anomaly of ~ 30°C is
844 predicted beneath the entire ocean down to ~ 200 km depth as a result of upper mantle upwelling. The
845 seismic anomaly could then be explained by this temperature anomaly and a resulting increase in the
846 degree of partial melt by up to 0.5% [Foulger, 2012]. Such a temperature anomaly is consistent with
847 the low values predicted by Ribe *et al.* [1995] who modeled the topography of the region, and the
848 petrological estimates of Hole and Natland [this volume]. Seismic tomography images are notoriously
849 variable in detail, in particular anomaly amplitudes [Foulger *et al.*, 2013], and we thus place most
850 significance on the correspondence between the shape of the predicted (Figure 19) and observed
851 (Figure 21) anomalies.

852 Our results differ from those of existing mechanical models in that breakup of the continental crust is
853 more protracted [*e.g.*, Brune *et al.*, 2014]. For example, Huisman and Beaumont [2011] showed that
854 extension of lithosphere with relatively weak crust results in pre-breakup wide-rift-mode extension for
855 ~35 Myr. Our model differs from theirs by having dense HVLC that delaminates as a consequence of
856 rifting thereby increasing heat flow into the crust. This enables wide rifting to persist for much longer
857 than where no HVLC is present, even in the absence of an especially weak lower crustal rheology.

858 The amount and detailed history of wide-mode extension is controlled by the thickness of the initial
859 crust and rheology-governing parameters such as initial thermal state, heat flow, radiogenic heat
860 production and crustal flow laws. We examined models that varied some of these parameters to
861 investigate the sensitivity of our results to the assumed initial conditions. We modeled crustal
862 thicknesses of 35 km for the region and 40 km for the orogen, and lithosphere thickness of 100 km
863 with quartzite-like crustal rheology. Similar results to those described above were obtained. Factors

864 we do not incorporate in our simple model that would further encourage crustal stretching and delay
 865 breakup include increased basal heat flow and/or internal heat production and inclusion of 3D effects
 866 that would permit ductile mid- and lower crust to flow along the strike of the Caledonides towards the
 867 GIFR during extension.

868 **6 Geochemistry**

869 All aspects of the petrology and geochemistry of igneous rocks in the NE Atlantic Realm are
 870 consistent with a model where Icelandic lower crust contains a substantial amount of continental
 871 crust. The geochemical and petrological work most powerful to test this model is that which addresses
 872 the composition and potential temperature (T_p) of the melt source.

873 *6.1 Composition of the melt source*

874 The source of Icelandic lavas cannot be explained by mantle peridotite alone [*e.g.*, Presnall &
 875 Gudfinnsson, 2011]. A component of continental material is required and some studies have presented
 876 evidence that this could be of Caledonian age [Breddam, 2002; Chauvel & Hemond, 2000; Korenaga
 877 & Kelemen, 2000]. It could come from subducted slabs still remaining in the shallow mantle, as has
 878 been proposed earlier [Foulger & Anderson, 2005; Foulger *et al.*, 2005]. The observations could also
 879 be explained by the upward flow of mantle melt through a substrate of stretched, magma-inflated
 880 continental crust similar to some HVLC beneath the passive margins.

881 *Titanium*: The petrology and geochemistry of igneous rocks along the mid-Atlantic ridge change
 882 radically at the Icelandic margin. Low-TiO₂ basalts are found on the Reykjanes and Kolbeinsey
 883 Ridges and in the rift zones of Iceland. These rocks do not follow the MORB array of Klein and
 884 Langmuir [1987] but have the least Na₈ and Ti₈ of the entire global array. These lavas are probably
 885 derived mostly from a peridotitic MORB source.

886 Basalts with high-TiO₂ and FeO(T) signatures occur in Iceland, Scotland, east and west Greenland,
 887 but not on the Reykjanes or Kolbeinsey Ridges. These basalts cannot come from MORB-source
 888 mantle—the source is required to have distinct Fe-Ti-rich material and other important geochemical
 889 indicators such as REE that are not found in MORB-source mantle. The extent of differentiation
 890 beneath Icelandic central volcanoes is also high enough to produce abundant silicic lavas—icelandite
 891 and rhyolite—in association with the FeO(T)-TiO₂-rich basalts. These rocks comprise 10% of the
 892 surface volcanics of Iceland but are not present on the adjacent submarine ridges and are uncommon
 893 on all other oceanic spreading plate boundaries.

894 A candidate for the source of such lavas is lower continental crust, possibly pyroxenite/eclogite
 895 arising from gabbro with elevated TiO₂ and FeO(T) at pressures in the eclogite facies, along with
 896 refractory sub-continental lithospheric mantle (SCLM), originally from the Greenland and European
 897 margins and still present in the central North Atlantic. A hybrid source of this sort can explain the
 898 diversity of Icelandic magmas [Foulger & Anderson, 2005; Foulger *et al.*, 2005; Korenaga, 2004;
 899 Korenaga & Kelemen, 2000]. Because there is no major isotopic anomaly, the source cannot be very
 900 old. Candidate material is common in continental lithosphere. For example, xenolith suites of lower
 901 crustal cumulates from Permian lamprophyres in Scotland have the required characteristics [Downes
 902 *et al.*, 2007; Hole *et al.*, 2015].

903 The close proximity of the low- and high-Ti, high-FeO(T) basalts suggests that their different sources
 904 are physically close together. It is clear that these sources have been tapped since the opening of the
 905 NE Atlantic as they are also seen in the same successions in the Skaergaard intrusion in east
 906 Greenland [Larsen *et al.*, 1999]. The high-TiO₂ and FeO(T) lavas found in Iceland are typical of lavas
 907 derived from sub-continental lithospheric mantle and pyroxenite. No more than 20 - 30% of
 908 pyroxenite in a hybrid source is required to explain the observations.

909 *Isotope ratios:* Elevated $^{87}\text{Sr}/^{86}\text{Sr}$ and Pb isotope ratios are found in basalts from east and southeast
 910 Iceland [Prestvik *et al.*, 2001]. This has been interpreted as requiring a component of continental
 911 material in the source beneath Iceland. That component could come from crust or detached SCLM
 912 buried beneath surface lavas [Foulger *et al.*, 2003].

913 *Zircons:* Archaean and Jurassic zircons with Lewisian (1.8 Ga) and Mesozoic (~126 - 242 Ma)
 914 inheritance ages have been reported from lavas in NE Iceland. This has been interpreted as indicating
 915 ancient continental lithosphere beneath Iceland [Paquette *et al.*, 2006; Schaltegger *et al.*, 2002]. A
 916 continental composition for Icelandic-type lower crust can explain these results.

917 *Water:* Water in basalt glass from the mid-Atlantic Ridge indicates elevated contents in the source
 918 from ~61°N across Iceland [Nichols *et al.*, 2002]. The water contents are estimated to be ~165 ppm at
 919 the southern end of the Reykjanes Ridge, rising to 620 - 920 ppm beneath Iceland. Such a component,
 920 and other volatiles such as CO_2 [Hole & Natland, this volume] decrease the solidus of a source rock
 921 and increase the volume of melt produced for a given T_P (Section 6.2).

922 6.2 Temperature of the melt source

923 The temperature of the melt source of Icelandic rocks is too low to be able to account for a 30-40-km-
 924 thick basaltic crust using any reasonable lithology [Hole & Natland, this volume]. It is therefore an
 925 inevitable conclusion that much of the lower crust beneath the GIFR must arise from a process other
 926 than high-temperature partial melting of mantle peridotite.

927 Geochemical work aimed at determining the potential temperature of NE Atlantic source rocks has
 928 used basalts from Iceland and high-MgO picrites from the Davis Strait [Clarke & Beutel, 2019; Hole
 929 & Natland, this volume]. The T_P for the source of MORB is generally used as the standard against
 930 which other calculated mantle temperatures are compared. The currently accepted value of this is
 931 $1350 \pm 40^\circ\text{C}$ (Table 3) [Hole & Natland, this volume].

932 A large range of temperatures, $T_P = 1400 - 1583^\circ\text{C}$, has been suggested for the mantle beneath Iceland
 933 [Hole & Millett, 2016; Putirka, 2008]. The breadth of this range in itself indicates how difficult it is to
 934 derive a repeatable, reliable T_P using geochemistry and petrology. Difficulties include the lack of
 935 surface samples that correspond to an original mantle melt—crystalline rocks essentially always
 936 contain xenocrysts, and no picritic glass has been found in the NE Atlantic Realm [Presnall &
 937 Gudfinnsson, 2007]. The unknown source composition also introduces uncertainty. The geochemistry
 938 of Icelandic lavas requires there to be a component of recycled surface materials in the source and
 939 variable volatile contents including water [Nichols *et al.*, 2002]. Ignoring any of these unknowns
 940 causes estimates of T_P to be erroneously high.

941 Crystallization temperatures estimated from olivine-spinel melt equilibration, the so-called
 942 “aluminum-in-olivine” method, are independent of whole-rock composition. The temperatures
 943 yielded by this method are $T_P \sim 1375^\circ\text{C}$ and $\sim 100^\circ\text{C}$ higher for the Davis Strait picrites (Table 3) [Hole
 944 & Natland, this volume]. A summary of global maximum petrological estimates of T_P and ranges of
 945 olivine-spinel equilibrium crystallization temperatures for magnesian olivine are shown in Figure 22.

946 Petrological estimates of the potential temperature T_P of the source of basalts in the NE Atlantic
 947 Realm suggest upper-bound T_P of $\sim 1450^\circ\text{C}$ for Iceland and $\sim 1500^\circ\text{C}$ for the picrites of Baffin Island,
 948 Disko Island and west Greenland [Hole & Natland, this volume]. There may thus have been a short-
 949 lived, localized burst of magma from a relatively hot source lasting $\sim 2 - 3$ Myr when propagation of
 950 the Labrador Sea spreading center was blocked at the Nagssugtoqidian orogen, but there is no
 951 compelling evidence for a T_P anomaly $> \sim 100^\circ\text{C}$ before or after this anywhere in the NE Atlantic
 952 Realm.

953 The melt volume produced at Iceland has also been used as a constraint in models for T_p . That work
 954 has assumed that the full thickness of the 30-40-km-thick seismic crustal layer is melt produced by
 955 steady state fractional melting of a peridotite mantle source. Production of just 20 km of igneous crust
 956 would require a T_p of ~1450 - 1550°C assuming a damp or dry peridotite source [Sarafian *et al.*,
 957 2017]. No credible lithology or temperature can explain the crustal thickness of ~40 km that has been
 958 measured for central Iceland [Darbyshire *et al.*, 1998a; Foulger *et al.*, 2003].

959 Crustal thickness beneath the active volcanic zones of Iceland varies from ~40 km (beneath
 960 Vatnajökull) to ~15 - 20 km (beneath the Reykjanes Peninsula extensional transform zone) [Foulger
 961 *et al.*, 2003]. If the full thickness of crust everywhere is formed from melting in the mantle,
 962 unrealistically large lateral variations in temperature of the source of ~150°C over distances of ~125
 963 km would be required [Hole & Natland, this volume].

964 6.3 $^3\text{He}/^4\text{He}$

965 Elevated $^3\text{He}/^4\text{He}$ values are commonly assumed to indicate a core-mantle boundary provenance for
 966 the melt source. This association was originally suggested when it was found that some lavas from
 967 Hawaii contain high- $^3\text{He}/^4\text{He}$ [Craig & Lupton, 1976]. It was reasoned that, over the lifetime of Earth,
 968 the $^3\text{He}/^4\text{He}$ of the mantle has progressively decreased from an original value of ~200 times the
 969 present-day atmospheric ratio (Ra) to $\sim 8 \pm 2$ Ra—the value most commonly observed in MORB. It
 970 was subsequently assumed that a lava with $^3\text{He}/^4\text{He}$ much larger than 8 Ra must have arisen from a
 971 primordial source, isolated for Earth's 4.6 Ga lifetime, deep in the mantle near the core-mantle
 972 boundary.

973 This theory has long been contested and it has been counter-proposed that the helium instead resided
 974 for a long time in depleted, unradiogenic materials such as olivine in the sub-continental lithospheric
 975 mantle [Anderson, 2000a; b; 2001; Anderson *et al.*, 2006; Foulger & Pearson, 2001; Natland, 2003;
 976 Parman *et al.*, 2005]. That theory would fit the high- $^3\text{He}/^4\text{He}$ values reported from Iceland and the
 977 Davis Strait [Starkey *et al.*, 2009; Stuart *et al.*, 2003] if the deeper parts of the crust beneath these
 978 regions contain ancient material, as we propose in this paper.

979 7 Discussion

980 7.1 The Greenland-Iceland-Faroe Ridge

981 The model presented here proposes that in general Icelandic-type upper crust is mafic in nature,
 982 equivalent to Layers 2 - 3 of oceanic crust, whilst Icelandic-type lower crust is magma-dilated
 983 continental crust. The pre-existing SCLM mostly delaminated during the stretching process (Section
 984 5) (Figure 18). The melt layer thus comprises Icelandic-type upper crust plus the melt that intruded
 985 into the continental crust below as plutons, dykes and sills. The location of Iceland with respect to the
 986 east Greenland and Faroe Volcanic margins fits the model of Geoffroy *et al.* [2015; submitted] of a
 987 dislocated C-block (Figure 5).

988 This new model contributes to the > 40-year controversy regarding whether the crust beneath Iceland
 989 is thick or thin. A “thin crust” model, generally assumed in the 1970s and 1980s, attributed Icelandic-
 990 type upper crust to the melt layer—the subaerial equivalent of oceanic crust—and the layer currently
 991 termed “Icelandic-type lower crust” to hot, partially molten mantle [Björnsson *et al.*, 2005]. From the
 992 1990s, long seismic explosion profiles using modern digital recording were shot and deep reflecting
 993 horizons were discovered. A “thick crust” model was then introduced that interpreted the layer
 994 previously thought to be hot, partially molten mantle as Icelandic-type lower crust, the equivalent of
 995 oceanic layer 3, and part of the melt layer.

996 Our findings support the thin-crust model with the caveat that Icelandic-type lower crust is indeed
 997 crust, and not hot mantle as previously proposed, but it is magma-inflated continental crust. This

998 model agrees with long-sideline magnetotelluric work in Iceland which detects a high-conductivity
 999 layer at ~10 - 20 km depth. This layer was proposed to mark the base of the crust [Beblo & Bjornsson,
 1000 1978; 1980; Beblo *et al.*, 1983; Eysteinsson & Hermance, 1985; Hermance & Grillot, 1974]. High-
 1001 conductivity layers are common in continental mid- and lower crust [*e.g.*, Muñoz *et al.*, 2008].
 1002 Explosion seismology and receiver functions find the thickness of Icelandic-type upper crust to be ~3
 1003 - 10 km (Figure 9; Figure 10) [Darbyshire *et al.*, 1998b; Foulger *et al.*, 2003] which is comparable
 1004 with the crustal thicknesses beneath the Reykjanes Ridge and the Kolbeinsey Ridge if additional
 1005 magma dilating the Icelandic-type lower crust is taken into consideration. This is nevertheless up to
 1006 ~40% thicker than the global average of 6 - 7 km. Mantle fusibility enhanced by pyroxenite and water
 1007 (Section 6), a moderate elevation in temperature (Section 6.2), and bursts of volcanism accompanying
 1008 frequent rift jumps (Section 4) can account for the enhanced melt volumes.

1009 The plate boundary traversing the GIFR cannot be likened to a conventional spreading ridge with
 1010 segments connected by linear transform faults as is commonly depicted in simplified illustrations.
 1011 Historically, motion in the GIFR region was postulated to have been taken up on a classic ~150-km-
 1012 long sinistral transform fault named the Faroe Transform Fault or the Iceland Faroe Fracture Zone
 1013 [Bott, 1985; Voppel *et al.*, 1979] and this idea was reiterated in subsequent work [*e.g.*, Blischke *et al.*,
 1014 2017; Guarnieri, 2015]. Locations proposed for this feature include the north edge of the Iceland
 1015 shelf, central Iceland, and the South Iceland Seismic Zone [Bott, 1974].

1016 There is, however, no observational evidence for such a structure [Gernigon *et al.*, 2015; Schiffer *et al.*
 1017 *et al.*, 2018] and it does not, even to a first order, fit the observations on the ground. Only a GIFR that
 1018 deforms as a broad zone of distributed extension and shear can account for the reality of the geology
 1019 of Iceland and adjacent regions [Schiffer *et al.*, 2018].

1020 Our model may provide a long-awaited explanation for why the JMMC broke off east Greenland.
 1021 Westerly migration of axes of extension on the GIFR may have changed the stress field in the
 1022 diffusely extending continental area to the north and encouraged extension there to coalesce on the
 1023 single most westerly zone which thereafter developed into the Kolbeinsey Ridge.

1024 7.2 Crustal flow

1025 Ductile crustal flow has been incorporated into earlier numerical models of continental breakup. A
 1026 ductile, low-viscosity layer that decouples the upper lithosphere from the lower was incorporated in
 1027 models of extending continental lithosphere by Huisman and Beaumont [2011; 2014]. Such a layer
 1028 enables ultrawide regions of thinned, unruptured continental crust to develop along with distal
 1029 extensional (sag) basins. Crustal thicknesses are maintained by widespread lateral flow of mid- and
 1030 lower-crustal material from beneath surrounding regions. Lower crust may well up, further delaying
 1031 full crustal breakup.

1032 In our model, subsidence resulting from progressive thinning or delamination of the mantle
 1033 lithosphere is mitigated by hot asthenosphere rising to the base of the crust. This abruptly raises
 1034 temperatures, increasing heat flow and further encourages ductile flow. Low extension rates, such as
 1035 have characterized the NE Atlantic, tend to prolong the time to breakup and encourage diffuse
 1036 extension because ductile flow and cooling can continue for longer. The crust may stretch unruptured
 1037 for tens of millions of years and widen by 100s of kilometers with axes of extension migrating
 1038 diachronously and laterally across the extending zone. Only after eventual rupture of the continental
 1039 lithosphere can sea-floor spreading begin. Until that occurs, geochemical signatures of continental
 1040 crust and mantle lithosphere are expected in overlying magmas that have risen through the continental
 1041 material.

1042 Depth-dependent stretching, in particular involving the lower-crustal ductile flow that we model in
 1043 Section 5, is both predicted by theory [McKenzie & Jackson, 2002] and required by observations
 1044 from many regions. These include amagmatic margins, the Basin Range province, western USA

1045 [Gans, 1987] and deformation at collision zones, *e.g.*, the Himalaya and Zagros mountain chains [*e.g.*,
 1046 Kuszniir & Karner, 2007; Royden, 1996; Shen *et al.*, 2001]. Lower-crustal flow is actually observed
 1047 where such crust is exhumed to the surface, *e.g.*, at Ivrea in the Italian Alps, where lower-crustal
 1048 granulite intruded by mafic plutons is exposed [*e.g.*, Quick *et al.*, 1995; Rutter *et al.*, 1993].

1049 7.3 *Magmatism*

1050 7.3.1 The concept of the North Atlantic Igneous Province

1051 The issues laid out in this paper bring into question the concept that the magmas popularly grouped
 1052 into the North Atlantic Igneous Province (NAIP) can be viewed as a single magmatic entity [Peace *et al.*
 1053 *et al.*, this volume]. The NAIP is generally considered to include the volcanic rocks in the region of the
 1054 Davis Strait, the volcanic margins of east Greenland and Scandinavia, and the magmatism of the
 1055 GIFR. These magmas are, however, only a subset of those in the region and many others are not
 1056 typically included [Peace *et al.*, this volume]. These include melt embedded in the “amagmatic”
 1057 margins of SW Greenland and Labrador, current volcanism at Jan Mayen, the Vestbakken Volcanic
 1058 Province ~300 km south of Svalbard, conjugates in NE Greenland [Á Horni *et al.*, 2016], magmatism
 1059 at the west end of the CGFZ [Keen *et al.*, 2014] and basaltic sills offshore Newfoundland detected in
 1060 ODP site 210-1276 that are thought to extend throughout an area of ~20,000 km² [Deemer *et al.*,
 1061 2010]. It is illogical to exclude these, especially since the Cretaceous(?) Anton Dohrn and Rockall
 1062 seamounts are included in the NAIP [Jones *et al.*, 1994].

1063 The grouping of a select subset of magmas in the NE Atlantic Realm into a single province is
 1064 predicated on and reinforces, the concept that they all arise from a single, generic source. A model of
 1065 such simplicity that fits all observations has been elusive for over half a century. The obvious
 1066 solution, and one that can readily account for the observations, is a model whereby each magmatic
 1067 event occurs in response to local lithospheric tectonics and melts are locally sourced.

1068 The same reasoning may well apply to other volcanic provinces, *e.g.*, the South Atlantic Volcanic
 1069 Province. Generally included in this are the Paraná and Etendeka flood basalts, the volcanic rocks of
 1070 the Rio Grande Rise and the Walvis Ridge, the currently active Tristan da Cunha archipelago and
 1071 even kimberlites and carbonatites in Angola and the Democratic Republic of the Congo [see Foulger,
 1072 2018 for a review]. These volcanic elements contrast with one another in the extreme and each most
 1073 likely erupted in reaction to local tectonic responses to global events and processes, with magmas
 1074 locally sourced.

1075 7.3.2 Magma volume

1076 Estimates for the total volume of the magma generally lumped together as the NAIP are 2 - 10 x 10⁶
 1077 km³ with a value of ~6.6 x 10⁶ km³ for the north Atlantic volcanic margins [Eldholm & Grue, 1994a].
 1078 Assuming these margins formed in ~3 Myr, Eldholm and Grue [1994a] calculate a magmatic rate of
 1079 2.2 km³/a and suggest the NAIP is one of the most voluminous igneous provinces in the world. That
 1080 calculation assumes that the HVLC beneath the *Inner* SDRs is all igneous and formed
 1081 contemporaneously with the volcanic margins. If this is not the case, the volume and magmatic rate
 1082 for the north Atlantic volcanic margins must be downward-revised by up to 30%, *i.e.* to ~4.4 x 10⁶
 1083 km³ for volume and 1.5 km³/a for magmatic rate. Eldholm and Grue [1994a] furthermore estimate a
 1084 magmatic rate of ~ 0.2 km³/a for Iceland. If the igneous crust on the GIFR is only 10 - 15 km thick,
 1085 this rate must be downward-revised to 0.12 - 0.08 km³/a. The magmatic rate per rift kilometer would
 1086 then be 2 - 3 x 10⁻⁴ km³/a compared with ~4.8 x 10⁻⁴ km³/a per rift kilometer for the global plate
 1087 boundary.

1088
 1089 These changes reconcile geological estimates with those derived from numerical modeling.
 1090 Magmatism at the NE Atlantic rifted margins has been simulated using models of decompression
 1091 melting in a convectively destabilized thermal boundary layer coupled with upper-mantle (“small-

1092 scale”) convection [Geoffroy *et al.*, 2007; Mutter & Zehnder, 1988; Simon *et al.*, 2009]. These
 1093 models explore whether the volumes and volume rates can be accounted for simply by breakup of the
 1094 100-200-km-thick lithosphere without additional *ad hoc* processes. Current numerical models slightly
 1095 under-predict traditional geological estimates but could be reconciled with estimates lowered to take
 1096 into account a wholly or partially continental affinity of HVLC.

1097 More accurate estimates of volume could also explain the extreme variations in magmatic thickness
 1098 over short distances required by assumptions of HVLC igneous affinity. For example, the radical
 1099 contrast between the unusually thin (4 - 7 km) oceanic crust beneath the Aegir Ridge [Greenhalgh &
 1100 Kuszniir, 2007] and a ~30 km igneous thickness beneath the adjacent GIFR defies reasonable
 1101 explanation but the problem vanishes if the latter assumption is dropped.

1102 7.3.3 The chevron ridges

1103 Lithosphere- and asthenosphere-related mechanisms compete to explain the chevron ridges that flank
 1104 the Reykjanes Ridge [Hey *et al.*, 2008; Jones *et al.*, 2002]. Martinez and Hey [this volume] suggest
 1105 that the required oscillatory changes in magmatic production result from axially propagating mantle
 1106 upwelling instabilities that travel with ridge-propagator tips along the Reykjanes Ridge. These
 1107 originate in Iceland and the gradient in mantle properties along the Reykjanes Ridge results in the
 1108 convective instabilities migrating systematically south along the Ridge. Upwelling is purely passive
 1109 and the propagators behave in a wave-like manner without the flow of actual mantle material along
 1110 the Ridge. In this model, the transition from linear to ridge/transform staircase plate boundary
 1111 geometry at ~37 - 38 Ma failed to eliminate the structure of the deeper asthenospheric melting zone
 1112 and the Reykjanes Ridge is restructuring itself to realign over that zone.

1113 Several of the propagators onset at the GIFR in concert with tectonic reorganizations there (Table 1)
 1114 [Benediktsdóttir *et al.*, 2012] inviting consideration of lithospheric triggers. The Reykjanes Ridge as a
 1115 whole is oblique to the direction of plate motion but its axis comprises an array of right-stepping *en*
 1116 *echelon* spreading segments, each of which strikes perpendicular to the direction of motion. Such
 1117 fabric resembles a left-lateral transtension zone.

1118 The diachronous chevron crustal fabric began to form at ~37 - 38 Ma when the Reykjanes Ridge
 1119 changed from a linear to a ridge-transform configuration with a ~30° counter-clockwise rotation in the
 1120 direction of plate motion (Section 2.2.2) [Gaina *et al.*, 2017]. From 25-15 Ma slow, counter-clockwise
 1121 rotation of the extension direction continued and from 15 Ma - present it rotated back [Gaina *et al.*,
 1122 2017]. Slow counter-clockwise migration of the spreading direction would gradually hinder strike-slip
 1123 motion on the transform segments and encourage evolution toward extension with a minor left-lateral
 1124 shear overprint. Very slow changes in the direction of extension might be insufficient to trigger a
 1125 sudden and major reorganization but enough to bring about the slow plate-boundary evolution
 1126 observed.

1127 Regardless of whether a lithosphere- or asthenosphere-related mechanism is responsible for the
 1128 chevron ridges, it is clear that shallow processes control them as their southerly propagation was
 1129 temporarily blocked by several previously existing transform faults north of the present reorganization
 1130 tip near the Bight transform fault. Furthermore, if their inception is related to tectonic reorganizations
 1131 on the GIFR, then conversely the time at which the propagators set off from the GIFR could indicate
 1132 the times of first-order tectonic reorganizations on the GIFR.

1133 The transform-eliminating rift propagators of the Reykjanes Ridge are unique in their degree of
 1134 development but not entirely unknown elsewhere. Examples outside the NE Atlantic include a
 1135 southward propagator eliminating a transform formerly at 21°40'N on the mid-Atlantic Ridge
 1136 [Dannowski *et al.*, 2011] and propagators on the faster-spreading (~100 km/Myr) NE Pacific plate
 1137 boundary that eliminated the Surveyor, Sila, Sedna and Pau transforms [Atwater & Severinghaus,
 1138 1989; Hey & Wilson, 1982; Shih & Molnar, 1975]. Propagating small-scale convective instabilities

1139 have also been postulated to form volcanic ridges and seamount chains that flank parts of the East
1140 Pacific Rise in a direction parallel to plate motion [e.g, Forsyth *et al.*, 2006].

1141 7.3.4 The North Atlantic geoid high

1142 The GIFR sits at the apex of a ~3000-km-long bathymetric and geoid high (up to ~4000 m and 80 m
1143 respectively) that stretches from the Azores to the Jan Mayen Fracture Zone [Carminati & Doglioni,
1144 2010; King, 2005; Marquart, 1991]. Without this high the Thulean land bridge and Iceland would not
1145 have been subaerial. Globally, the only other comparable geoid high extends through Indonesia and
1146 Melanesia and to the Tonga Trench. Major geoid highs with lower amplitudes or smaller spatial
1147 extents are associated with the SW Indian Ocean and the Andean mountain chain.

1148 The geoid highs associated with Indonesia, Melanesia and Tonga, and the Andean mountain chain are
1149 a consequence of accumulations of dense subducted slabs. The geoid high of the north Atlantic
1150 corresponds closely to the pre-breakup Caledonian orogen plus the south European/North African
1151 Hercynian orogen (Figure 23). A possible explanation for part of the geoid anomaly is thus residual,
1152 dense, subducted Caledonian and Hercynian slabs along with continental lower crust and mantle
1153 lithosphere distributed in the shallow mantle. Henry Dick and colleagues have long argued that the
1154 petrology and geochemistry of magmas on the SW Indian ridge require SCLM in the melt source
1155 [Cheng *et al.*, 2016; Dick, 2015; Gao *et al.*, 2016; Zhou & Dick, 2013]. That ridge is the current locus
1156 of extension between Africa and Antarctica which separated as part of Pangaea breakup beginning in
1157 the Jurassic. By analogy with the NE Atlantic, continental material might also remain in the mantle
1158 beneath the ocean there and the SW Indian geoid high might thus be explained in a similar way to that
1159 of the north Atlantic.

1160 7.3.5 Regions analogous to the GIFR

1161 There are clear parallels between the GIFR and the Davis Strait. The structure and tectonic
1162 development of the latter show similar characteristics to the GIFR but to a less extreme degree (Figure
1163 24). The Davis Strait is colinear with the GIFR and both function as transtensional shear zones. Its
1164 primary feature is the long Ungava Fault Complex [Peace *et al.*, 2017]. This is underlain by ~8 km of
1165 oceanic crust beneath which is ~8 km of HVLC with V_p up to 7.4 - 7.5 km/s [Chalmers & Pulvertaft,
1166 2001; Funck *et al.*, 2006; Funck *et al.*, 2007; Srivastava *et al.*, 1982] and density of 2850 - 3050 kg/m³
1167 [Suckro *et al.*, 2013]. These values are similar to those of Icelandic-type lower crust.

1168 Like the GIFR, the bathymetric high that contains the 550-km-long Davis Strait is elongated in the
1169 direction approximately perpendicular to plate motion. It has water depths of < 700 m, contrasting
1170 with the adjacent > 2000-m-deep Labrador Sea and Baffin Bay. At the Davis Strait north-propagating
1171 rifting stalled at the confluence of the Nagssugtoqidian and Rinkian orogens and continued displaced
1172 by several hundred kilometers in a right-stepping sense. In the case of the GIFR, both north- and
1173 south-propagating oceanic rifting stalled at the confluence of the Nagssugtoqidian and Caledonian
1174 orogens.

1175 The Jan Mayen Fracture Zone formed where a major, pre-existing transverse structure formed a
1176 barrier to the south-propagating Mohns Ridge. It was also an episodic transtensional structure, has a
1177 history of migration of the locus of deformation, bathymetric highs and unusual volcanism, *e.g.*, on
1178 the island of Jan Mayen and in the submarine Traill Ø and Vøring Spur igneous complexes [Gernigon
1179 *et al.*, 2009; Kandilarov *et al.*, 2015]. Continental crust is possibly trapped between parallel segments
1180 of the Zone.

1181 7.3.6 Regions analogous to the NE Atlantic Realm

1182 The history, structure, tectonics and petrology of the NE Atlantic Realm are unusually complex but it
1183 represents an extreme example and not a unique case. Other regions that show similar features suggest

1184 that the style of breakup it exemplifies is generic. The NE Atlantic Realm may owe its extremity to
 1185 the facts that the NE Atlantic was formed by two opposing propagators that stalled at a barrier, an
 1186 unusually large microcontinent was captured, and the spreading rate was and is exceptionally slow.

1187 The South Atlantic Igneous Province also includes regions of shallow sea-floor, anomalously thick
 1188 crust, anomalous volcanism and continental crust distributed in the ocean. It has a history of stalled
 1189 spreading-ridge propagation, coincidence with a major pre-existing transverse structure and both
 1190 shear and extensional deformation in a zone several hundred kilometers broad in the direction
 1191 perpendicular to plate motion [Foulger, 2018; Kuszniir & al., 2018]. Graça *et al.* [2019] recently
 1192 presented evidence that the Rio Grande Rise, which contains continental material [Santos Ventura *et*
 1193 *al.*, 2019], and parts of the Walvis Ridge were once joined, but split apart by at least four ridge jumps.
 1194 Such a process is very similar to that which we propose for the GIFR.

1195 The Lomonosov Ridge in the Arctic ocean can be viewed as an incipient microcontinent. West of
 1196 India, the Laxmi basin comprises a pair of aborted conjugate volcanic passive margins with Outer
 1197 SDRs that appear to be underlain by HVLC and flank an intra-oceanic microcontinent—a C-block
 1198 [Geoffroy *et al.*, submitted; Guan *et al.*, 2019; Nemčok & Rybár, 2017]. The Seychelles region in the
 1199 West Indian Ocean, the Galapagos Islands region in the east Pacific [Foulger, 2010, p 100-101] and
 1200 the Shatsky Rise [Korenaga & Sager, 2012; Sallares & Charvis, 2003] all display analogous features.
 1201 Regions currently in the process of breaking up in a similar mode include the Afar area [Acton *et al.*,
 1202 1991], the Imperial and Mexicali Valleys and Baja California (California and Mexico). The
 1203 abundance of continental crustal fragments in the oceans is becoming increasingly clear, with much
 1204 originating at locations where continental breakup was complicated by lithospheric heterogeneities.

1205 Despite the very different structure and context, tectonics comparable to those observed on the GIFR
 1206 and in Iceland are also observed on the East Pacific Rise (EPR). There, “dueling” overlapping
 1207 propagating ridge pairs with intermediate bookshelf shearing build ridge-perpendicular and ridge-
 1208 oblique zones of crustal complexity (Figure 25) [Perram *et al.*, 1993]. In oceanic settings overlapping
 1209 ridge tips tend to form where lithosphere is weak and to migrate along-strike. Overlapping spreading
 1210 centers are kinematically unstable and the tips inevitably fail episodically and are replaced by new
 1211 ones. An unusual facet of the development of the GIFR that is not reported from the East Pacific Rise
 1212 is the switching of the sense of overlap when the Aegir Ridge was replaced by the Kolbeinsey Ridge.

1213 Comparable styles of deformation are also observed in the Japan-, Manus-, Lau- and Mariana Trench
 1214 back-arc basins [Kurashimo *et al.*, 1996; Martinez *et al.*, 2018; Taylor *et al.*, 1994]. Beneath back-arc
 1215 basins the hydrous mantle environment above the dewatering slab does not become dehydrated and
 1216 the attendant increase in viscosity tends to localize upwelling melt. As a result, extension does not
 1217 become focused in a single rift zone but remains distributed between multiple, parallel rifts. Magnetic
 1218 anomalies are disorganized and water also reduces the solidus, increasing melt production [Dunn &
 1219 Martinez, 2011; Martinez *et al.*, 2018].

1220 On land, similar petrologies, including high-TiO₂ basalts, association with abundant rhyolite, and
 1221 likely provenance of the source in subcontinental material are observed in flood basalts that erupted
 1222 through continental lithosphere. These include the Central Atlantic Magmatic Province [Peace *et al.*,
 1223 this volume], the Deccan traps and the Columbia River Basalts.

1224 **8 Conclusions**

1225 Our main conclusions may be summarized:

- 1226 1. Disintegration of the Laurasian collage of cratons and orogens to form the Labrador Sea, Baffin
 1227 Bay and the NE Atlantic Ocean lasted several tens of millions of years and occurred piecewise
 1228 and diachronously via rift propagation.

- 1229 2. The GIFR formed where the south-propagating Aegir Ridge and the north-propagating,
 1230 Reykjanes Ridge stalled at the junction of the Nagssugtoqidian and Caledonian orogens. The
 1231 intervening ~300-km wide (northerly) and ~150-km long (easterly) continental block, the Iceland
 1232 Microcontinent, along with flanking areas, extended by distributed, magma-assisted continental
 1233 extension via multiple parallel migrating rifts with diffuse shear zones between them. The
 1234 continental crust was capped by surface lavas. It stretched to form the 1000-km long Thulean
 1235 continental land bridge which was not overrun by oceanic waters until ~10 -15 Ma.
- 1236 3. Magma-assisted continental extension was enabled by ductile flow of low-viscosity mid- and
 1237 lower crust.
- 1238 4. Icelandic-type crust comprises the 3 - 10 km thick upper crust, equivalent to oceanic layers 2 - 3,
 1239 underlain by lower crust up to ~ 30 km thick comprising magma-inflated continental crust.
- 1240 5. The melt layer that caps the GIFR comprises the Icelandic-type upper crust plus magma injected
 1241 into the Icelandic-type lower crust, and has a total thickness of ~10 - 15 km.
- 1242 6. The petrology and geochemistry of Icelandic lavas is consistent with inclusion of a component
 1243 from underlying continental crust.
- 1244 7. A largely continental Icelandic-type lower crust is consistent with the fact that no reasonable
 1245 models of temperature or mantle petrology can generate the ~40 km of melt necessary to explain
 1246 its entire thickness as wholly oceanic.
- 1247 8. The chevron ridges that flank the Reykjanes Ridge form in association with small-offset
 1248 propagators initiated by tectonic reorganizations on the unstable GIFR.
- 1249 9. The GIFR tectonically decouples the oceanic regions to the north and south.
- 1250 10. The continuity of continental crust beneath the GIFR means that, at this latitude, Laurasia still has
 1251 not yet entirely broken up. An implication of this is that the GIFR could be considered to be a
 1252 new kind of plate boundary.
- 1253 11. A model whereby continental breakup is characterized by diachronous rifting, strong influence
 1254 from pre-existing structures, distributed continental material in the new oceans, and anomalous
 1255 volcanism matches many other oceanic regions.

1256

1257 *Acknowledgments*

1258 Erin K. Beutel and D. Barrie Clarke made valuable contributions to the discussions that led to this
 1259 manuscript. CS's postdoctoral fellowship at Durham University was financed by the Carlsberg
 1260 Foundation. F. Martinez and R. Hey are supported by US NSF grants OCE-1154071 and OCE-
 1261 1756760. A. Peace's postdoctoral fellowship at Memorial University of Newfoundland was funded by
 1262 the Hibernia project geophysics support fund. M. Stoker acknowledges the award of Visiting
 1263 Research Fellow at the Australian School of Petroleum.

1264

1265 Table 1: Chronology of major tectonic events in the NE Atlantic. Timescale after Gradstein *et al.*
 1266 [2012]. Chevron ridge # after Jones *et al.* [2002].
 1267

Date (Ma)	Chevron ridge #	Magnetic chron	Event
58-57		C26	Beginning of opening of the Labrador Sea.
56-52		C24-22	First magnetic anomaly on the proto-Reykjanes Ridge.
54		C24r	Beginning of opening of the North Atlantic Ocean on the Aegir Ridge and west of the Lofoten margin.
54-ca 46		C24-21	Rift to drift transition, Faroe-Shetland and Hatton margins.
54.2-50			Spreading propagated from the Greenland Fracture Zone south to the Jan Mayen Fracture Zone.
52		C23	Aegir Ridge reaches its maximum southerly extent.
50-48		C21	~30-40° clockwise rotation of direction of plate motion .
48		C22-21	Onset of fan-shaped spreading about the Aegir Ridge. Pulse of extension in the southern JMMC. No major change south of the GIFR.
40		C18	Counter-clockwise rotation of direction of plate motion.
38-37	7	C17	Reykjanes Ridge becomes stair-step. First chevron ridge begins to form.
36		C13	Cessation of spreading in the Labrador Sea.
33-29		C12-10	Counter-clockwise rotation of direction of plate motion.
31-28	6	C12-10	Extinction of the ultra-slow Aegir Ridge. Second chevron ridge begins to form about the Reykjanes Ridge
24		C6/7	First unambiguous magnetic anomaly about the Kolbeinsey Ridge.
15-10		C5A/C5	Breaching of the Thulean land bridge.
14	5		Rift jump in Iceland from North West Syncline to Snæfellsnes Zone and Húnaflói Volcanic Zone, propagator “Loki” starts to travel south down Reykjanes Ridge forming third chevron ridge.
9	4		Propagator “Fenrir” starts to travel south down Reykjanes Ridge forming fourth chevron ridge.
7	3		Extinction of Snæfellsnes Zone, propagator “Sleipnir” starts to travel south down Reykjanes Ridge forming fifth chevron ridge.
5	2		Propagator “Hel” starts to travel south down Reykjanes Ridge forming sixth chevron ridge.
2	1		EVZ in Iceland forms, propagator “Frigg” starts to travel south down Reykjanes Ridge forming seventh chevron ridge.

1268

1269 Table 2: Rift zones indicated by geological observations on land in Iceland.

1270

Name	Acronym	Tectonic status
North West Syncline	NWS	Extinct
Austurbrún Syncline	AS	Extinct
East Iceland Zone	EIZ	Extinct
Snæfellsnes Zone	SZ	Oblique, non extensional
Húnaflói Volcanic Zone	HVZ	Extinct
Mödrudalsfjallgardar Zone	MZ	Extinct
Reykjanes Peninsula Zone	RPZ	Oblique, extensional
Western Volcanic Zone	WVZ	Active, waning
Hofsjökull Zone	HZ	Active, very short
Northern Volcanic Zone	NVZ	Active
Öræfajökull-Snæfell Zone	ÖVZ	Active, non extensional
Eastern Volcanic Zone	EVZ	Active, propagating

1271

1272

1273 Table 3: Potential temperatures required to produce 20 km of melt for various source compositions
1274 [from Hole & Natland, this volume].

1275

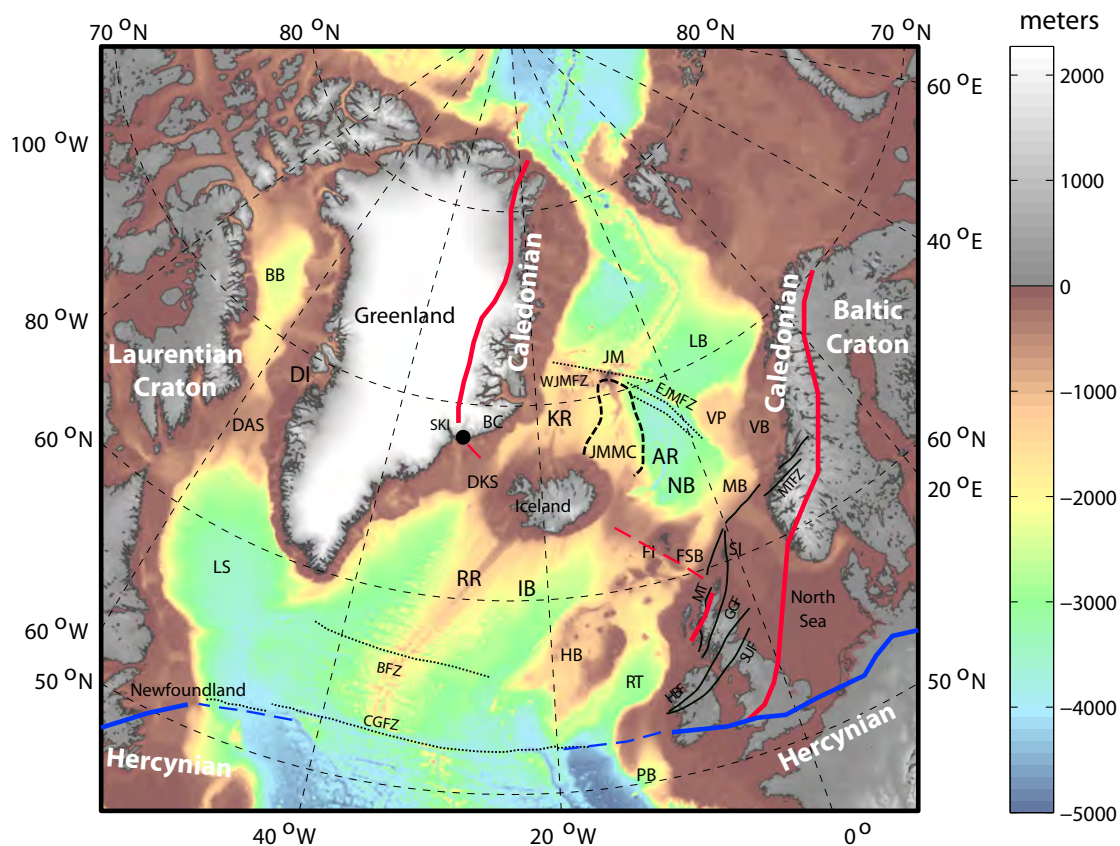
Source composition	T_P °C
dry peridotite	1550
dry peridotite + 10% pyroxenite	1540
dry peridotite + 40% pyroxenite	1470
damp peridotite + pyroxenite	1450
damp peridotite	1450
pyroxenite	1325-1450
Baffin Island picrites (T_{Ol-sp})	1500

1276

1277

1278

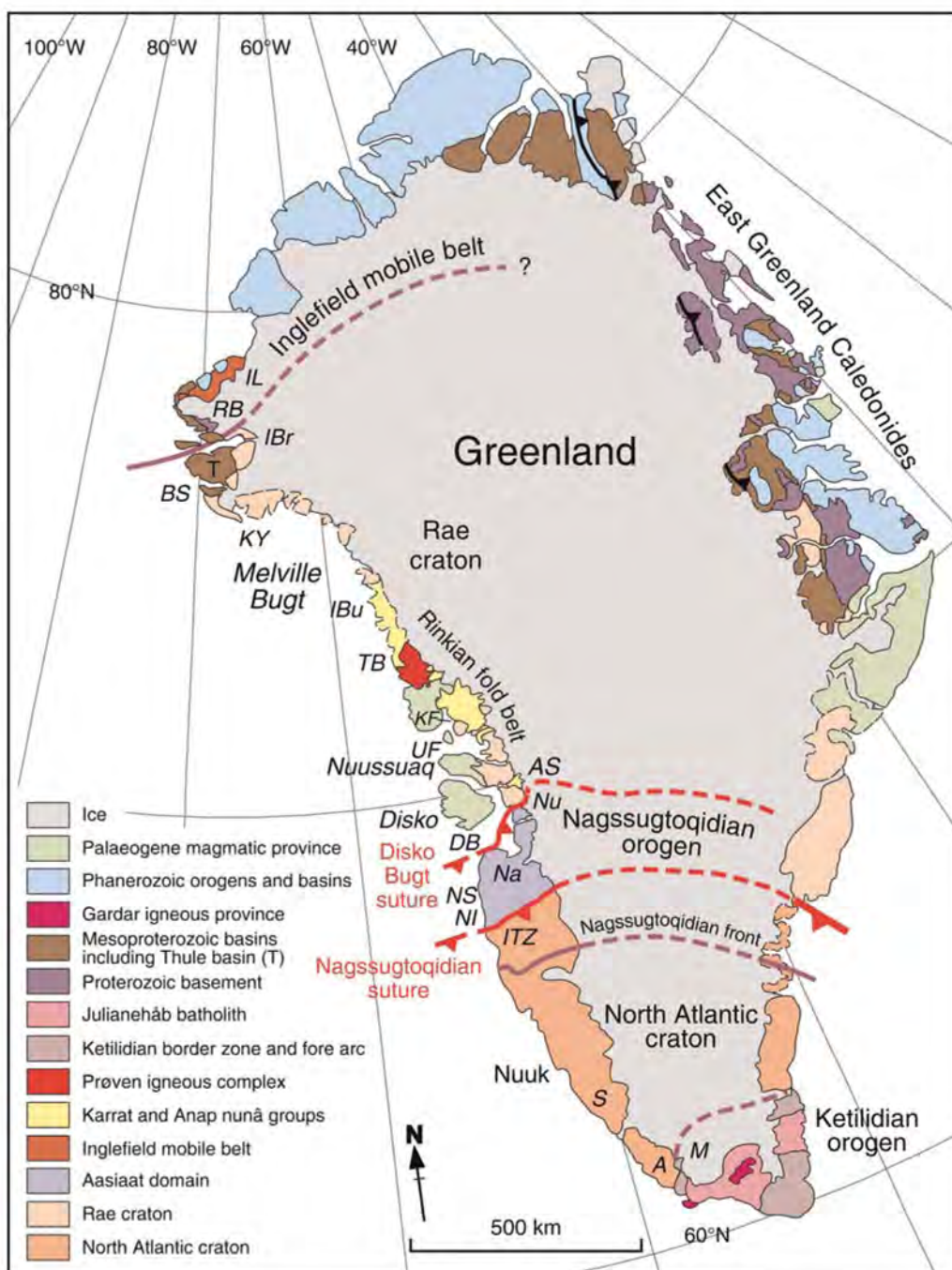
1279
1280



1281
1282
1283
1284
1285
1286
1287
1288
1289
1290
1291
1292
1293
1294
1295
1296

Figure 1: Regional map of the North East Atlantic Realm showing features and places mentioned in the text. Bathymetry is shown in color and topography in land areas in gray. BB: Baffin Bay, DAS: Davis Strait, DI: Disko Island, LS: Labrador Sea, CGFZ: Charlie-Gibbs Fracture Zone, BFZ: Bight Fracture Zone, RR: Reykjanes Ridge, IB: Iceland basin, DKS: Denmark Strait, SKI: Skaergaard intrusion, BC: Blosseville coast, KR: Kolbeinsey Ridge, JMMC: Jan Mayen Microcontinent Complex, AR: Aegir Ridge, NB: Norway basin, WJMFZ, EJMfZ: West and East Jan Mayen Fracture Zones, JM: Jan Mayen, LB: Lofoten basin, VP: Vøring Plateau, VB: Vøring basin, MB: Møre basin, FI: Faroe Islands, SI: Shetland Islands, FSB: Faroe-Shetland basin, MT: Moine Thrust, GGF: Great Glen Fault, HBF: Highland Boundary Fault, SUF: Southern Upland Fault, MTFZ: Møre-Trøndelag Fault Zone, HB: Hatton basin, RT: Rockall Trough, PB: Porcupine basin. Red lines: boundaries of the Caledonian orogen and associated thrusts, blue lines: northern boundary of the Hercynian orogen, both dashed where extrapolated into the younger Atlantic Ocean.

1297

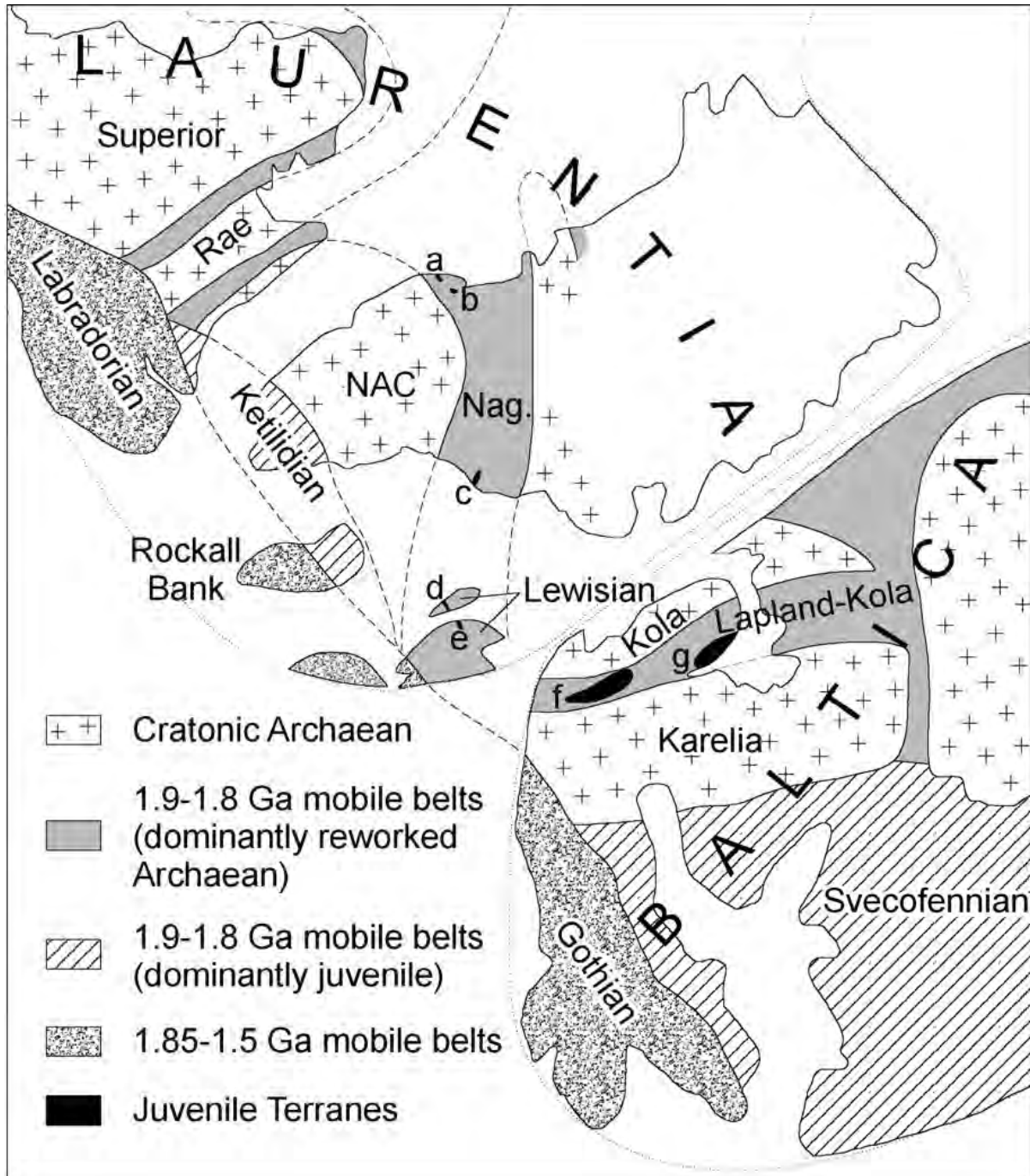


1298

1299

1300 Figure 2: Schematic map of Greenland showing features referred to in the text. A: Arsuk, AS: Ataa
 1301 Sund, BS: Bylot Sund, DB: Disko Bugt, IBr: Inglefield Bredning, IBu: Inussulik Bugt, IL: Inglefield
 1302 Land, ITZ: Ikertoq thrust zone, KF: Karrat Fjord, KY: Kap York, M: Midternæs, Na: Naternaq, NI:
 1303 Nordre Isortoq, NS: Nordre Strømfjord, Nu: Nunatarsuaq, RB: Rensselaer Bugt, S: Sermilik, T: Thule
 1304 basin, TB: Tasiussaqa Bugt, UF: Uummannaq Fjord [from St-Onge *et al.*, 2009].

1305

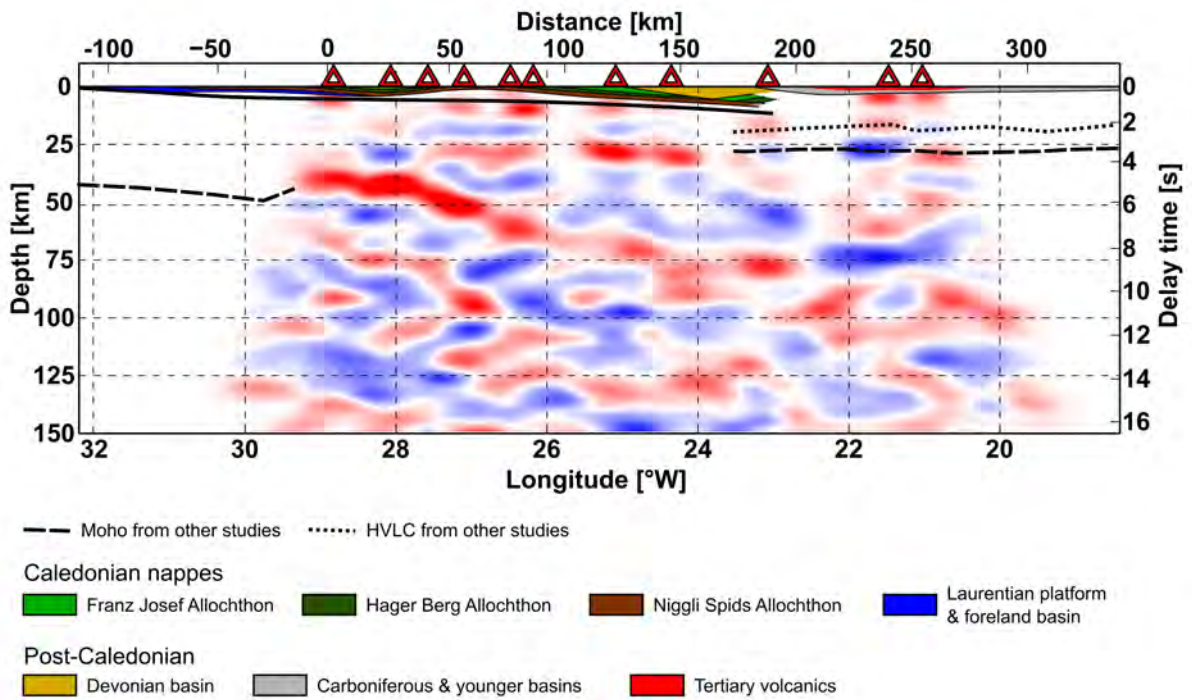


1306

1307

1308 Figure 3: Reconstruction of the North Atlantic Realm at 1265 Ma. NAC: North Atlantic Craton, Nag:
 1309 Nagssugtoqidian. Juvenile terranes: a: Sissimuit Charnockite, b: Arfersiorfic diorite, c: Ammassalik
 1310 Intrusive Complex, d: South Harris Complex, e: Loch Maree Group, f: Lapland-Kola Granulite Belt,
 1311 g: Tersk and Umba terranes [from Mason *et al.*, 2004].
 1312

1313



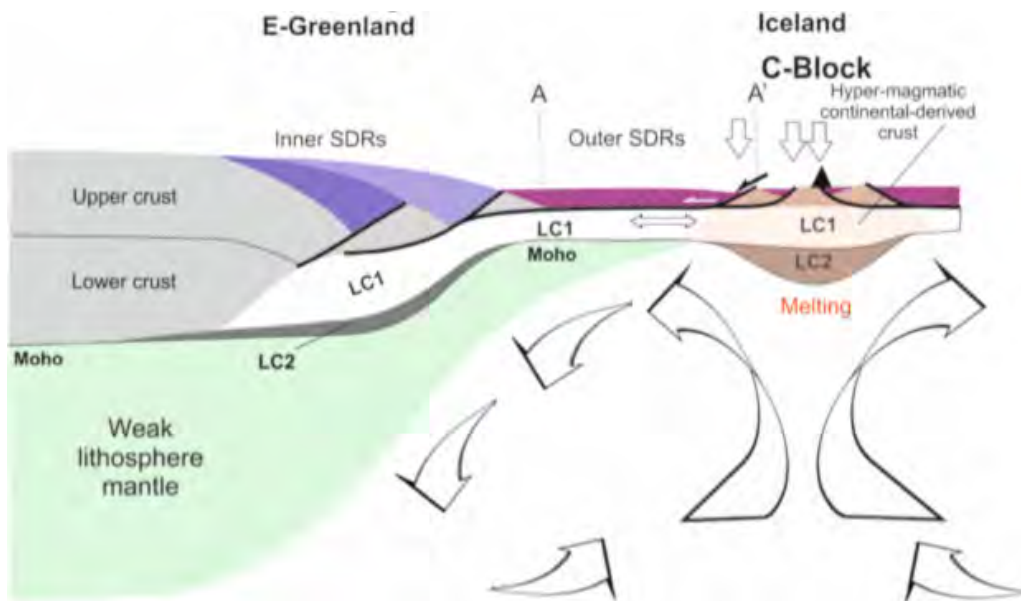
1314

1315

1316 Figure 4: Receiver function image of the crust and upper mantle under central east Greenland from
 1317 Schiffer *et al.* [2014] showing the Central Fjord structure. A geological cross-section based on Gee
 1318 [2015] is overlain showing the Caledonian nappes and foreland basin, and the Devonian basin.
 1319 Younger sedimentary basins are from Schlindwein & Jokat [2000]. Extrapolated Moho depths are
 1320 from Schiffer *et al.* [2016].

1321

1322

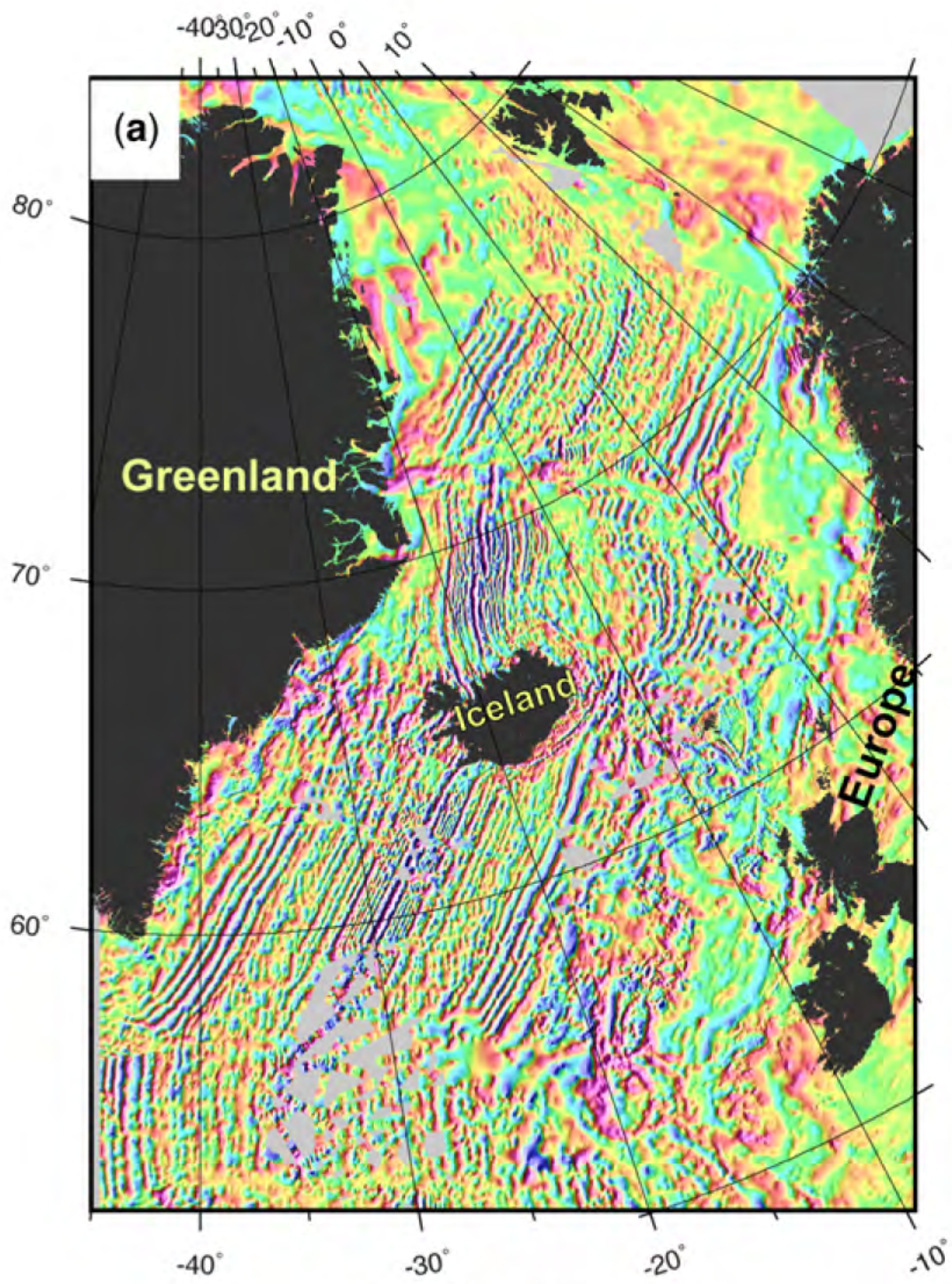


1323

1324

1325

1326 Figure 5: Schematic diagram illustrating the generalized structure of Inner- and Outer-SDRs and a
1327 possible “C-Block” under Iceland. Outer-SDRs comprise thick subaerial eruptive layers underlain by
1328 hyper-extended middle crust and high- V_p mafic material of uncertain affinity but similar in structure
1329 to massively sill-intruded lower crust. Ductile flow and magma-assisted inflation can extend such
1330 crust to many times its original length. Material eroded from the underlying lithospheric mantle may
1331 be distributed in the direction of extension and incorporated in the underlying asthenosphere. LC1:
1332 sill-injected continent-derived ductile crust. LC2: highly reflective, undeformed layer, tectonically
1333 disconnected from LC1, and with much higher V_p (7.6-7.8 km/s) [adapted from Geoffroy *et al.*,
1334 submitted].



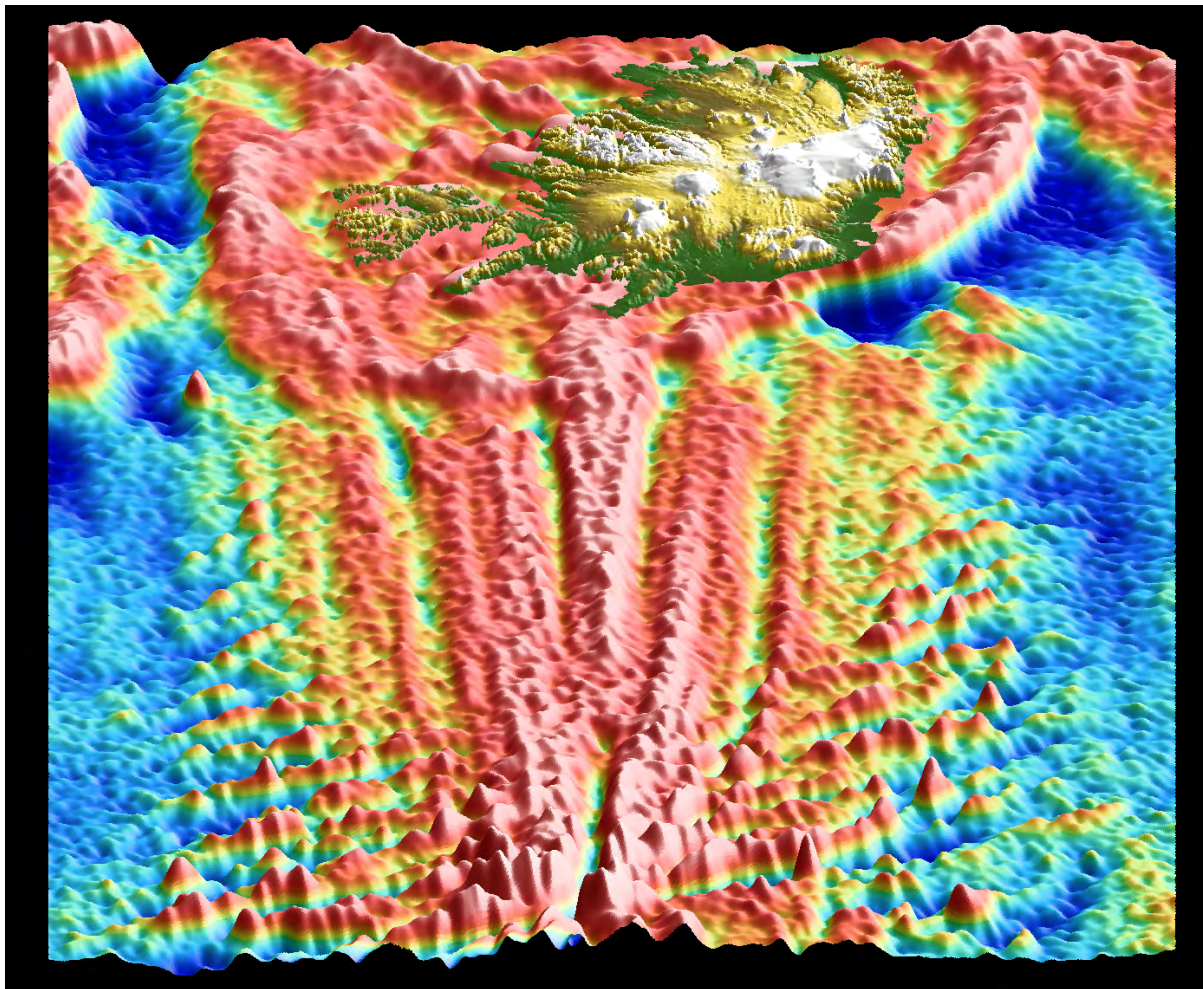
1335

1336

1337 Figure 6: Magnetic anomalies in the North Atlantic Ocean [from Gaina *et al.*, 2017].

1338

1339



1340

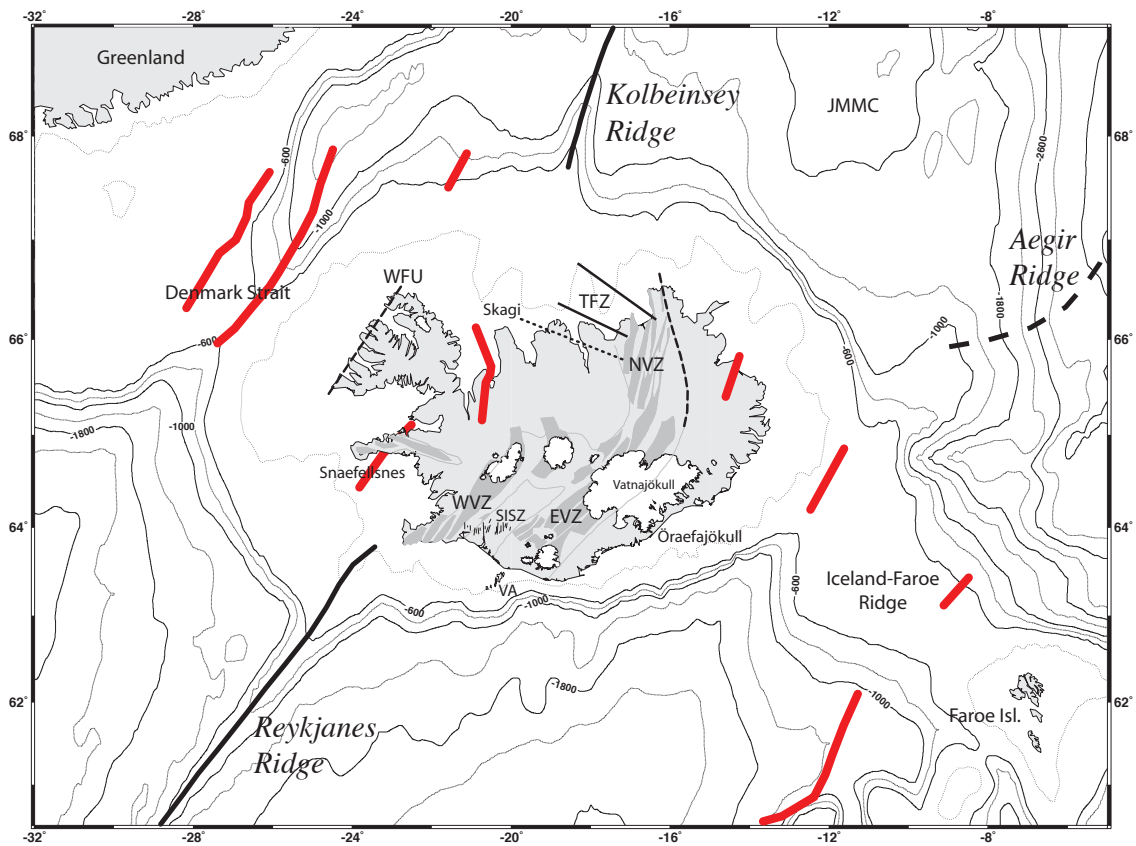
1341

1342 Figure 7: Perspective view along the Reykjanes Ridge looking towards Iceland showing the flanking
1343 chevron ridges converging with the spreading axis. Fracture-zone traces delineating former transform
1344 faults that have been eliminated can be seen as oblique cross-cutting structures in the lower part of the
1345 figure. Submarine areas show satellite-derived Free Air gravity anomalies from Sandwell *et al.* [2014]
1346 with the land topography of Iceland superimposed.

1347

1348

1349
1350

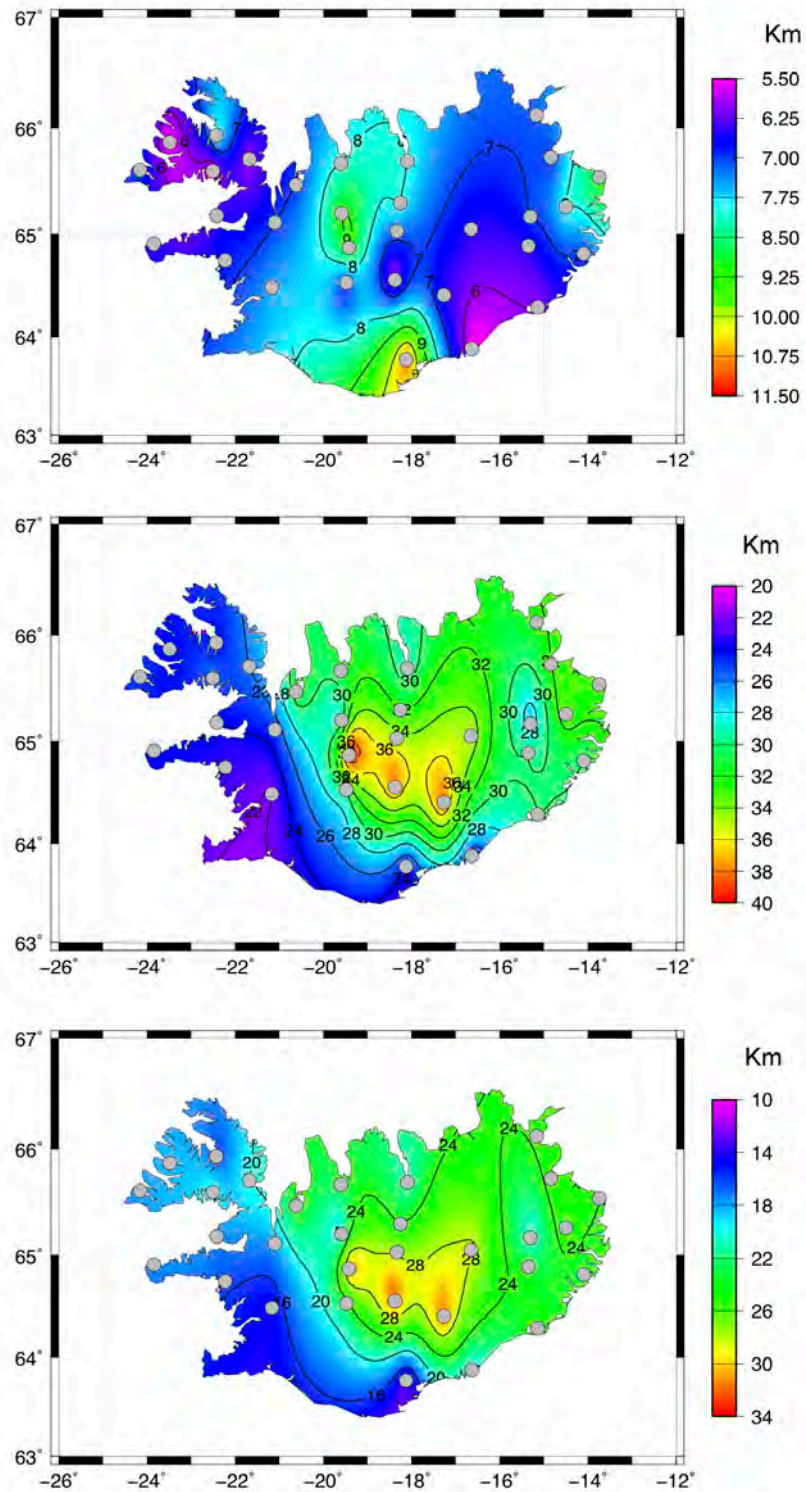


1351
1352

1353 Figure 8: The Greenland-Iceland-Faroe Ridge and surrounding areas showing bathymetry and
 1354 tectonic features. JMMC: Jan Mayen Microcontinent Complex. Thick black lines: axes of Reykjanes
 1355 and Kolbeinsey Ridges, thin gray lines on land: outlines of neovolcanic zones, dark grey: currently
 1356 active extensional volcanic systems, dashed black lines: extinct rifts on land, thin black lines:
 1357 individual faults of the South Iceland Seismic Zone (SISZ), white: glaciers. WVZ, EVZ, NVZ:
 1358 Western, Eastern, Northern Volcanic Zones, TFZ: Tjörnes Fracture Zone comprising two main shear
 1359 zones and one (dotted) known only from earthquake epicenters (see also Figure 15). Thick red lines:
 1360 extinct rift zones from Hjartarson *et al.* [2017].
 1361

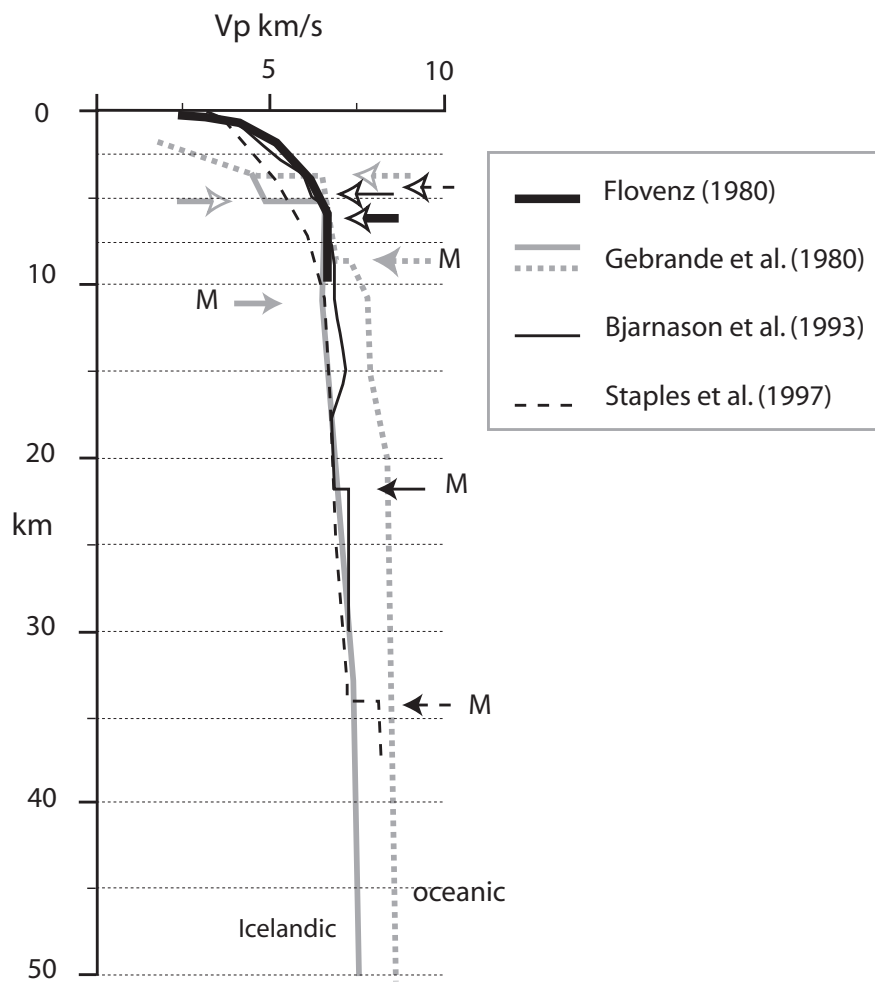
1362
1363
1364

1365

1366
1367

1368 Figure 9: Compilation of results from receiver function analysis in Iceland. Top: Depth to the base of
 1369 the upper crust, middle: depth to the base of the lower crust, bottom: thickness of the lower crust [data
 1370 from Foulger *et al.*, 2003].

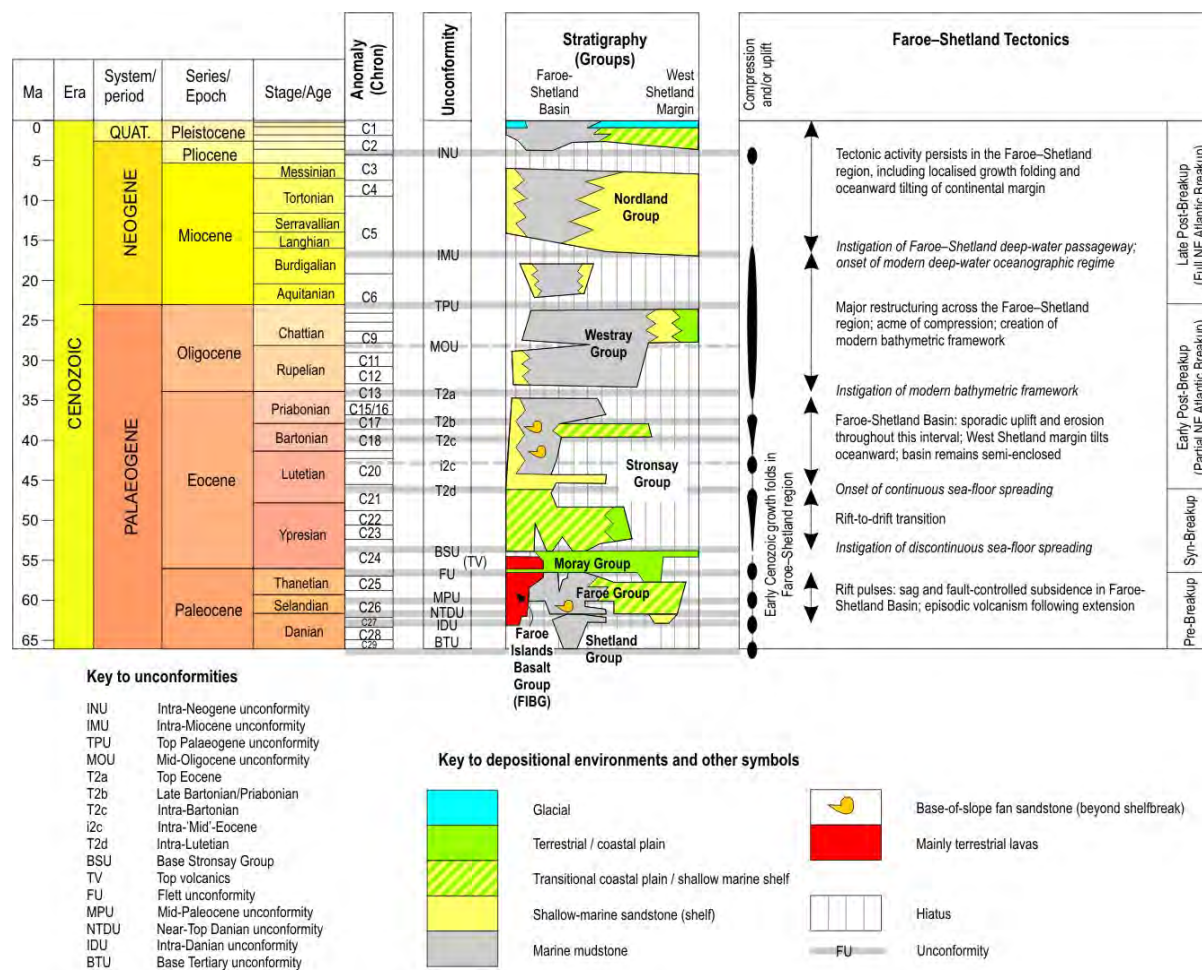
1371



1372
1373

1374 Figure 10: Velocity-depth profiles showing the average one-dimensional seismic structure of
 1375 Icelandic-type crust from explosion profiles shot in Iceland and in 10-Ma oceanic crust south of
 1376 Iceland [Gebrande *et al.*, 1980]. Open-headed arrows, estimates of the base of the upper crust from
 1377 various studies; solid-headed arrows, estimates of the base of the lower crust; M, proposed Moho
 1378 identifications [from Bjarnason *et al.*, 1993; Flovenz, 1980; Foulger *et al.*, 2003; Staples *et al.*, 1997].

1379
1380

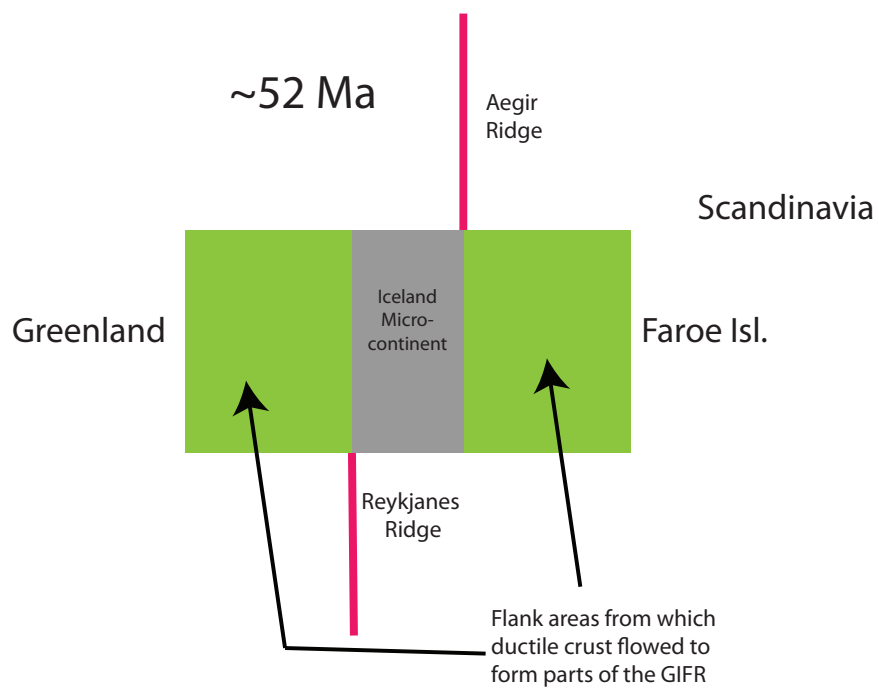


1381

1382

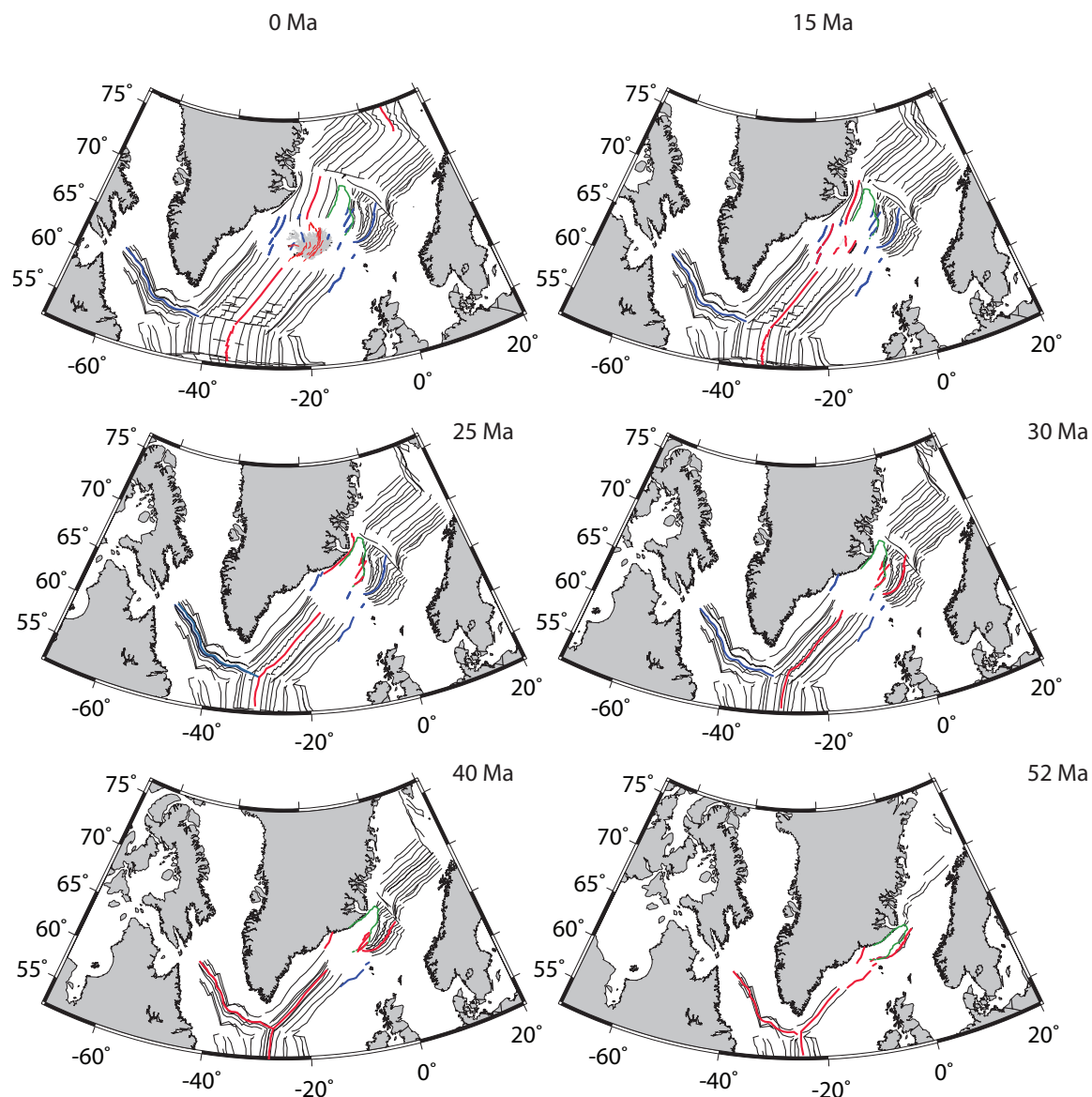
1383 Figure 11: Cenozoic tectonostratigraphy for the Faroe-Shetland basin. The compilation of the
 1384 stratigraphy and Faroe-Shetland tectonics is based mainly on Stoker *et al.* [2013; 2018; 2005b].
 1385 Additional information: ‘Stratigraphy’ and ‘Unconformity’ columns [Mudge, 2015], ‘Faroe-Shetland
 1386 Tectonics’ column [Blischke *et al.*, 2017; Dean *et al.*, 1999; Ellis & Stoker, 2014; Johnson *et al.*,
 1387 2005; Ólavsdóttir *et al.*, 2013a; Stoker *et al.*, 2012; Stoker *et al.*, 2005a], timescale [Gradstein *et al.*,
 1388 2012].

1389



1390
1391

1392 Figure 12: Schematic diagram illustrating the Iceland Microcontinent.



1393

1394

1395

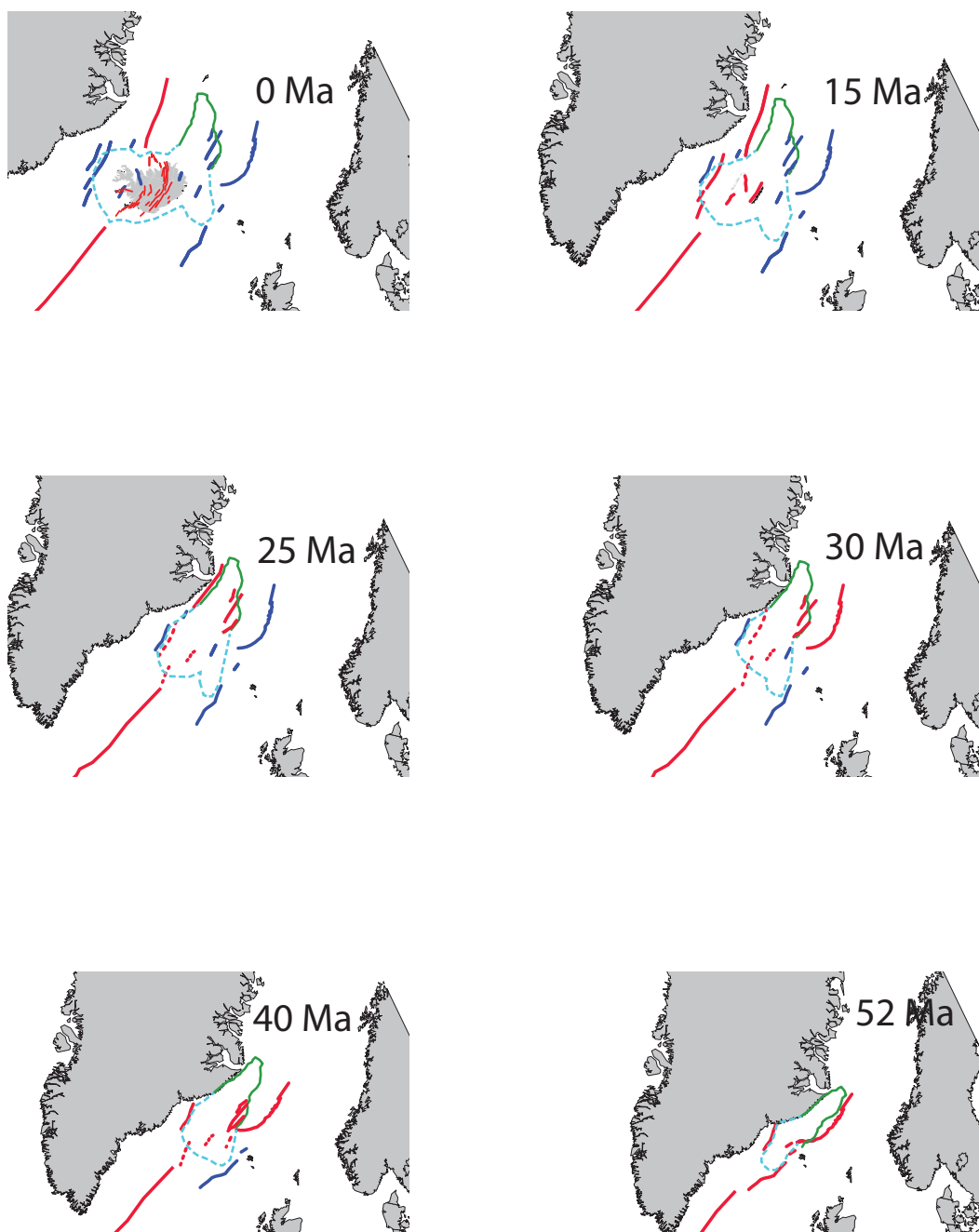
1396 Figure 13: Locations of known extensional axes during opening of the NE Atlantic Ocean. Basemap
 1397 and magnetic chrons (black lines) from GPlates using a Lambert Conformal Conic projection.

1398 Isochrons are from Müller *et al.* [2016]. Spreading ridges: Red—active, blue—extinct. Locations of
 1399 some extinct offshore spreading axes are from Hjartarson *et al.* [2017] and Brandsdóttir *et al.* [2015].

1400 Green: approximate boundary of Jan Mayen Microplate Complex. Areas where there is no direct
 1401 evidence for rifts or spreading axes are left white.

1402

1403

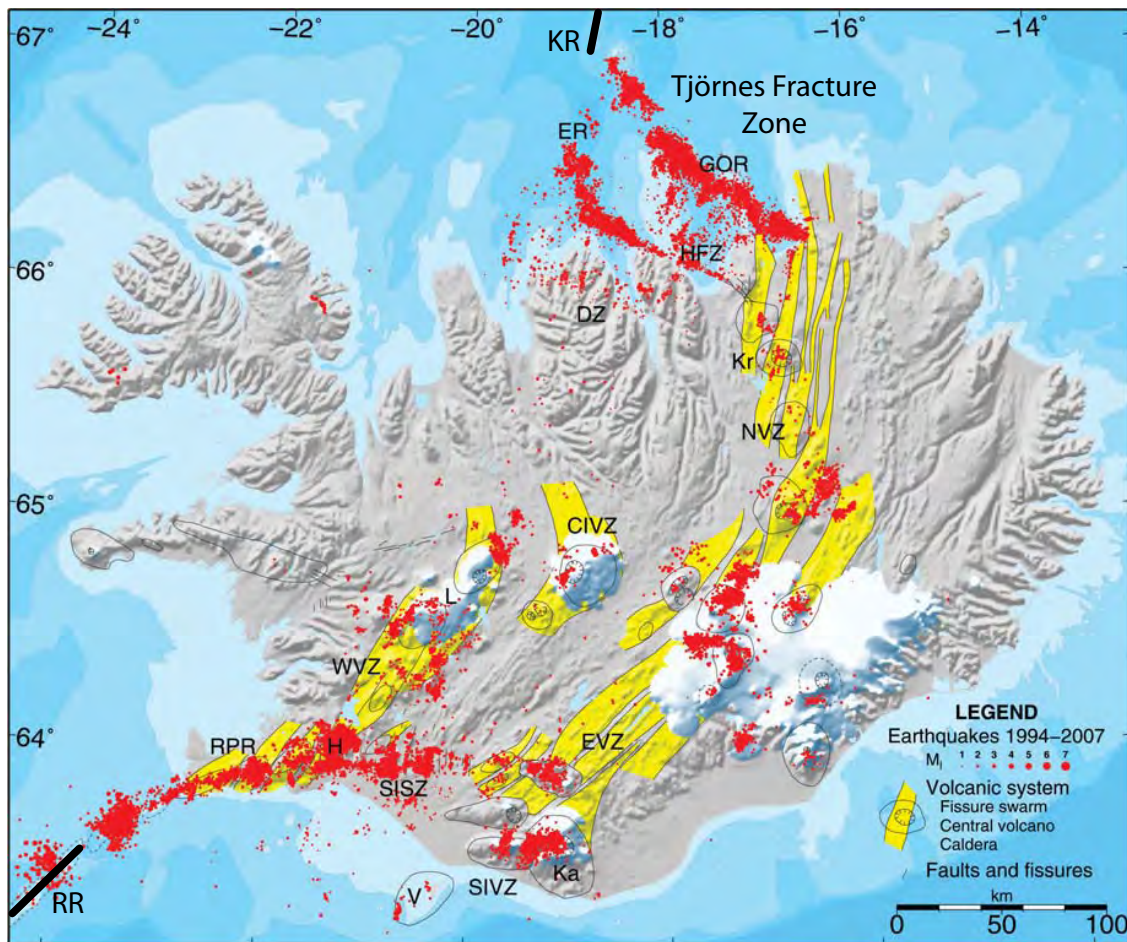


1404

1405

1406 Figure 14: Speculative reconstruction of the sequence of extensional deformation on the GIFR and
 1407 surroundings. Outline of land areas and locations of known extensional axes are from Figure 13 with
 1408 the latter shown as solid lines. Red: active, blue: extinct. Dashed lines show speculative positions of
 1409 ridges at times when observational data are lacking. Green solid line: approximate boundary of Jan
 1410 Mayen Microplate Complex. Pale blue dashed line: approximate boundary of Iceland Microcontinent.
 1411 This, and the Jan Mayen Microplate Complex expand with time as a result of magma inflation and
 1412 ductile flow.

1413

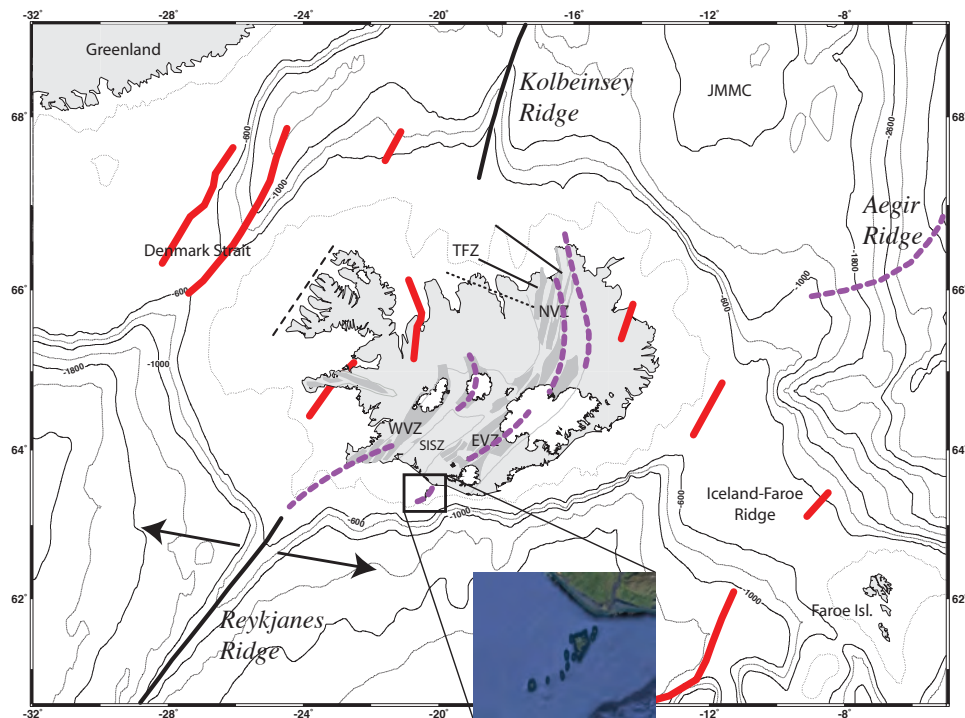


1414

1415

1416 Figure 15: Map of Iceland from Einarsson [2008] showing earthquakes 1994–2007 from the database
 1417 of the Icelandic Meteorological Office. Yellow: volcanic systems. The Tjörnes Fracture Zone
 1418 comprises GOR: the Grímsey Oblique Rift, HFZ: the Húsavík-Flatey Zone, ER: the Eyjafjardaráll
 1419 Rift, DZ: the Dalvík Zone. Other abbreviations are RR: Reykjanes Ridge, KR: Kolbeinsey Ridge,
 1420 RPR: Reykjanes Peninsula Rift Zone (also known as the Reykjanes Peninsula extensional transform
 1421 zone), WVZ: Western Volcanic Zone, SISZ: South Iceland Seismic Zone, EVZ: Eastern Volcanic
 1422 Zone, CIVZ: Central Iceland Volcanic Zone, NVZ: Northern Volcanic Zone, SIVZ: South Iceland
 1423 Volcanic Zone, Kr, Ka, H and L: the central volcanoes Krafla, Katla, Hengill and Langjökull, V: the
 1424 Vestmannaeyjar archipelago.

1425



1426

1427

1428

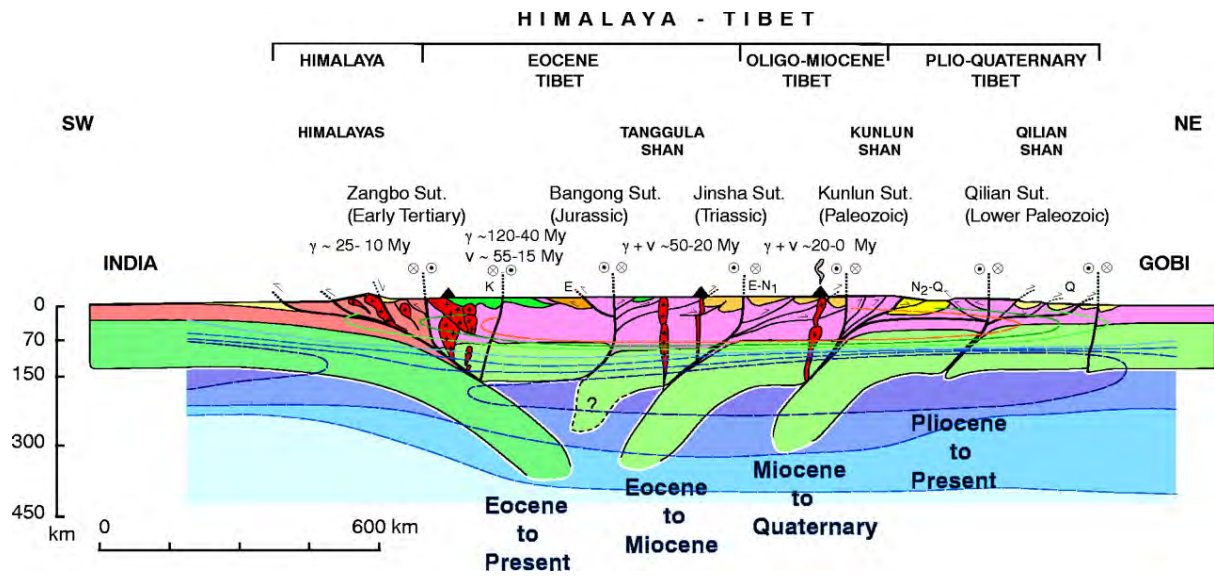
1429

1430 Figure 16: Similar to Figure 8 but showing additionally lines of curved sections of plate boundary that
 1431 resemble curving, approaching crack tips (dashed magenta lines). Inset: expanded view of
 1432 Vestmannaeyjar archipelago. Bold arrows: current direction of regional plate motion. For other details
 1433 and abbreviations see caption of Figure 8.

1434

1435

1436

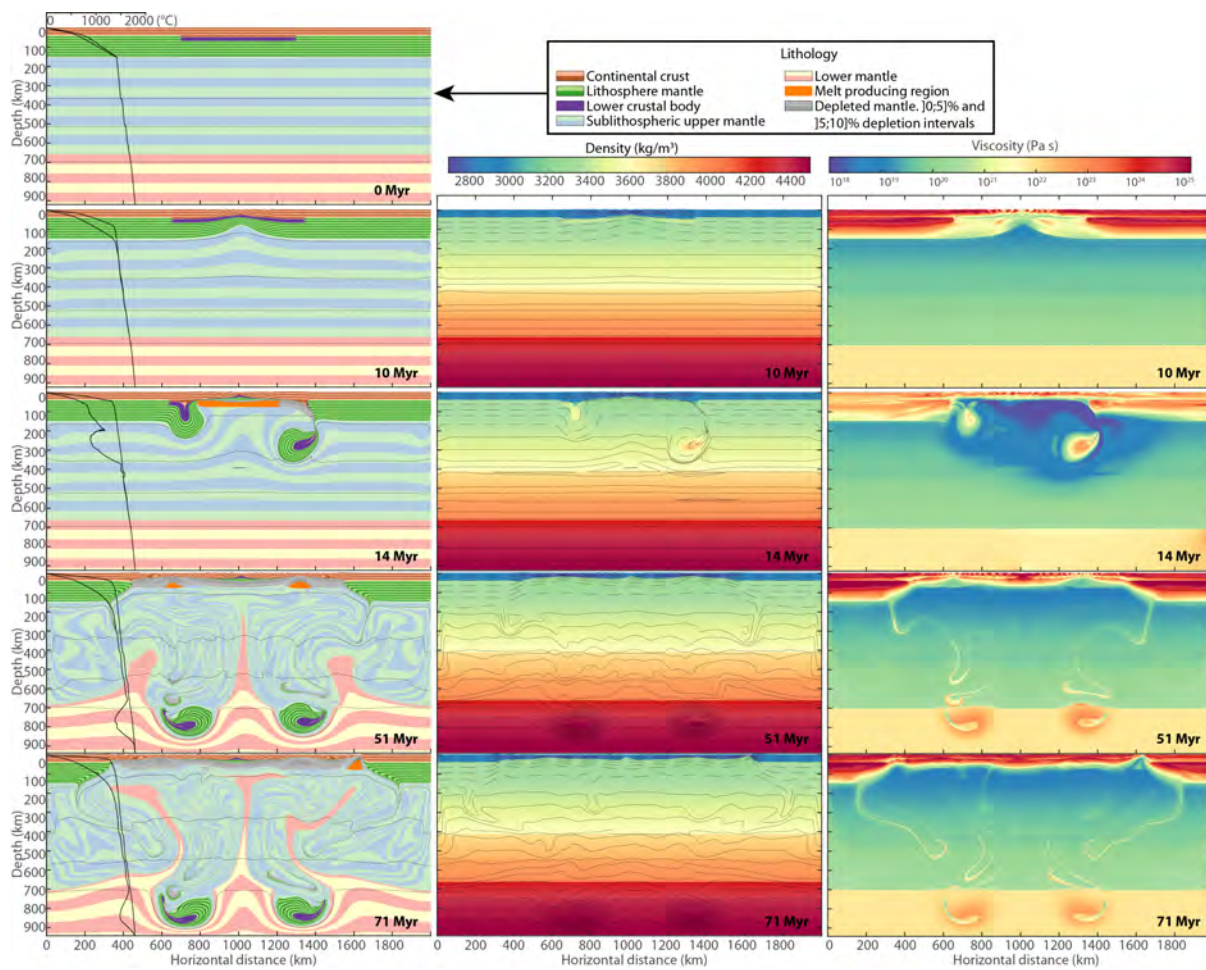


1437

1438

1439

1440 Figure 17: Schematic figure of the lithospheric structure of a well-studied, currently intact orogen—
 1441 the Himalaya-Tibet orogen. Green: lithospheric mantle, red and pink: crust or intrusives, yellow and
 1442 dark green: sedimentary basins. The orogen is underlain by an array of trapped fossil slabs that
 1443 thicken the crust locally. Deeper parts of the slabs are in the dense eclogite facies and negatively
 1444 buoyant [from Tapponnier *et al.*, 2001].



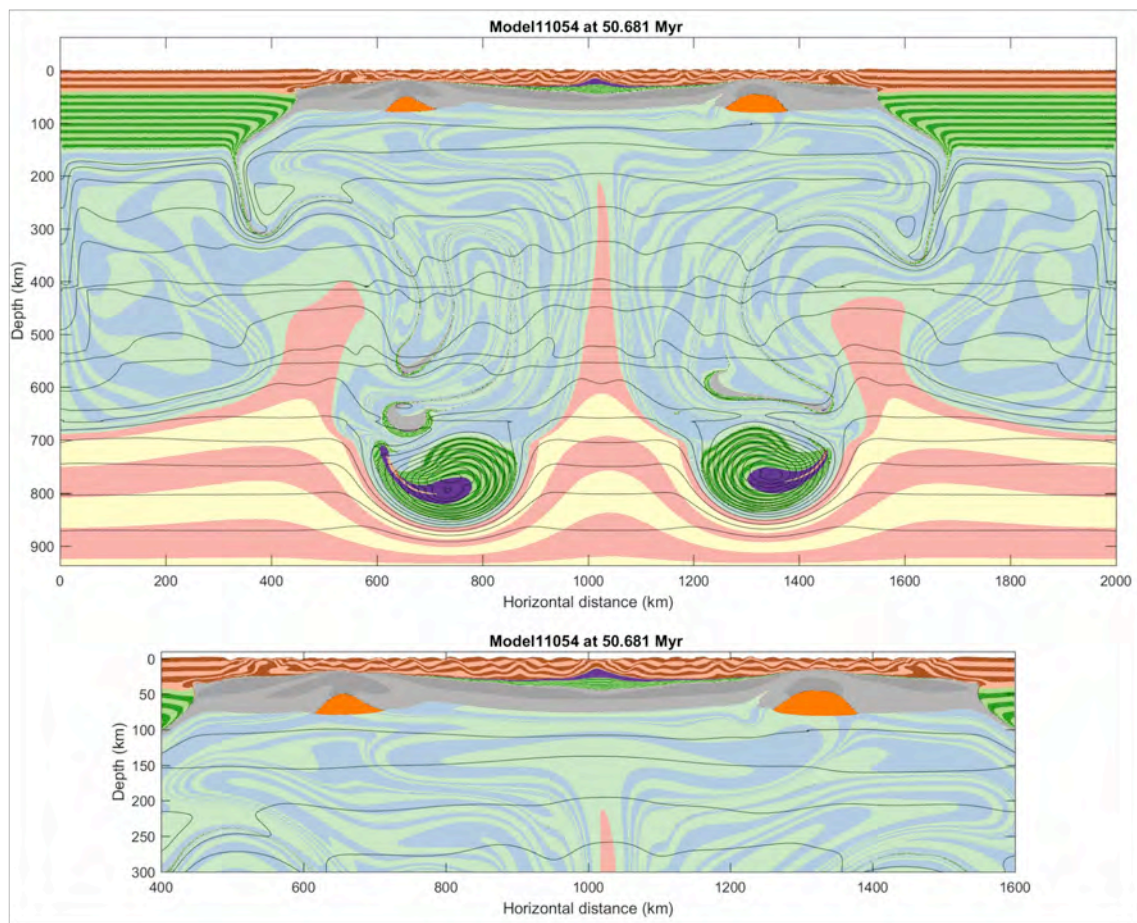
1445

1446

1447

1448 Figure 18: Simplified thermo-mechanical model of Cenozoic extension of the western frontal thrust of
 1449 the Caledonian suture. Left panels: Lithology at selected times, thick black lines: minimum/maximum
 1450 temperature profiles as a function of depth, thin black lines: isotherms from 1400°C with 100°C
 1451 intervals. Upper left panel: initial model configuration. Central panels: density evolution, dashed
 1452 black lines: isotherms from 0°C to 1400°C at 200°C intervals, full black lines: isotherms from 1450°C
 1453 at 25°C intervals. Right panels: effective viscosity evolution.

1454



1455
1456

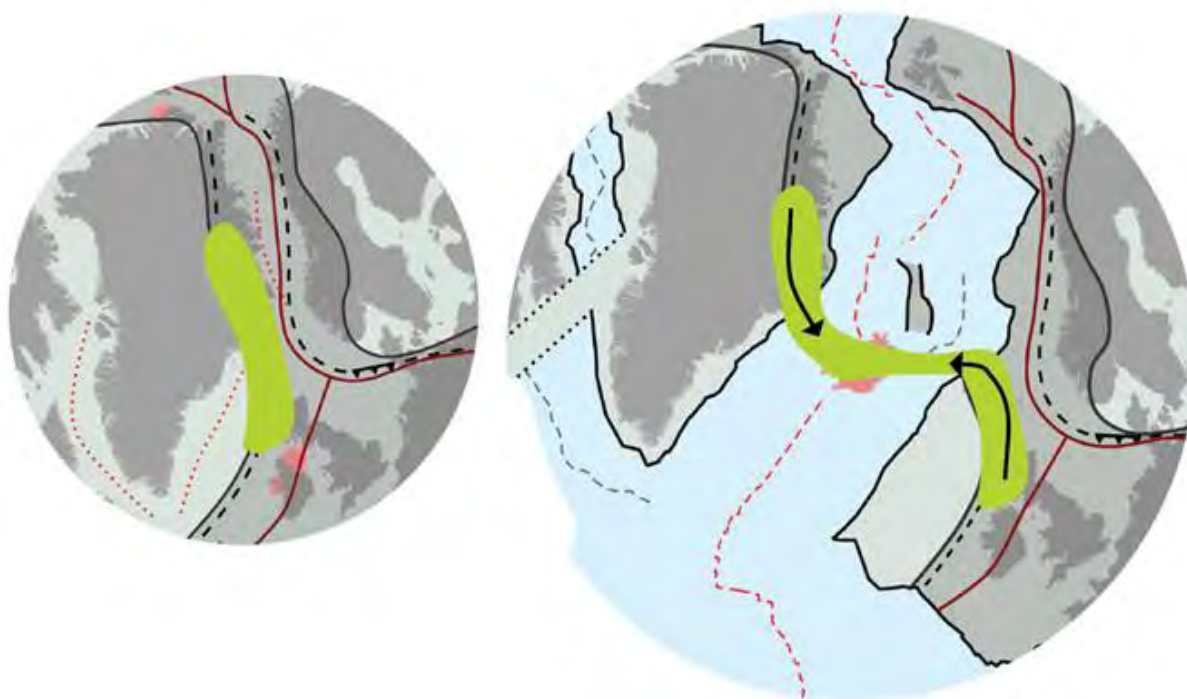
1457 Figure 19: Expanded view of the lithology panel for 50.6 Myr, from Figure 18. See that Figure for
1458 details.

1459

1460

1461

1462



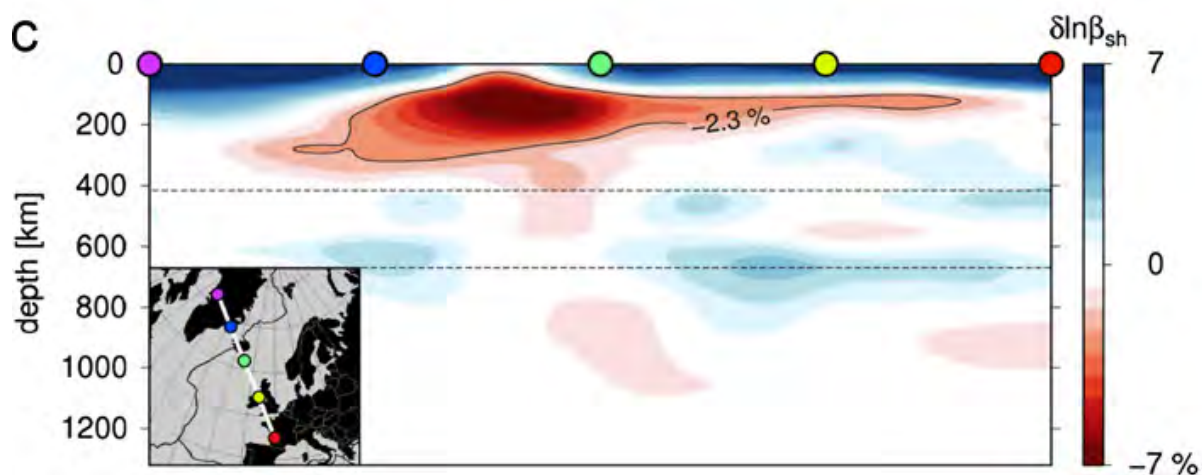
1463

1464

1465

1466 Figure 20: Map view sketch of our model. Green: the Caledonian frontal thrust zone where the crust is
 1467 relatively thick prior to breakup, arrows: lateral inflow of weak lower crust into the extending,
 1468 thinning zone. The persistence of continental crust beneath the GIFR maintains a warm, weak
 1469 lithosphere and encourages distributed deformation and lateral rift jumps to persist.

1470

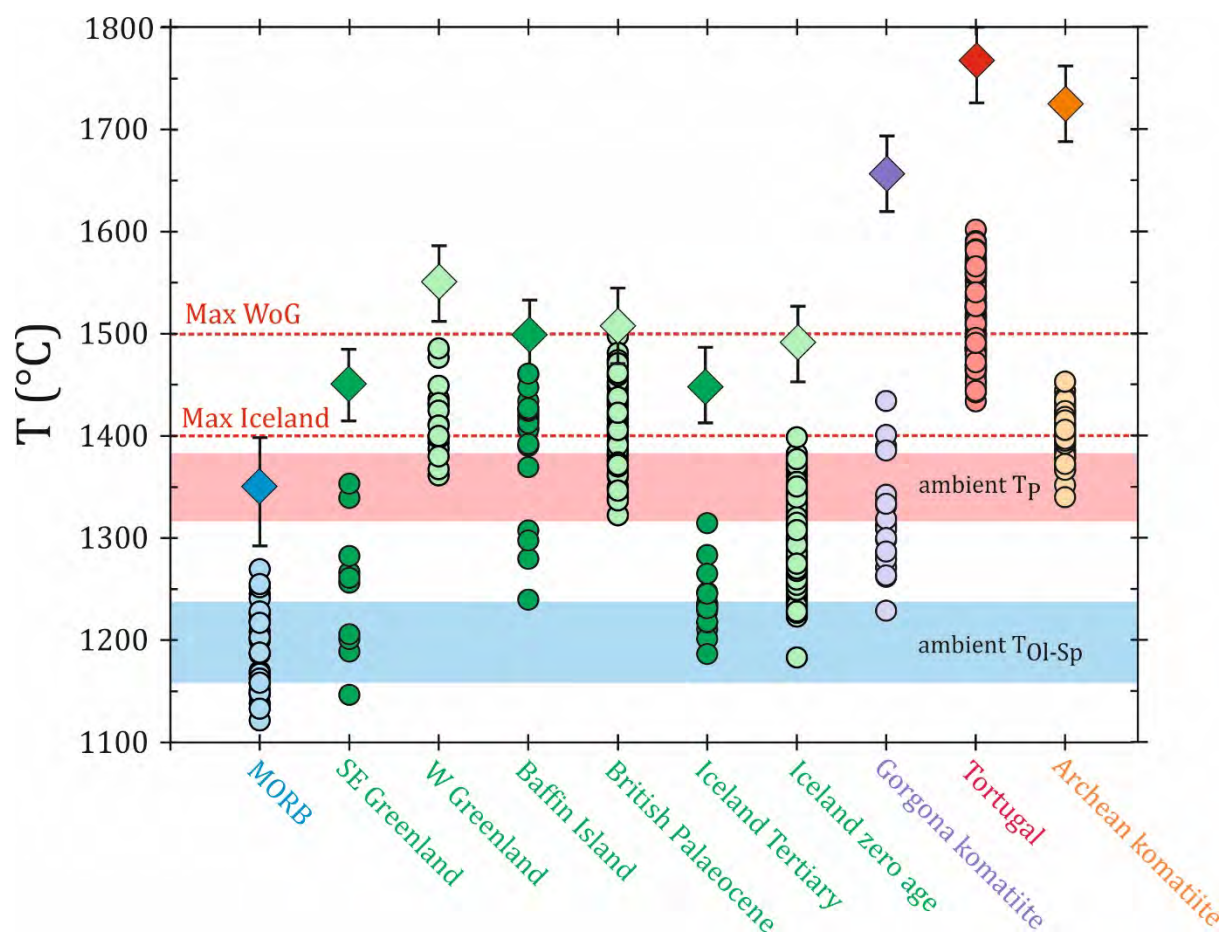


1471

1472

1473

1474 Figure 21: Cross section through the full-waveform inversion tomographic model of Rickers *et al.*
 1475 [2013]. Colored dots are spaced at intervals of 1000 km. Compare with lower left panel of Figure 18.
 1476



1477

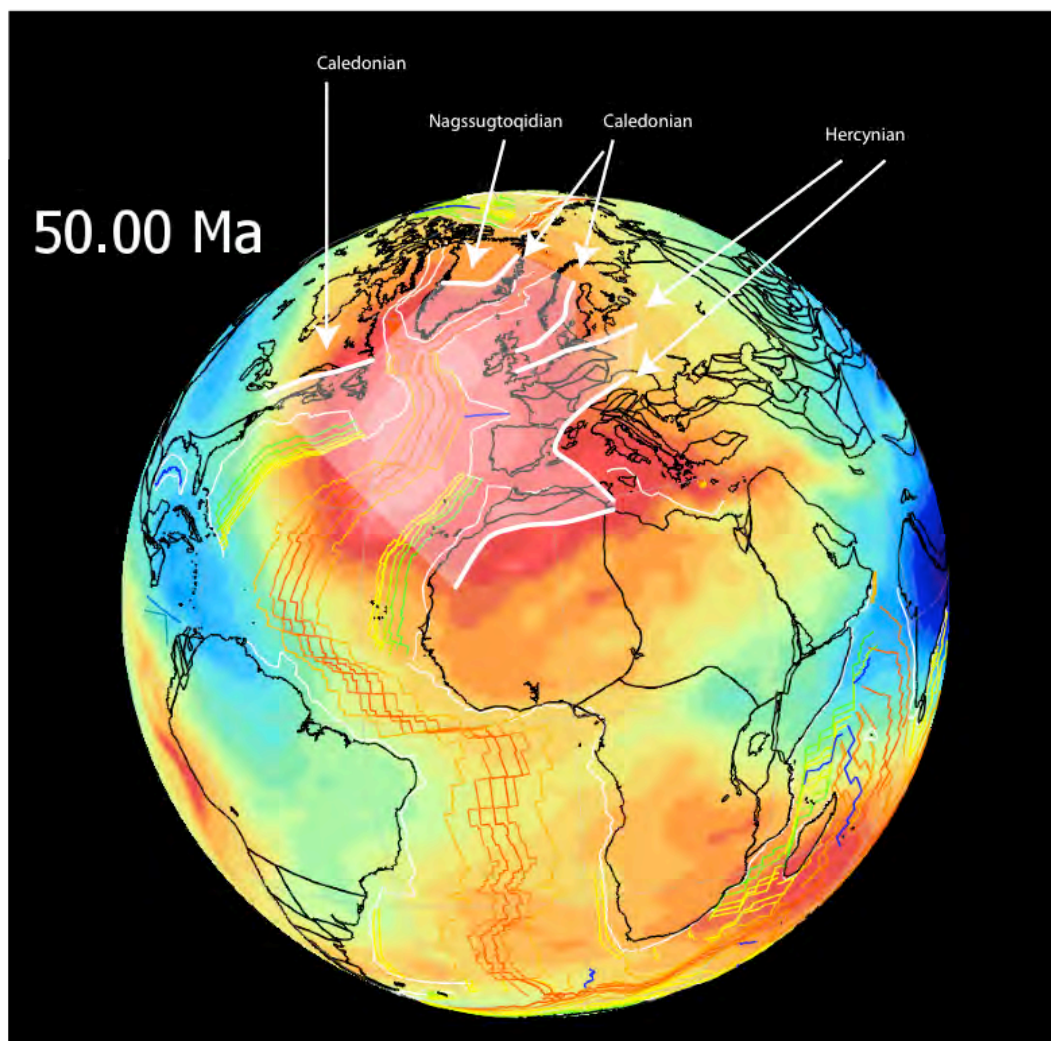
1478

1479 Figure 22: Summary of global maximum petrological estimates of T_p (diamonds $\pm 40^\circ\text{C}$; Herzberg &
 1480 Asimow [2015]) and olivine-spinel equilibrium crystallization temperatures (T_{Ol-Sp}) for magnesian
 1481 olivine (dots). The lower light-blue shaded region represents the range of T_{Ol} for olivine which
 1482 crystallized from near-primary magmas formed at ambient $T_p \sim 1350 \pm 40^\circ\text{C}$ (upper pink-shaded
 1483 region). The horizontal dashed lines represent the maximum estimated T_p for Iceland and West of
 1484 Greenland (WoG; Disko Island, Baffin Island) from Hole and Natland [this volume]. Data sources for
 1485 T_{Ol-Sp} : MORB, Gorgona komatiite and Archean komatiite: Coogan *et al.* [2014], British Palaeocene,
 1486 Baffin Island, West Greenland (Disko Island): Coogan *et al.* [2014], Spice *et al.* [2016], Iceland:
 1487 Matthews *et al.* [2016], Spice *et al.* [2016], Tortugal: Trela *et al.* (2017). Petrological estimates from
 1488 Herzberg and Asimow [2008; 2015], Hole [2015], Hole and Millett [2016] and Trela *et al.* [2017].

1489

1490

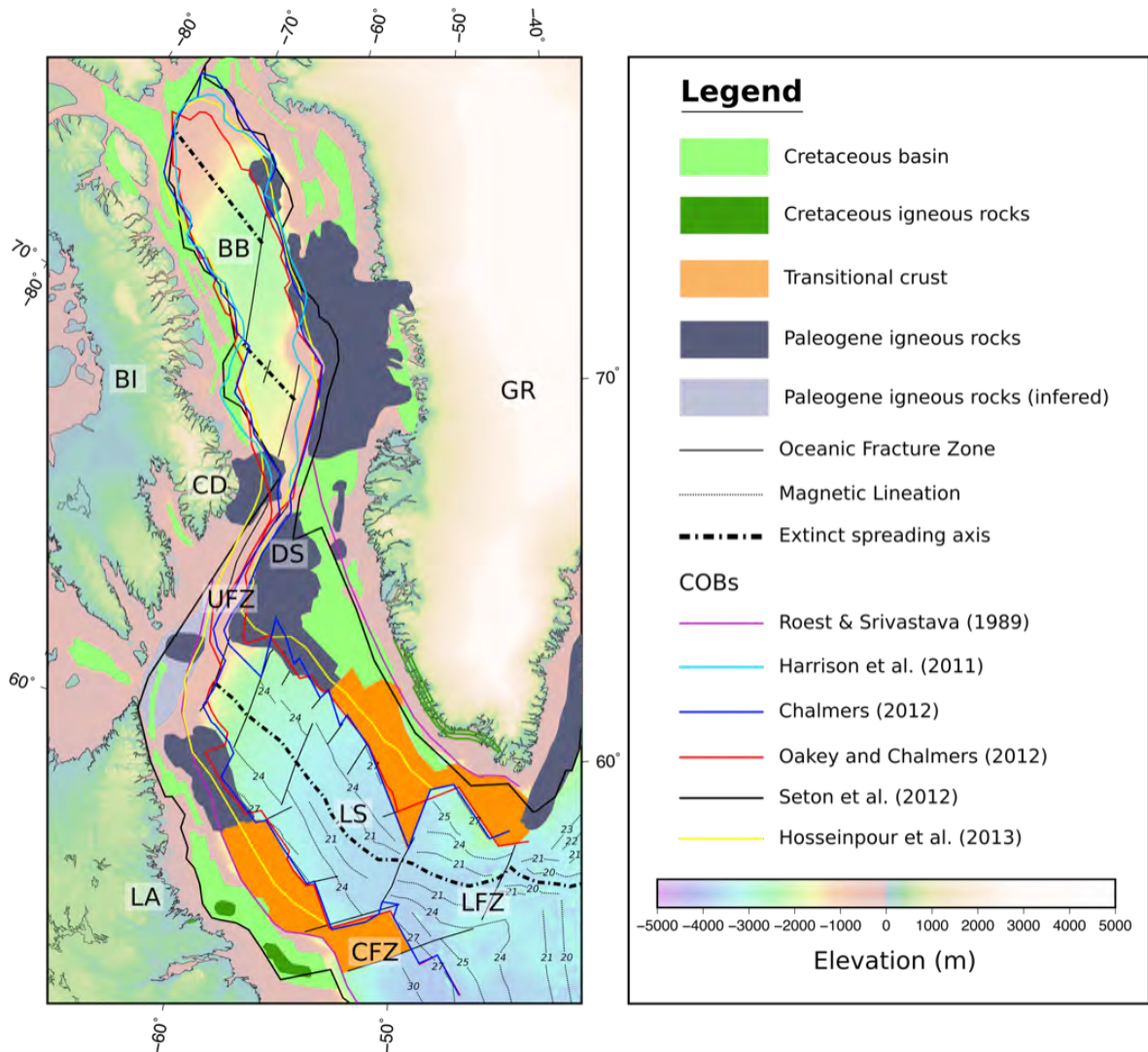
1491
1492



1493
1494
1495

1496 Figure 23: Continents reassembled to 50 Ma with the location of the future NE Atlantic centered over
1497 the present-day geoid high (red area). Thick white lines outline the Caledonian, Nagssugtoqidian, and
1498 Hercynian orogens. The area encompassed by these orogens is shaded and corresponds to the majority
1499 of the region of the geoid high.

1500
1501



1502

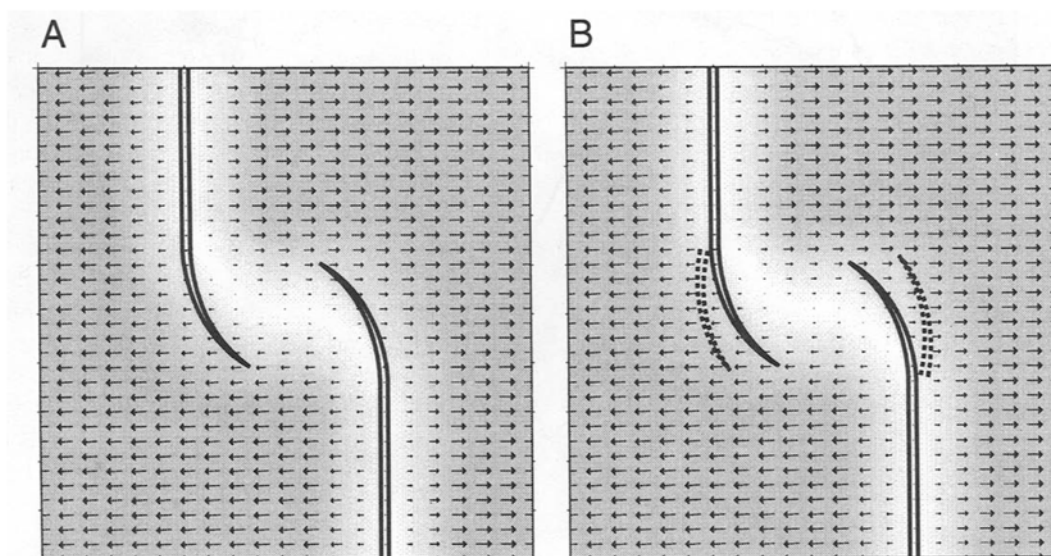
1503

1504 Figure 24: Structural map of the oceanic region west of Greenland showing Cretaceous basins and the
 1505 extent of Paleogene volcanics, including inferred continuation as shown in Abdelmalak *et al.* [2018].
 1506 Different proposed continent-ocean boundaries are also shown. The magnetic lineations and fracture
 1507 zones are reproduced from Chalmers [2012]. BB: Baffin Bay, BI: Baffin Island, CFZ: Cartwright
 1508 Fracture Zone, DS: Davis Strait, GR: Greenland, LFZ: Leif Fracture Zone, LS: Labrador Sea, UFZ:
 1509 Ungava Fault Zone, LA: Labrador. Elevation data are from Smith and Sandwell [1997].

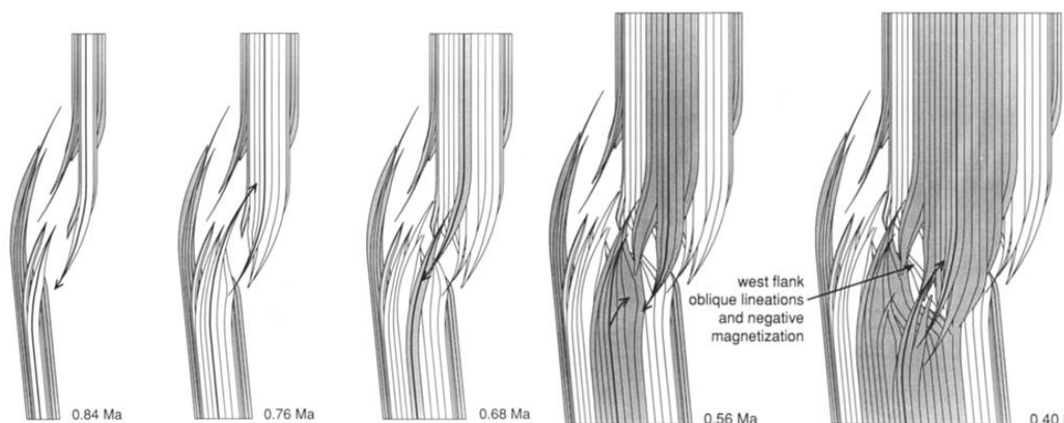
1510

1511

1512



1513



1514

1515

1516 Figure 25: Schematic diagrams showing models of spreading ridge evolution observed on the East
 1517 Pacific Rise. Top panels: ridges in the region $26^{\circ}\text{S} - 32^{\circ}\text{S}$ between the Easter and Juan Fernandez
 1518 microplates. Parallel, solid lines: active ridges, parallel dashed lines: extinct ridges. The structure is
 1519 modeled as a brittle layer overlying and weakly coupled with an underlying ductile layer.
 1520 Deformation in this layer is shown by shading with gray indicating uniform motion and white
 1521 indicating little or no motion. Arrows show displacement. Extension occurs in the overlap zone on
 1522 curved, overlapping ridges that progressively migrate outward, are removed from the magma supply,
 1523 become extinct, and are replaced by new ridges. Distributed bookshelf faulting occurs in the overlap
 1524 zone [from Martínez *et al.*, 1997]. Bottom panels: Model for the evolution of the East Pacific Rise at
 1525 $20^{\circ}40'\text{S}$ showing a possible origin of rotated blocks. Shading indicates magnetization polarities. The
 1526 ridge tips alternate between propagation and retreat, leading to the term “dueling propagators” [from
 1527 Perram *et al.*, 1993].

1528

1529

1530
1531

References

- 1532 Á Horni, J., J. R. Hopper, and e. al. (2016), Regional distribution of volcanism within the North
1533 Atlantic Igneous Province, *in* The North-East Atlantic Region: A Reappraisal of Crustal
1534 Structure, Tectono-Stratigraphy and Magmatic Evolution, edited by G. Péron-Pinvidic, J.
1535 Hopper, M. S. Stoker, C. Gaina, H. Doornenbal, T. Funck and U. Ártng, Geological Society,
1536 London, Special Publications.
- 1537 Abdelmalak, M. M., J. I. Faleide, S. Planke, L. Gernigon, D. Zastrozhnov, G. E. Shephard, and R.
1538 Myklebust (2017), The T-Reflection and the Deep Crustal Structure of the Vøring Margin,
1539 Offshore mid-Norway, *Tectonics*, 36, 2497-2523.
- 1540 Abdelmalak, M. M., S. Planke, S. Polteau, E. H. Hartz, J. I. Faleide, C. Tegner, D. A. Jerram, J. M.
1541 Millett, and R. Myklebust (2018), Breakup volcanism and plate tectonics in the NW Atlantic,
1542 *Tectonophysics*.
- 1543 Acton, G. D., S. Stein, and J. F. Engeln (1991), Block rotation and continental extension in Afar: A
1544 comparison to oceanic microplate systems, *Tectonics*, 10, 501-526.
- 1545 Ady, B. E., and R. C. Whittaker (2018), Examining the influence of tectonic inheritance on the
1546 evolution of the North Atlantic using a palinspastic deformable plate reconstruction, Geological
1547 Society, London, Special Publications, 470, SP470.479.
- 1548 Amundsen, H. E. F., U. Schaltegger, B. Jamtveit, W. L. Griffin, Y. Y. Podladchikov, T. Torsvik, and
1549 K. Gronvold (2002), Reading the LIPs of Iceland and Mauritius, *Proceedings of the 15th*
1550 *Kongsberg Seminar*, Kongsberg, Norway.
- 1551 Andersen, M. S., T. Nielsen, A. B. Sørensen, L. O. Boldreel, and A. Kuijpers (2000), Cenozoic
1552 sediment distribution and tectonic movements in the Faroe region, *Global and Planetary Change*,
1553 24, 239-259.
- 1554 Anderson, D. L. (2000a), The statistics of helium isotopes along the global spreading ridge system
1555 and the Central Limit Theorem, *Geophys. Res. Lett.*, 27, 2401-2404.
- 1556 Anderson, D. L. (2000b), The statistics and distribution of helium in the mantle, *Int. Geol. Rev.*, 42,
1557 289-311.
- 1558 Anderson, D. L. (2001), A statistical test of the two reservoir model for helium, *Earth planet. Sci.*
1559 *Lett.*, 193, 77-82.
- 1560 Anderson, D. L., G. R. Foulger, and A. Meibom (2006), Helium: Fundamental models, edited, G. R.
1561 Foulger, <http://www.mantleplumes.org/>.
- 1562 Angenheister, G., H. Gebrande, H. Miller, P. Goldflam, W. Weigel, W. R. Jacoby, G. Palmason, S.
1563 Bjornsson, P. Einarsson, N. I. Pavlenkova, S. M. Zverev, I. V. Litvinenko, B. Loncarevic, and S.
1564 C. Solomon (1980), Reykjanes ridge Iceland seismic experiment (RRISP 77), *J. Geophys.*, 47,
1565 228-238.
- 1566 Artemieva, I. M., and H. Thybo (2013), EUNaseis: A seismic model for Moho and crustal structure
1567 in Europe, Greenland, and the North Atlantic region, *Tectonophysics*, 609, 97-153.
- 1568 Atwater, T., and J. Severinghaus (1989), Tectonic maps of the northeast Pacific, *in* The Eastern
1569 Pacific Ocean and Hawaii, edited by E. L. Winterer, D. M. Hussong and R. W. Decker, pp. 15-
1570 20, Geological Society of America, Boulder, Colorado.
- 1571 Barnett-Moore, N., D. R. Müller, S. Williams, J. Skogseid, and M. Seton (2018), A reconstruction of
1572 the North Atlantic since the earliest Jurassic, *Basin Research*, 30, 160-185.
- 1573 Bauer, K., S. Neben, B. Schreckenberger, R. Emmermann, K. Hinz, N. Fechner, K. Gohl, A. Schulze,
1574 R. B. Trumbull, and K. Weber (2000), Deep structure of the Namibia continental margin as
1575 derived from integrated geophysical studies, *J. Geophys. Res.*, 105, 25829–25853.
- 1576 Beblo, M., and A. Bjornsson (1978), Magnetotelluric investigation of the lower crust and upper
1577 mantle beneath Iceland, *J. Geophys.*, 45, 1-16.
- 1578 Beblo, M., and A. Bjornsson (1980), Model of Electrical-Resistivity beneath Ne Iceland, Correlation
1579 with Temperature, *Journal of Geophysics-Zeitschrift Fur Geophysik*, 47, 184-190.
- 1580 Beblo, M., A. Bjornsson, K. Arnason, B. Stein, and P. Wolfgram (1983), Electrical conductivity
1581 beneath Iceland - Constraints imposed by magnetotelluric results on temperature, partial melt,
1582 crust and mantle structure, *J. Geophys.*, 53, 16-23.

- 1583 Benediktsdóttir, Á., R. Hey, F. Martinez, and Á. Höskuldsson (2012), Detailed tectonic evolution of
 1584 the Reykjanes Ridge during the past 15 Ma, *Geochem. Geophys. Geosys.*, 13.
- 1585 Benson, R. N. (2003), Age Estimates of the Seaward-Dipping Volcanic Wedge, Earliest Oceanic
 1586 Crust, and Earliest Drift-Stage Sediments Along the North American Atlantic Continental
 1587 Margin, *in* The Central Atlantic Magmatic Province: Insights from Fragments of Pangea, edited
 1588 by W. Hames, J. Mchone, P. Renne and C. Ruppel, pp. 61–75, American Geophysical Union.
- 1589 Bergerat, F., and J. Angelier (2000), The South Iceland Seismic Zone: tectonic and sismotectonic
 1590 analyses revealing the evolution from rifting to transform motion, *J. Geodyn.*, 29, 211-231.
- 1591 Berzin, R., O. Oncken, J. H. Knapp, A. Pérez-Estaún, T. Hismatulin, N. Yunusov, and A. Lipilin
 1592 (1996), Orogenic Evolution of the Ural Mountains: Results from an Integrated Seismic
 1593 Experiment, *Science*, 274, 220.
- 1594 Bingen, B., and G. Viola (2018), The early-Sveconorwegian orogeny in southern Norway: Tectonic
 1595 model involving delamination of the sub-continental lithospheric mantle, *Precamb. Res.*, 313,
 1596 170-204.
- 1597 Bjarnason, I. T., W. Menke, O. G. Flovenz, and D. Caress (1993), Tomographic image of the mid-
 1598 Atlantic plate boundary in south-western Iceland, *J. Geophys. Res.*, 98, 6607-6622.
- 1599 Björnsson, A., G. Johnsen, S. Sigurdsson, G. Thorbergsson, and E. Tryggvason (1979), Rifting of the
 1600 Plate Boundary in North Iceland 1975-1978, *J. Geophys. Res.*, 84, 3029-3038.
- 1601 Björnsson, A., H. Eysteinnsson, and M. Beblo (2005), Crustal formation and magma genesis beneath
 1602 Iceland: magnetotelluric constraints, *in* Plates, Plumes, and Paradigms, edited by G. R. Foulger,
 1603 J.H. Natland, D.C. Presnall and D.L. Anderson, pp. 665-686, Geological Society of America.
- 1604 Blischke, A., C. Gaina, J. R. Hopper, G. Peron-Pinvidic, B. Brandsdóttir, P. Guarnieri, O. Erlendsson,
 1605 and K. Gunnarsson (2017), The Jan Mayen microcontinent: an update of its architecture,
 1606 structural development and role during the transition from the Ægir Ridge to the mid-oceanic
 1607 Kolbeinsey Ridge, *in* The NE Atlantic Region: A Reappraisal of Crustal Structure,
 1608 Tectonostratigraphy and Magmatic Evolution, edited by G. Peron-Pinvidic, J. R. Hopper, M. S.
 1609 Stoker, C. Gaina, J. C. Doornenbal, T. Funck and U. E. Arting, pp. 299-337, Geological Society,
 1610 London, Special Publications.
- 1611 Bohnhoff, M., and J. Makris (2004), Crustal structure of the southeastern Iceland-Faeroe Ridge (IFR)
 1612 from wide aperture seismic data, *J. Geodyn.*, 37, 233-252.
- 1613 Bonatti, E. (1985), Punctiform initiation of seafloor spreading in the Red Sea during transition from a
 1614 continental to an oceanic rift, *Nature*, 316, 33.
- 1615 Bott, M. H. P. (1974), Deep structure, evolution and origin of the Icelandic transverse ridge, *in*
 1616 *Geodynamics of Iceland and the North Atlantic Area*, edited by L. Kristjansson, pp. 33-48, D.
 1617 Reidel Publishing Company, Dordrecht.
- 1618 Bott, M. H. P. (1985), Plate tectonic evolution of the Icelandic transverse ridge and adjacent regions,
 1619 *JGR*, 90, 9953-9960.
- 1620 Bott, M. H. P., J. Sunderland, P. J. Smith, U. Casten, and S. Saxov (1974), Evidence for continental
 1621 crust beneath the Faeroe Islands, *Nature*, 248, 202.
- 1622 Bourgeois, O., O. Dauteuil, and E. Hallot (2005), Rifting above a mantle plume: structure and
 1623 development of the Iceland Plateau, *Geodinamica Acta*, 18, 59-80.
- 1624 Brandsdóttir, B., E. E. E. Hooff, R. Mjelde, and Y. Murai (2015), Origin and evolution of the
 1625 Kolbeinsey Ridge and Iceland Plateau, N-Atlantic, *Geochem. Geophys. Geosys.*, 16, 612–634.
- 1626 Breddam, K. (2002), Kistufell: Primitive melt from the Iceland mantle plume, *J. Pet.*, 43, 345-373.
- 1627 Breivik, A. J., R. Mjelde, J. I. Faleide, and Y. Murai (2006), Rates of continental breakup magmatism
 1628 and seafloor spreading in the Norway Basin–Iceland plume interaction, *Journal of Geophysical*
 1629 *Research: Solid Earth*, 111.
- 1630 Breivik, A. J., R. Mjelde, J. I. Faleide, and Y. Murai (2012), The eastern Jan Mayen microcontinent
 1631 volcanic margin, *Geophys. J. Int.*, 188, 798-818.
- 1632 Bronner, A., D. Sauter, G. Manatschal, G. Péron-Pinvidic, and M. Munsch (2011), Magmatic
 1633 breakup as an explanation for magnetic anomalies at magma-poor rifted margins, *Nature*
 1634 *Geoscience*, 4, 549.
- 1635 Brooks, C. K. (2011), The East Greenland rifted volcanic margin, *Geological Survey of Denmark and*
 1636 *Greenland Bulletin*, 24, 1-96.

- 1637 Brune, S., C. Heine, M. Pérez-Gussinyé, and S. V. Sobolev (2014), Rift migration explains
1638 continental margin asymmetry and crustal hyper-extension, *Nature Communications*, 5.
- 1639 Buck, R. W. (1986), Small-scale convection induced by passive rifting: the cause for uplift of rift
1640 shoulders, *Earth planet. Sci. Lett.*, 77, 362–372.
- 1641 Buck, W. R. (1991), Modes of continental lithospheric extension, *Journal of Geophysical Research:*
1642 *Solid Earth*, 96, 20161-20178.
- 1643 Buitter, S. J. H., and T. H. Torsvik (2014), A review of Wilson Cycle plate margins: A role for mantle
1644 plumes in continental break-up along sutures?, *Gondwana Research*, 26, 627-653.
- 1645 Carminati, E., and C. Doglioni (2010), North Atlantic geoid high, volcanism and glaciations,
1646 *Geophys. Res. Lett.*, 37.
- 1647 Chalmers, J. A. (2012), Labrador Sea, Davis Strait, and Baffin Bay, *in* *Regional Geology and*
1648 *Tectonics: Phanerozoic Passive Margins, Cratonic Basins and Global Tectonic Maps*, edited by
1649 D. G. Roberts and A. W. Bally, pp. 384-435, Elsevier, Boston.
- 1650 Chalmers, J. A., and K. H. Laursen (1995), Labrador Sea: The extent of continental and oceanic crust
1651 and the timing of the onset of seafloor spreading, *Marine and Petroleum Geology*, 12, 205–217.
- 1652 Chalmers, J. A., and T. C. R. Pulvertaft (2001), Development of the continental margins of the
1653 Labrador Sea: a review, *Geological Society, London, Special Publications*, 187, 77.
- 1654 Chauvel, C., and C. Hemond (2000), Melting of a complete section of recycled oceanic crust: Trace
1655 element and Pb isotopic evidence from Iceland, *Geochem. Geophys. Geosys.*, 1, 1999GC000002.
- 1656 Chauvet, F., L. Geoffroy, H. Guillou, R. Maury, B. Le Gall, A. Agranier, and A. Viana (2019),
1657 Eocene continental breakup in Baffin Bay 757.
- 1658 Cheng, H., H. Zhou, Q. Yang, L. Zhang, F. Ji, and H. Dick (2016), Jurassic zircons from the
1659 Southwest Indian Ridge, *Scientific Reports*, 6, 26260.
- 1660 Chenin, P., G. Manatschal, L. L. Lavier, and D. Erratt (2015), Assessing the impact of orogenic
1661 inheritance on the architecture, timing and magmatic budget of the North Atlantic rift system: a
1662 mapping approach, *Journal of the Geological Society*, 172, 711.
- 1663 Christensen, N. I. (2004), Serpentinites, Peridotites, and Seismology, *Int. Geol. Rev.*, 46, 795-816.
- 1664 Čížková, H., A. P. van den Berg, W. Spakman, and C. Matyska (2012), The viscosity of Earth's lower
1665 mantle inferred from sinking speed of subducted lithosphere, *Phys. Earth Planet. Int.*, 200-201,
1666 56-62.
- 1667 Clarke, D. B., and E. K. Beutel (2019), Davis Strait Paleocene Picrites: Products of a Plume or
1668 Plates?, *Earth-Science Reviews*, this volume.
- 1669 Clerc, C., L. Jolivet, and J.-C. Ringenbach (2015), Ductile extensional shear zones in the lower crust
1670 of a passive margin, *Earth planet. Sci. Lett.*, 431, 1-7.
- 1671 Connelly, J. N., K. Thrane, A. W. Krawiec, and A. A. Garde (2006), Linking the Palaeoproterozoic
1672 Nagssugtoqidian and Rinkian orogens through the Disko Bugt region of West Greenland, *Journal*
1673 *of the Geological Society*, 163, 319.
- 1674 Connolly, J. A. D. (2005), Computation of phase equilibria by linear programming: A tool for
1675 geodynamic modeling and its application to subduction zone decarbonation, *Earth planet. Sci.*
1676 *Lett.*, 236, 524-541.
- 1677 Coogan, L. A., A. D. Saunders, and R. N. Wilson (2014), Aluminum-in-olivine thermometry of
1678 primitive basalts: Evidence of an anomalously hot mantle source for large igneous provinces,
1679 *Chem. Geol.*, 368, 1-10.
- 1680 Craig, H., and J. E. Lupton (1976), Primordial neon, helium, and hydrogen in oceanic basalts, *Earth*
1681 *planet. Sci. Lett.*, 31, 369-385.
- 1682 Dalhoff, F., L. M. Larsen, J. R. Ineson, S. Stouge, J. A. Bojesen-Koefoed, S. Lassen, A. Kuijpers, J.
1683 A. Rasmussen, and H. Nøhr-Hansen (2006), Continental crust in the Davis Strait: new evidence
1684 from seabed sampling, *Geological Survey of Denmark and Greenland Bulletin*, 10, 33–36.
- 1685 Dannowski, A., I. Grevemeyer, J. Phipps Morgan, C. R. Ranero, M. Maia, and G. Klein (2011),
1686 Crustal structure of the propagating TAMMAR ridge segment on the Mid-Atlantic Ridge,
1687 21.5°N, *Geochemistry, Geophysics, Geosystems*, 12.
- 1688 Darbyshire, F. A., I. T. Bjarnason, R. S. White, and O. G. Flovenz (1998a), Crustal structure above
1689 the Iceland mantle plume imaged by the ICEMELT refraction profile, *Geophys. J. Int.*, 135,
1690 1131-1149.

- 1691 Darbyshire, F. A., I. T. Bjarnason, R. S. White, and I. G. Flovenz (1998b), Crustal structure above the
 1692 Iceland mantle plume imaged by the ICEMELT refraction profile, *Geophys. J. Int.*, 135, 1131-
 1693 1149.
- 1694 Darbyshire, F. A., T. Dahl-Jensen, T. B. Larsen, P. H. Voss, and G. Joyal (2018), Crust and
 1695 uppermost-mantle structure of Greenland and the Northwest Atlantic from Rayleigh wave group
 1696 velocity tomography, *Geophys. J. Int.*, 212, 1546-1569.
- 1697 Dean, K., K. McLachlan, and A. Chambers (1999), Rifting and the development of the Faeroe-
 1698 Shetland Basin, *Proceedings of the 5th Conference Petroleum Geology of Northwest Europe*,
 1699 London, pp. 533–544.
- 1700 Deemer, S., C. A. Hurich, and J. Hall (2010), Post-rift flood-basalt-like volcanism on the
 1701 Newfoundland Basin nonvolcanic margin: The U event mapped with spectral decomposition
 1702 494, 1-16 pp.
- 1703 Denk, T., F. Grímsson, R. Zetter, and L. A. Simonarson (2011), The Biogeographic History of Iceland
 1704 – The North Atlantic Land Bridge Revisited, *in* *Late Cainozoic Floras of Iceland*, edited, pp.
 1705 647-668, Springer Science+Business Media B.V.
- 1706 Detrick, R. S., J. G. Sclater, and J. Thiede (1977), The subsidence of aseismic ridges, *Earth planet.*
 1707 *Sci. Lett.*, 34, 185-196.
- 1708 Dewey, J. F., and R. A. Strachan (2003), Changing Silurian–Devonian relative plate motion in the
 1709 Caledonides: sinistral transpression to sinistral transtension, *Journal of the Geological Society*,
 1710 160, 219.
- 1711 Dick, H. J. B. (2015), The Southwest Indian Ridge: Remelting the Gondwanan Mantle, *Acta*
 1712 *Geologica Sinica - English Edition*, 89, 27-27.
- 1713 Doré, A. G., E. R. Lundin, C. Fichler, and O. Olesen (1997), Patterns of basement structure and
 1714 reactivation along the NE Atlantic margin, *J. geol. Soc. Lon.*, 154, 85–92.
- 1715 Downes, H., B. G. J. Upton, A. D. J. Connolly, and J.-L. Bodinier (2007), Petrology and
 1716 geochemistry of a cumulate xenolith suite from Bute: evidence for late Palaeozoic crustal
 1717 underplating beneath SW Scotland, *Journal of the Geological Society, London*, 164, 1217–1231.
- 1718 Du, Z., and G. R. Foulger (1999), The crustal structure beneath the Northwest Fjords, Iceland, from
 1719 receiver functions and surface waves, *Geophys. J. Int.*, 139, 419-432.
- 1720 Du, Z., G. R. Foulger, B. R. Julian, R. M. Allen, G. Nolet, W. J. Morgan, B. H. Bergsson, P.
 1721 Erlendsson, S. Jakobsdottir, S. Ragnarsson, R. Stefansson, and K. Vogfjord (2002), Crustal
 1722 structure beneath western and eastern Iceland from surface waves and receiver functions,
 1723 *Geophys. J. Int.*, 149, 349-363.
- 1724 Du, Z. J., and G. R. Foulger (2001), Variation in the crustal structure across central Iceland, *Geophys.*
 1725 *J. Int.*, 145, 246-264.
- 1726 Dunbar, J. A., and D. S. Sawyer (1988), Continental rifting at pre-existing lithospheric weaknesses,
 1727 *Nature*, 333, 450.
- 1728 Dunn, R., and F. Martinez (2011), Contrasting crustal production and rapid mantle transitions beneath
 1729 backarc ridges, *Nature*, 469, 198–202.
- 1730 Eagles, G., L. Pérez-Díaz, and N. Scarselli (2015), Getting over continent ocean boundaries, *Earth-*
 1731 *Science Reviews*, 151, 244-265.
- 1732 Ebbing, J., E. Lundin, O. Olesen, and E. K. Hansen (2006), The mid-Norwegian margin: a discussion
 1733 of crustal lineaments, mafic intrusions, and remnants of the Caledonian root by 3D density
 1734 modelling and structural interpretation, *Journal of the Geological Society*, 163, 47.
- 1735 Ebbing, J., R. W. England, T. Korja, T. Lauritsen, O. Olesen, W. Stratford, and C. Weidle (2012),
 1736 Structure of the Scandes lithosphere from surface to depth, *Tectonophysics*, 536-537, 1-24.
- 1737 Ebdon, C. C., P. J. Granger, H. D. Johnson, and A. M. Evans (1995), Early Tertiary evolution and
 1738 sequence stratigraphy of the Faeroe-Shetland Basin: implications for hydrocarbon prospectivity,
 1739 *in* *The Tectonics, Sedimentation and Palaeoceanography of the North Atlantic Region*, edited by
 1740 R. A. Scrutton, M. S. Stoker, G. B. Shimmield and A. W. Tudhope, pp. 51–69, Geological
 1741 Society, London, Special Publications, London.
- 1742 Einarsson, P. (1988), The South Iceland Seismic Zone, *Episodes*, 11, 34-35.
- 1743 Einarsson, P. (1991), Earthquakes and present-day tectonism in Iceland, *Tectonophysics*, 189, 261-
 1744 279.

- 1745 Einarsson, P. (2008), Plate boundaries, rifts and transforms in Iceland, *Jökull*, 58, 35-58.
- 1746 Eldholm, O., and K. Grue (1994a), North Atlantic volcanic margins: Dimensions and production
1747 rates, *J. Geophys. Res.*, 99, 2955–2968.
- 1748 Eldholm, O., and K. Grue (1994b), North Atlantic volcanic margins: Dimensions and production
1749 rates, *Journal of Geophysical Research: Solid Earth*, 99, 2955-2968.
- 1750 Eldholm, O., J. Thiede, and E. Taylor (1989), Evolution of the Vøring Volcanic Margin, *Proceedings
1751 of the ODP, Scientific Results*, pp 1033-1065 104.
- 1752 Elliott, G. M., and L. M. Parson (2008), Influence of margin segmentation upon the break-up of the
1753 Hatton Bank rifted margin, NE Atlantic, *Tectonophysics*, 457, 161-176.
- 1754 Ellis, D., and M. S. Stoker (2014), The Faroe–Shetland Basin: a regional perspective from the
1755 Paleocene to the present day and its relationship to the opening of the North Atlantic Ocean, *in
1756 Hydrocarbon Exploration to Exploitation West of Shetlands*, edited by S. J. C. Cannon and D.
1757 Ellis, Geological Society, London, London.
- 1758 Engeln, J. F., S. Stein, J. Werner, and R. G. Gordon (1988), Microplate and shear zone models for
1759 oceanic spreading center reorganizations, *Journal of Geophysical Research: Solid Earth*, 93,
1760 2839-2856.
- 1761 Escartin, J., G. Hirth, and B. Evans (2001), Strength of slightly serpentinitized peridotites: Implications
1762 for the tectonics of oceanic lithosphere, *Geology*, 29, 1023-1026.
- 1763 Eysteinnsson, H., and J. Hermance (1985), Magnetotelluric measurements across the eastern
1764 neovolcanic zone in south Iceland, *JGR*, 90, 10,093-010,103.
- 1765 Fichler, C., T. Odinsen, H. Rueslåtten, O. Olesen, J. E. Vindstad, and S. Wienecke (2011), Crustal
1766 inhomogeneities in the Northern North Sea from potential field modeling: Inherited structure and
1767 serpentinites?, *Tectonophysics*, 510, 172-185.
- 1768 Flovenz, O. G. (1980), Seismic structure of the Icelandic crust above layer three and the relation
1769 between body wave velocity and the alteration of the basaltic crust, *J. Geophys.*, 47, 211-220.
- 1770 Forsyth, D. W., N. Harmon, D. S. Scheirer, and R. A. Duncan (2006), Distribution of recent
1771 volcanism and the morphology of seamounts and ridges in the GLIMPSE study area:
1772 Implications for the lithospheric cracking hypothesis for the origin of intraplate, non-hot spot
1773 volcanic chains, *J. Geophys. Res.*, 111, B11407.
- 1774 Fossen, H. (2010), Extensional tectonics in the North Atlantic Caledonides: a regional view,
1775 Geological Society, London, Special Publications, 335, 767.
- 1776 Foulger, G. R. (2006), Older crust underlies Iceland, *Geophys. J. Int.*, 165, 672-676.
- 1777 Foulger, G. R. (2010), *Plates vs Plumes: A Geological Controversy*, Wiley-Blackwell, Chichester,
1778 U.K., xii+328 pp.
- 1779 Foulger, G. R. (2012), Are 'hot spots' hot spots?, *J. Geodyn.*, 58, 1-28.
- 1780 Foulger, G. R. (2018), Origin of the South Atlantic igneous province, *J. Volc. Geotherm. Res.*, 355, 2-
1781 20.
- 1782 Foulger, G. R., and D. G. Pearson (2001), Is Iceland underlain by a plume in the lower mantle?
1783 Seismology and helium isotopes, *Geophys. J. Int.*, 145, F1-F5.
- 1784 Foulger, G. R., and D. L. Anderson (2005), A cool model for the Iceland hot spot, *J. Volc. Geotherm.
1785 Res.*, 141, 1-22.
- 1786 Foulger, G. R., Z. Du, and B. R. Julian (2003), Icelandic-type crust, *Geophys. J. Int.*, 155, 567-590.
- 1787 Foulger, G. R., J. H. Natland, and D. L. Anderson (2005), A source for Icelandic magmas in remelted
1788 Iapetus crust, *J. Volc. Geotherm. Res.*, 141, 23-44.
- 1789 Foulger, G. R., C. H. Jahn, G. Seeber, P. Einarsson, B. R. Julian, and K. Heki (1992), Post-rifting
1790 stress relaxation at the divergent plate boundary in Northeast Iceland, *Nature*, 358, 488-490.
- 1791 Foulger, G. R., G. F. Panza, I. M. Artemieva, I. D. Bastow, F. Cammarano, J. R. Evans, W. B.
1792 Hamilton, B. R. Julian, M. Lustrino, H. Thybo, and T. B. Yanovskaya (2013), Caveats on
1793 tomographic images, *Terra Nova*, 25, 259-281.
- 1794 Fountain, D. M., T. M. Boundy, H. Austrheim, and P. Rey (1994), Eclogite-facies shear zones—deep
1795 crustal reflectors?, *Tectonophysics*, 232, 411-424.
- 1796 Funck, T., H. R. Jackson, S. A. Dehler, and I. D. Reid (2006), A refraction seismic transect from
1797 Greenland to Ellesmere Island, Canada: The crustal structure in southern Nares Strait,
1798 *Polarforschung*, 74, 94–112.

- 1799 Funck, T., H. R. Jackson, K. E. Loudon, and F. Klingelhoefer (2007), Seismic study of the transform-
 1800 rifted margin in Davis Strait between Baffin Island (Canada) and Greenland: What happens when
 1801 a plume meets a transform, *J. Geophys. Res.*, 112, B04402.
- 1802 Funck, T., M. S. Andersen, J. Keser Neish, and T. Dahl-Jensen (2008), A refraction seismic transect
 1803 from the Faroe Islands to the Hatton-Rockall Basin, *Journal of Geophysical Research: Solid*
 1804 *Earth*, 113.
- 1805 Funck, T., K. Gohl, V. Damm, and I. Heyde (2012), Tectonic evolution of southern Baffin Bay and
 1806 Davis Strait: Results from a seismic refraction transect between Canada and Greenland, *J.*
 1807 *Geophys. Res.*, 117, B04107.
- 1808 Funck, T., W. H. Geissler, G. S. Kimbell, S. Gradmann, O. Erlendsson, K. McDermott, and U. K.
 1809 Petersen (2016), Moho and basement depth in the NE Atlantic Ocean based on seismic refraction
 1810 data and receiver functions, *in* *The NE Atlantic Region: A Reappraisal of Crustal Structure,*
 1811 *Tectonostratigraphy and Magmatic Evolution*, edited by G. Peron-Pinvidic, J. R. Hopper, M. S.
 1812 Stoker, C. Gaina, J. C. Doornenbal, T. Funck and U. E. Arting, pp. 207 - 231, Geological
 1813 Society, London, Special Publications, London.
- 1814 Funck, T., W. H. Geissler, G. S. Kimbell, S. Gradmann, Ö. Erlendsson, K. McDermott, and U. K.
 1815 Petersen (2017), Moho and basement depth in the NE Atlantic Ocean based on seismic refraction
 1816 data and receiver functions, Geological Society, London, Special Publications, 447, 207.
- 1817 Gaina, C., L. Gernigon, and P. Ball (2009), Palaeocene–Recent plate boundaries in the NE Atlantic
 1818 and the formation of the Jan Mayen microcontinent, *Journal of the Geological Society, London,*
 1819 166, 1–16.
- 1820 Gaina, C., A. Nasuti, G. S. Kimbell, and A. Blischke (2017), Break-up and seafloor spreading
 1821 domains in the NE Atlantic, Geological Society, London, Special Publications, 447, 393–417.
- 1822 Gans, P. B. (1987), An open-system, two-layer crustal stretching model for the Eastern Great Basin,
 1823 *Tectonics*, 6, 1–12.
- 1824 Gao, C., H. J. B. Dick, Y. Liu, and H. Zhou (2016), Melt extraction and mantle source at a Southwest
 1825 Indian Ridge Dragon Bone amagmatic segment on the Marion Rise, *Lithos*, 246–247, 48–60.
- 1826 Garde, A. A., M. A. Hamilton, B. Chadwick, J. Grocott, and K. J. McCaffrey (2002), The Ketilidian
 1827 orogen of South Greenland: geochronology, tectonics, magmatism, and fore-arc accretion during
 1828 Palaeoproterozoic oblique convergence, *Canadian Journal of Earth Sciences*, 39, 765–793.
- 1829 Gasser, D. (2014), The Caledonides of Greenland, Svalbard and other Arctic areas: status of research
 1830 and open questions, Geological Society, London, Special Publications, 390, 93.
- 1831 Gebrande, H., H. Miller, and P. Einarsson (1980), Seismic structure of Iceland along RRISP-Profile I,
 1832 *J. Geophys.*, 47, 239–249.
- 1833 Gee, D. G., H. Fossen, N. Henriksen, and A. K. Higgins (2008a), From the Early Paleozoic Platforms
 1834 of Baltica and Laurentia to the Caledonide Orogen of Scandinavia and Greenland, *Episodes*, 31,
 1835 44–51.
- 1836 Gee, D. G., H. Fossen, N. Henriksen, and K. Higgins (2008b), From the early Paleozoic platforms of
 1837 Baltica and Laurentia to the Caledonide orogen of Scandinavia and Greenland, *Episodes*, 44–51.
- 1838 Gee, J. (2015), Caledonides of Scandinavia, Greenland, and Svalbard, *in* *Reference Module in Earth*
 1839 *Systems and Environmental Sciences*, edited by S. A. Elias, Elsevier.
- 1840 Geoffroy, L. (2005), Volcanic passive margins, *Comptes Rendus Geoscience*, 337, 1395–1408.
- 1841 Geoffroy, L., E. B. Burov, and P. Werner (2015), Volcanic passive margins: another way to break up
 1842 continents, *Scientific Reports*, 5, 14828.
- 1843 Geoffroy, L., C. Aubourg, J.-P. Callot, and J.-A. Barrat (2007), Mechanisms of crustal growth in large
 1844 igneous provinces: The north Atlantic province as a case study, *in* *Plates, Plumes, and Planetary*
 1845 *Processes*, edited by G. R. Foulger and D. M. Jurdy, pp. 747–774, Geological Society of
 1846 America, Boulder, CO.
- 1847 Geoffroy, L., H. Guan, L. Gernigon, G. R. Foulger, and P. Werner (submitted), C-Blocks and the
 1848 extent of continental material in oceans: the Laxmi Basin case study, *Geophys. J. Int.*
- 1849 Gernigon, L., J.-C. Ringenbach, S. Planke, and B. L. Gall (2004), Deep structures and breakup along
 1850 volcanic rifted margins: insights from integrated studies along the outer Vøring Basin (Norway),
 1851 *Marine and Petroleum Geology*, 21, 363–372.

- 1852 Gernigon, L., A. Blischke, A. Nasuti, and M. Sand (2015), Conjugate volcanic rifted margins,
 1853 seafloor spreading, and microcontinent: Insights from new high-resolution aeromagnetic surveys
 1854 in the Norway Basin, *Tectonics*, 34.
- 1855 Gernigon, L., F. Lucazeau, F. Brigaud, e.-C. Ringenbach, S. Planke, and B. L. Gall (2006), A
 1856 moderate melting model for the Vøring margin (Norway) based on structural observations and a
 1857 thermo-kinematical modelling: Implication for the meaning of the lower crustal bodies,
 1858 *Tectonophysics*, 412, 255-278.
- 1859 Gernigon, L., C. Gaina, O. Olesen, P. J. Ball, G. Péron-Pinvidic, and T. Yamasaki (2012), The
 1860 Norway Basin revisited: From continental breakup to spreading ridge extinction, *Marine and*
 1861 *Petroleum Geology*, 35, 1-19.
- 1862 Gernigon, L., D. Franke, L. Geoffroy, C. Schiffer, G. R. Foulger, M. Stoker, and e. al. (this volume),
 1863 Crustal fragmentation, magmatism, and the diachronous breakup of the Norwegian-Greenland
 1864 Sea, *Earth-Science Reviews*.
- 1865 Gernigon, L., O. Olesen, J. Ebbing, S. Wienecke, C. Gaina, J. O. Mogaard, M. Sand, and R.
 1866 Myklebust (2009), Geophysical insights and early spreading history in the vicinity of the Jan
 1867 Mayen Fracture Zone, Norwegian–Greenland Sea, *Tectonophysics*, 468, 185–205.
- 1868 Gerya, T. (2011), Origin and models of oceanic transform faults, *Tectonophysics*.
- 1869 Gillard, M., D. Sauter, J. Tugend, S. Tomasi, M.-E. Epin, and G. Manatschal (2017), Birth of an
 1870 oceanic spreading center at a magma-poor rift system, *Scientific Reports*, 7, 15072.
- 1871 Goodwin, T., D. Cox, and J. Trueman (2009), Paleocene sedimentary models in the sub-basalt around
 1872 the Munkagrinnur–East Faroes Ridge, *Proceedings of the Faroe Islands Exploration Conference*,
 1873 2nd Conference, pp. 267–285.
- 1874 Graça, M. C., N. Kuszniir, and N. S. Gomes Stanton (2019), Crustal thickness mapping of the central
 1875 South Atlantic and the geodynamic development of the Rio Grande Rise and Walvis Ridge,
 1876 *Marine and Petroleum Geology*, 101, 230-242.
- 1877 Gradstein, F. M., J. G. Ogg, M. D. Schmitz, and G. M. Ogg (2012), *The Geologic Time Scale 2012*,
 1878 Elsevier, Amsterdam.
- 1879 Greenhalgh, E. E., and N. J. Kuszniir (2007), Evidence for thin oceanic crust on the extinct Aegir
 1880 Ridge, Norwegian Basin, NE Atlantic derived from satellite gravity inversion, *Geophys. Res.*
 1881 *Lett.*, 34, L06305.
- 1882 Grocott, J., and K. J. W. McCaffrey (2017), Basin evolution and destruction in an Early Proterozoic
 1883 continental margin: the Rinkian fold–thrust belt of central West Greenland, *Journal of the*
 1884 *Geological Society*.
- 1885 Guan, H., L. Geoffroy, L. Gernigon, F. Chauvet, C. Grigné, and P. Werner (2019), Magmatic ocean-
 1886 continent transitions, *Marine and Petroleum Geology*, 104, 438-450.
- 1887 Guarnieri, P. (2015), Pre-break-up palaeostress state along the East Greenland margin, *J. geol. Soc.*
 1888 *Lon.*, 172, 727–739.
- 1889 Gudlaugsson, S. T., K. Gunnarsson, M. Sand, and J. Skogseid (1988), Tectonic and volcanic events at
 1890 the Jan Mayen Ridge microcontinent, *in* *Early Tertiary Volcanism and the Opening of the NE*
 1891 *Atlantic*, edited by A. C. Morton and L. M. Parson, pp. 85-93, *Geological Society Special*
 1892 *Publications*.
- 1893 Gudmundsson, O. (2003), The dense root of the Iceland crust, *Earth planet. Sci. Lett.*, 206, 427-440.
- 1894 Haller, J. (1971), *Geology of the East Greenland Caledonides*, Interscience, New York.
- 1895 Hansen, J., D. A. Jerram, K. McCaffrey, and S. R. Passey (2009), The onset of the North Atlantic
 1896 Igneous Province in a rifting perspective, *Geological Magazine*, 146, 309-325.
- 1897 Harry, D. L., D. S. Sawyer, and W. P. Leeman (1993), The mechanics of continental extension in
 1898 western North America: implications for the magmatic and structural evolution of the Great
 1899 Basin, *Earth planet. Sci. Lett.*, 117, 59-71.
- 1900 Heki, K., G. R. Foulger, B. R. Julian, and C.-H. Jahn (1993), Plate dynamics near divergent
 1901 boundaries: Geophysical implications of postrifting crustal deformation in NE Iceland, *J.*
 1902 *Geophys. Res.*, 98, 14279-14297.
- 1903 Henriksen, N. (1999), Conclusion of the 1:500 000 mapping project in the Caledonian fold belt in
 1904 North-East Greenland, *Geology of Greenland Survey Bulletin*, 183, 10-22.

- 1905 Henriksen, N., and A. K. Higgins (1976), East Greenland Caledonian fold belt, *in* *Geology of*
 1906 *Greenland*, edited by A. Escher and W. S. Watt, pp. 182–246, Geological Survey of Greenland,
 1907 Copenhagen.
- 1908 Hermance, J. F., and L. R. Grillo (1974), Constraints on temperatures beneath Iceland from
 1909 magnetotelluric data, *Phys. Earth Planet. Int.*, 8, 1-12.
- 1910 Heron, P., A. Peace, K. McCaffrey, J. K. Welford, R. Wilson, and R. N. Pysklywec (2019),
 1911 Segmentation of rifts through structural inheritance: Creation of the Davis Strait, *Tectonics*, in
 1912 press.
- 1913 Herzberg, C., and P. D. Asimow (2008), Petrology of some oceanic island basalts: PRIMELT2.XLS
 1914 software for primary magma calculation, *Geochemistry, Geophysics, Geosystems*, 9.
- 1915 Herzberg, C., and P. D. Asimow (2015), PRIMELT3 MEGA.XLSM software for primary magma
 1916 calculation: Peridotite primary magma MgO contents from the liquidus to the solidus,
 1917 *Geochemistry, Geophysics, Geosystems*, 16, 563-578.
- 1918 Hey, R., F. Martinez, Á. Höskuldsson, and Á. Benediksdóttir (2008), Propagating Rift Origin of the
 1919 V-Shaped Ridges South of Iceland, paper presented at IAVCEI 2008 General assembly, 17-22
 1920 August, 2008.
- 1921 Hey, R., F. Martinez, A. Höskuldsson, and A. Benediksdóttir (2010), Propagating rift model for the
 1922 V-shaped ridges south of Iceland, *Geochem. Geophys. Geosys.*, 11.
- 1923 Hey, R., F. Martinez, Á. Höskuldsson, D. E. Eason, J. Sleeper, S. Thordarson, Á. Benediksdóttir, and
 1924 S. Merkurjev (2016), Multibeam investigation of the active North Atlantic plate boundary
 1925 reorganization tip, *Earth planet. Sci. Lett.*, 435, 115-123.
- 1926 Hey, R. N., and D. S. Wilson (1982), Propagating rift explanation for the tectonic evolution of the
 1927 northeast Pacific—the pseudomovie, *Earth planet. Sci. Lett.*, 58, 167-188.
- 1928 Hjartarson, A., O. Erlendsson, and A. Blischke (2017), The Greenland–Iceland–Faroe Ridge
 1929 Complex, *in* *The NE Atlantic Region: A Reappraisal of Crustal Structure, Tectonostratigraphy*
 1930 *and Magmatic Evolution*, edited by G. Peron-Pinvidic, J. R. Hopper, M. S. Stoker, C. Gaina, J.
 1931 C. Doornenbal, T. Funck and U. E. Arting, pp. 127-148, Geological Society, London, Special
 1932 Publications.
- 1933 Hofton, M. A., and G. R. Foulger (1996a), Post-rifting anelastic deformation around the spreading
 1934 plate boundary, north Iceland, 2: Implications of the model derived from the 1987-1992
 1935 deformation field, *J. Geophys. Res.*, 101, 25,423 - 425,436.
- 1936 Hofton, M. A., and G. R. Foulger (1996b), Post-rifting anelastic deformation around the spreading
 1937 plate boundary, north Iceland, 1: Modeling of the 1987-1992 deformation field using a
 1938 viscoelastic Earth structure, *JGR*, 101, 25,403 - 425,421.
- 1939 Holbrook, W. S., H. C. Larsen, J. Korenaga, T. Dahl-Jensen, I. D. Reid, P. B. Kelemen, J. R. Hopper,
 1940 G. M. Kent, D. Lizarralde, S. Bernstein, and R. S. Detrick (2001), Mantle thermal structure and
 1941 active upwelling during continental breakup in the north Atlantic, *Earth planet. Sci. Lett.*, 190,
 1942 251-266.
- 1943 Holdsworth, R. E., A. Morton, D. Frei, A. Gerdes, R. A. Strachan, E. Dempsey, C. Warren, and A.
 1944 Whitham (2018), The nature and significance of the Faroe-Shetland Terrane: linking Archaean
 1945 basement blocks across the North Atlantic, *Precamb. Res.*, in press.
- 1946 Hole, M. J. (2015), The generation of continental flood basalts by decompression melting of internally
 1947 heated mantle, *Geology*, 43, 311-314.
- 1948 Hole, M. J., and J. M. Millett (2016), Controls of mantle potential temperature and lithospheric
 1949 thickness on magmatism in the North Atlantic Igneous Province, *J. Pet.*, 57, 417-436.
- 1950 Hole, M. J., and J. H. Natland (this volume), Magmatism in the North Atlantic Igneous Province;
 1951 mantle temperatures, rifting and geodynamics, *Earth-Science Reviews*.
- 1952 Hole, M. J., R. M. Ellam, D. I. M. Macdonald, and S. P. Kelley (2015), Gondwana break-up related
 1953 magmatism in the Falkland Islands, *J. geol. Soc. Lon.*, 173, 108–126.
- 1954 Hopper, J. R., T. Dahl-Jensen, W. S. Holbrook, H. C. Larsen, D. Lizarralde, J. Korenaga, G. M. Kent,
 1955 and P. B. Kelemen (2003), Structure of the SE Greenland margin from seismic reflection and
 1956 refraction data: Implications for nascent spreading center subsidence and asymmetric crustal
 1957 accretion during North Atlantic opening, *Journal of Geophysical Research: Solid Earth*, 108.

- 1958 Huismans, R., and C. Beaumont (2011), Depth-dependent extension, two-stage breakup and cratonic
 1959 underplating at rifted margins, *Nature*, 473, 74.
- 1960 Huismans, R. S., and C. Beaumont (2014), Rifted continental margins: The case for depth-dependent
 1961 extension, *Earth planet. Sci. Lett.*, 407, 148-162.
- 1962 Jamtveit, B., R. Brooker, K. Brooks, L. M. Larsen, and T. Pedersen (2001), The water content of
 1963 olivines from the North Atlantic Volcanic Province, *Earth planet. Sci. Lett.*, 186, 401-415.
- 1964 Johannesson, H., and K. Saemundsson (1998), Geological Map of Iceland at 1/500 000, Geological
 1965 Map of Iceland, 1:500 000. Bedrock Geology.
- 1966 Johnson, H., J. D. Ritchie, K. Hitchen, D. B. McInroy, and G. S. Kimbell (2005), Aspects of the
 1967 Cenozoic deformational history of the northeast Faroe-Shetland Basin, Wyville-Thomson Ridge
 1968 and Hatton Bank areas, *Proceedings of the Petroleum Geology: NW Europe and Global
 1969 Perspectives*, 6th Conference, pp. 993–1007.
- 1970 Jones, E. J. W., R. Siddall, M. F. Thirlwall, P. N. Chroston, and A. J. Lloyd (1994), Anton Dohrn
 1971 Seamount and the evolution of the Rockall Trough, *Oceanologica Acta*, 17, 237-247.
- 1972 Jones, S. M. (2003), Test of a ridge–plume interaction model using oceanic crustal structure around
 1973 Iceland, *Earth planet. Sci. Lett.*, 208, 205-218.
- 1974 Jones, S. M., N. White, and J. Maclennan (2002), V-shaped ridges around Iceland; implications for
 1975 spatial and temporal patterns of mantle convection, *Geochem. Geophys. Geosys.*, 3,
 1976 2002GC000361.
- 1977 Kandilarov, A., R. Mjelde, E. Flueh, and R. B. Pedersen (2015), Vp/Vs-ratios and anisotropy on the
 1978 northern Jan Mayen Ridge, North Atlantic, determined from ocean bottom seismic data, *Polar
 1979 Science*, 9, 293-310.
- 1980 Karato, S.-i., and P. Wu (1993), Rheology of the Upper Mantle: A Synthesis, *Science*, 260, 771.
- 1981 Keen, C. E., and R. R. Boutilier (1995), Lithosphere-asthenosphere interactions below rifts, *Rifted
 1982 Ocean-Continent Boundaries*, 17-30.
- 1983 Keen, C. E., L. T. Dafoe, and K. Dickie (2014), A volcanic province near the western termination of
 1984 the Charlie-Gibbs Fracture Zone at the rifted margin, offshore northeast Newfoundland,
 1985 *Tectonics*, 33, 1133–1153.
- 1986 Keen, C. E., K. Dickie, and L. T. Dafoe (2018), Structural characteristics of the ocean-continent
 1987 transition along the rifted continental margin, offshore central Labrador, *Marine and Petroleum
 1988 Geology*, 89, 443-463.
- 1989 King, S. D. (2005), North Atlantic topographic and geoid anomalies: the result of a narrow ocean
 1990 basin and cratonic roots?, *in Plates, Plumes, and Paradigms*, edited by G. R. Foulger, J.H.
 1991 Natland, D.C. Presnall and D.L. Anderson, pp. 653-664, Geological Society of America,
 1992 Boulder, CO.
- 1993 Klein, E. M., and C. H. Langmuir (1987), Global correlations of ocean ridge basalt chemistry with
 1994 axial depth and crustal thickness, *J. Geophys. Res.*, 92, 8089-8115.
- 1995 Kodaira, S., R. Mjelde, K. Gunnarsson, H. Shiobara, and H. Shimamura (1998), Structure of the Jan
 1996 Mayen microcontinent and implications for its evolution, *Geophys. J. Int.*, 132, 383-400.
- 1997 Korenaga, J. (2004), Mantle mixing and continental breakup magmatism, *Earth planet. Sci. Lett.*, 218,
 1998 463-473.
- 1999 Korenaga, J., and P. B. Kelemen (2000), Major element heterogeneity in the mantle source of the
 2000 north Atlantic igneous province, *Earth planet. Sci. Lett.*, 184, 251-268.
- 2001 Korenaga, J., and W. W. Sager (2012), Seismic tomography of Shatsky Rise by adaptive importance
 2002 sampling, *Journal of Geophysical Research: Solid Earth*, 117.
- 2003 Korenaga, J., P. B. Kelemen, and W. S. Holbrook (2002), Methods for resolving the origin of large
 2004 igneous provinces from crustal seismology, *J. Geophys. Res.*, 107, 2178,
 2005 doi:2110.1029/2001JB001030.
- 2006 Krabbendam, M. (2001), When the Wilson Cycle breaks down: how orogens can produce strong
 2007 lithosphere and inhibit their future reworking, Geological Society, London, Special Publications,
 2008 184, 57.
- 2009 Kumar, P., R. Kind, K. Priestley, and T. Dahl-Jensen (2007), Crustal structure of Iceland and
 2010 Greenland from receiver function studies, *Journal of Geophysical Research: Solid Earth*, 112.

- 2011 Kurashimo, E., M. Shinohara, K. Suyehiro, J. Kasahara, and N. Hirata (1996), Seismic evidence for
 2012 stretched continental crust in the Japan Sea, *Geophys. Res. Lett.*, 23, 3067-3070.
- 2013 Kuszniir, N., and e. al. (2018), Intra-ocean Ridge Jumps, *Oceanic Plateaus & Upper Mantle*
 2014 Inheritance, *Earth Science Reviews*, submitted.
- 2015 Kuszniir, N. J., and G. D. Karner (2007), Continental lithospheric thinning and breakup in response to
 2016 upwelling divergent mantle flow: application to the Woodlark, Newfoundland and Iberia
 2017 margins, *in* *Imaging, Mapping and Modelling Continental Lithosphere Extension and Breakup*,
 2018 edited by G. D. Karner, G. Manatschal and L. M. Pinheiro, pp. 389-419, Geological Society of
 2019 London, Special Publications.
- 2020 Lamers, E., and S. M. M. Carmichael (1999), The Paleocene deepwater sandstone play West of
 2021 Shetland, *Proceedings of the Petroleum Geology of Northwest Europe, 5th Conference*, pp. 645–
 2022 659.
- 2023 Larsen, L. M., R. Waagstein, A. K. Pedersen, and M. Storey (1999), Trans-Atlantic correlation of the
 2024 Palaeogene volcanic successions in the Faeroe Islands and East Greenland, *Journal of the*
 2025 *Geological Society*, 156, 1081-1095.
- 2026 Larsen, L. M., L. M. Heaman, R. A. Creaser, R. A. Duncan, R. Frei, and M. Hutchinson (2009),
 2027 Tectonomagnetic events during stretching and basin formation in the Labrador Sea and the Davis
 2028 Strait: evidence from age and composition of Mesozoic to Palaeogene dyke swarms in West
 2029 Greenland, *Journal of the Geological Society, London*, 166, 999–1012.
- 2030 Lundin, E., and T. Doré (2005), The fixity of the Iceland "hotspot" on the Mid-Atlantic Ridge:
 2031 observational evidence, mechanisms and implications for Atlantic volcanic margins, *in* *Plates,*
 2032 *Plumes, and Paradigms*, edited by G. R. Foulger, J.H. Natland, D.C. Presnall and D.L. Anderson,
 2033 pp. 627-652, Geological Society of America.
- 2034 Lundin, E. R., and A. G. Doré (2011), Hyperextension, serpentinitization, and weakening: A new
 2035 paradigm for rifted margin compressional deformation, *Geology*, 39, 347-350.
- 2036 Lundin, E. R., and A. G. Doré (2018), Non-Wilsonian break-up predisposed by transforms: examples
 2037 from the North Atlantic and Arctic, *in* *Fifty Years of the Wilson Cycle Concept in Plate*
 2038 *Tectonics*, edited by R. W. Wilson, G. A. Houseman, K. J. W. Mccaffrey, A. G. Doré and S. J.
 2039 H. Buiter, Geological Society, London, Special Publications.
- 2040 Lundin, E. R., A. G. Doré, and T. F. Redfield (2018), Magmatism and extension rates at rifted
 2041 margins, *Petroleum Geoscience*.
- 2042 Manton, B., S. Planke, D. Zastrozhnov, M. M. Abdelmalak, J. Millett, D. Maharjan, S. Polteau, J. I.
 2043 Faleide, L. Gernigon, and R. Myklebust (2018), Pre-Cretaceous Prospectivity of the Outer Møre
 2044 and Vøring Basins Constrained by New 3D Seismic Data, paper presented at 80th EAGE
 2045 Conference and Exhibition.
- 2046 Marquart, G. (1991), Interpretations of Geoid Anomalies around the Iceland Hotspot, *Geophys. J. Int.*,
 2047 106, 149-160.
- 2048 Martinez, F., and R. N. Hey (this volume), Reykjanes Ridge evolution by plate kinematics and
 2049 propagating small-scale mantle convection within a regional upper mantle anomaly, *Earth-*
 2050 *Science Reviews*.
- 2051 Martinez, F., R. J. Stern, K. A. Kelley, Y. Ohara, J. D. Sleeper, J. M. Ribeiro, and M. Brounce (2018),
 2052 Diffuse extension of the southern Mariana margin, *J. Geophys. Res.*, 123, 892–916.
- 2053 Martínez, F., R. N. Hey, and P. D. Johnson (1997), The East ridge system 28.5–32°S East Pacific rise:
 2054 Implications for overlapping spreading center development, *Earth planet. Sci. Lett.*, 151, 13-31.
- 2055 Mason, A. J., R. R. Parrish, and T. S. Brewer (2004), U–Pb geochronology of Lewisian orthogneisses
 2056 in the Outer Hebrides, Scotland: implications for the tectonic setting and correlation of the South
 2057 Harris Complex, *Journal of the Geological Society*, 161, 45.
- 2058 Matthews, S., O. Shorttle, and J. Maclennan (2016), The temperature of the Icelandic mantle from
 2059 olivine-spinel aluminum exchange thermometry, *Geochemistry, Geophysics, Geosystems*, 17,
 2060 4725-4752.
- 2061 McKenzie, D., and J. Jackson (2002), Conditions for flow in the continental crust, *Tectonics*, 21, 5-1-
 2062 5-7.
- 2063 Meissner, R. (1999), Terrane accumulation and collapse in central Europe: seismic and rheological
 2064 constraints, *Tectonophysics*, 305, 93-107.

- 2065 Menke, W. (1999), Crustal isostasy indicates anomalous densities beneath Iceland, *Geophys. Res.*
 2066 *Lett.*, 26, 1215-1218.
- 2067 Menke, W., and V. Levin (1994), Cold crust in a hot spot, *Geophys. Res. Lett.*, 21, 1967-1970.
- 2068 Menke, W., V. Levin, and R. Sethi (1995), Seismic attenuation in the crust at the mid-Atlantic plate
 2069 boundary in south-west Iceland, *Geophys. J. Int.*, 122, 175-182.
- 2070 Meyer, R., J. G. H. Hertogen, R. B. Pedersen, L. Viereck-Götte, and M. Abratis (2009), Elements and
 2071 isotopic measurements of magmatic rock samples from ODP Hole 104-642E, in Supplement to:
 2072 Meyer, R. et al. (2009): Interaction of mantle derived melts with crust during the emplacement of
 2073 the Vøring Plateau, N.E. Atlantic. *Marine Geology*, 261(1-4), 3-16, edited, PANGAEA.
- 2074 Mjelde, R., A. Goncharov, and R. D. Müller (2013), The Moho: Boundary above upper mantle
 2075 peridotites or lower crustal eclogites? A global review and new interpretations for passive
 2076 margins, *Tectonophysics*, 609, 636-650.
- 2077 Mjelde, R., S. Kodaira, H. Shimamura, T. Kanazawa, H. Shiobara, E. W. Berg, and O. Riise (1997),
 2078 Crustal structure of the central part of the Vøring Basin, mid-Norway margin, from ocean bottom
 2079 seismographs, *Tectonophysics*, 277, 235-257.
- 2080 Mjelde, R., R. Aurvåg, S. Kodaira, H. Shimamura, K. Gunnarsson, A. Nakanishi, and H. Shiobara
 2081 (2002), Vp/Vs-ratios from the central Kolbeinsey Ridge to the Jan Mayen Basin, North Atlantic;
 2082 implications for lithology, porosity and present-day stress field, *Mar. Geophys. Res.*, 23, 123-
 2083 145.
- 2084 Mjelde, R., P. Digranes, H. Shimamura, H. Shiobara, S. Kodaira, H. Brekke, T. Egebjerg, N. Sørenes,
 2085 and S. Thorbjørnsen (1998), Crustal structure of the northern part of the Vøring Basin, mid-
 2086 Norway margin, from wide-angle seismic and gravity data, *Tectonophysics*, 293, 175-205.
- 2087 Mjelde, R., P. Digranes, M. Van Schaack, H. Simamura, H. Shiobara, S. Kodaira, O. Naess, N.
 2088 Sørenes, and E. Vagnes (2001), Crustal structure of the outer Voring Plateau, offshore Norway,
 2089 from ocean bottom seismic and gravity data, *J. Geophys. Res.*, 106, 6769-6791.
- 2090 Mudge, D. C. (2015), Regional controls on Lower Tertiary sandstone distribution in the North Sea
 2091 and NE Atlantic margin basins, *in* Tertiary Deep-Marine Reservoirs of the North Sea Region,
 2092 edited by T. McKie, P. T. S. Rose, A. J. Hartley, D. W. Jones and T. L. Armstrong, pp. 17-42,
 2093 Geological Society, London, Special Publications.
- 2094 Müller, R. D., M. Seton, S. Zahirovic, S. E. Williams, K. J. Matthews, N. M. Wright, G. E. Shephard,
 2095 K. T. Maloney, N. Barnett-Moore, M. Hosseinpour, D. J. Bower, and J. Cannon (2016), Ocean
 2096 basin evolution and global-scale plate reorganization events since Pangea breakup, *Ann. Rev.*
 2097 *Earth Planet. Sci.*, 44, 107.
- 2098 Muñoz, G., A. Mateus, J. Pous, W. Heise, F. Monteiro Santos, and E. Almeida (2008), Unraveling
 2099 middle-crust conductive layers in Paleozoic Orogens through 3D modeling of magnetotelluric
 2100 data: The Ossa-Morena Zone case study (SW Iberian Variscides), *Journal of Geophysical*
 2101 *Research: Solid Earth*, 113.
- 2102 Müntener, O., G. Manatschal, L. Desmurs, and T. Pettke (2010), Plagioclase Peridotites in Ocean-
 2103 Continent Transitions: Refertilized Mantle Domains Generated by Melt Stagnation in the
 2104 Shallow Mantle Lithosphere, *J. Pet.*, 51, 255-294.
- 2105 Mutter, J. C., and C. M. Zehnder (1988), Deep crustal structure and magmatic processes; the inception
 2106 of seafloor spreading in the Norwegian-Greenland Sea, *in* Early Tertiary volcanism and the
 2107 opening of the NE Atlantic, edited by A. C. Morton and L. M. Parson, pp. 35-48.
- 2108 Natland, J. H. (2003), Capture of helium and other volatiles during the growth of olivine phenocrysts
 2109 in picritic basalts from the Juan Fernandez Islands, *J. Pet.*, 44, 421-456.
- 2110 Nemčok, M., and S. Rybár (2017), Rift-drift transition in a magma-rich system: the Gop Rift-Laxmi
 2111 Basin case study, West India, Geological Society, London, Special Publications, 445, 95.
- 2112 Nichols, A. R. L., M. R. Carroll, and A. Hoskuldsson (2002), Is the Iceland hot spot also wet?
 2113 Evidence from the water contents of undegassed submarine and subglacial pillow basalts, *Earth*
 2114 *planet. Sci. Lett.*, 202, 77-87.
- 2115 Nirrengarten, M., G. Manatschal, J. Tugend, N. Kuznir, and D. Sauter (2018), Kinematic Evolution
 2116 of the Southern North Atlantic: Implications for the Formation of Hyperextended Rift Systems,
 2117 *Tectonics*, 37, 89-118.

- 2118 O'Reilly, B. M., F. Hauser, A. W. B. Jacob, and P. M. Shannon (1996), The lithosphere below the
2119 Rockall Trough: wide-angle seismic evidence for extensive serpentinisation, *Tectonophysics*,
2120 255, 1-23.
- 2121 Oakey, G. N., and J. A. Chalmers (2012), A new model for the Paleogene motion of Greenland
2122 relative to North America: Plate reconstructions of the Davis Strait and Nares Strait regions
2123 between Canada and Greenland, *Journal of Geophysical Research: Solid Earth*, 117.
- 2124 Ólavsdóttir, J., L. O. Boldreel, and M. S. Andersen (2010), Development of a shelf-margin delta due
2125 to uplift of Munkagrúnnut Ridge at the margin of Faroe-Shetland Basin: a seismic sequence
2126 stratigraphic study, *Petroleum Geoscience*, 16, 91-103.
- 2127 Ólavsdóttir, J., M. S. Andersen, and L. O. Boldreel (2013a), Seismic stratigraphic analysis of the
2128 Cenozoic sediments in the NW Faroe–Shetland Basin Implications for inherited structural
2129 control of sediment distribution, *Marine and Petroleum Geology*, 46, 19–35.
- 2130 Ólavsdóttir, J., M. S. Andersen, and L. O. Boldreel (2013b), Seismic stratigraphic analysis of the
2131 Cenozoic sediments in the NW Faroe Shetland Basin—Implications for inherited structural
2132 control of sediment distribution, *Marine and Petroleum Geology*, 46, 19-35.
- 2133 Ólavsdóttir, J., Ó. R. Eidesgaard, and M. S. Stoker (2017), The stratigraphy and structure of the
2134 Faroese continental margin, *in* *The NE Atlantic Region: A Reappraisal of Crustal Structure,*
2135 *Tectonostratigraphy and Magmatic Evolution*, edited by G. Péron-Pinvidic, J. R. Hopper, M. S.
2136 Stoker, C. Gaina, J. C. Doornenbal, T. Funck and U. E. Ártung, pp. 339–356, Geological Society,
2137 London, Special Publications, London.
- 2138 Palmason, G. (1971), Crustal structure of Iceland from explosion seismology, *Soc. Sci. Isl. Greinar V*,
2139 187 pp., Reykjavik.
- 2140 Paquette, J., O. Sigmarrsson, and M. Tiepolo (2006), Continental basement under Iceland revealed by
2141 old zircons, paper presented at American Geophysical Union, Fall Meeting.
- 2142 Parman, S. W., Kurz, M.D. , S. R. Hart, and T. L. Grove (2005), Helium solubility in olivine and
2143 implications for high $^3\text{He}/^4\text{He}$ in ocean island basalts, *Nature*, 437, 1140-1143.
- 2144 Passey, S. R., and D. W. Jolley (2009), A revised lithostratigraphic nomenclature for the Palaeogene
2145 Faroe Islands basalt Group, NE Atlantic ocean, *Earth and Environmental Science Transaction of*
2146 *the Royal Society of Edinburgh*, 99, 127-158.
- 2147 Peace, A., K. McCaffrey, J. Imber, J. Hunen, R. Hobbs, and R. Wilson (2018), The role of pre-
2148 existing structures during rifting, continental breakup and transform system development,
2149 offshore West Greenland, *Basin Research*, 30, 373-394.
- 2150 Peace, A., K. McCaffrey, J. Imber, J. Phethean, G. Nowell, K. Gerdes, and E. Dempsey (2016), An
2151 evaluation of Mesozoic rift-related magmatism on the margins of the Labrador Sea: Implications
2152 for rifting and passive margin asymmetry, *Geosphere*, 12.
- 2153 Peace, A. J., D. Franke, A. Doré, G. R. Foulger, N. Kuszniir, J. G. McHone, J. Phethean, S. Rocchi, S.
2154 Schiffer, M. Schnabel, and J. K. Welford (this volume), Pangea dispersal and Large Igneous
2155 Provinces – in search for causative mechanisms, *Earth-Science Reviews*.
- 2156 Peace, A. L., G. R. Foulger, C. Schiffer, and K. J. W. McCaffrey (2017), Evolution of Labrador Sea-
2157 Baffin Bay: Plate or plume processes?, *Geoscience Canada*, 44, 91-102.
- 2158 Peace, A. L., E. D. Dempsey, C. Schiffer, J. K. Welford, and J. W. Ken (submitted), Evidence for
2159 basement reactivation during the opening of the Labrador Sea from the Makkovik Province,
2160 Labrador, Canada: Insights from field-data and numerical models, *Geosciences*.
- 2161 Perlt, J., M. Heinert, and W. Niemeier (2008), The continental margin in Iceland — A snapshot
2162 derived from combined GPS networks, *Tectonophysics*, 447, 155-166.
- 2163 Peron-Pinvidic, G., and G. Manatschal (2010), From microcontinents to extensional allochthons:
2164 witnesses of how continents rift and break apart?, *Petroleum Geoscience*, 16, 1-10.
- 2165 Peron-Pinvidic, G., G. Manatschal, and P. T. Osmundsen (2013), Structural comparison of archetypal
2166 Atlantic rifted margins: A review of observations and concepts, *Marine and Petroleum Geology*,
2167 43, 21-47.
- 2168 Peron-Pinvidic, G., L. Gernigon, C. Gaina, and P. Ball (2012), Insights from the Jan Mayen system in
2169 the Norwegian–Greenland sea—I. Mapping of a microcontinent, *Geophys. J. Int.*, 191, 385-412.

- 2170 Perram, L. J., M.-H. Cormier, and K. C. Macdonald (1993), Magnetic and tectonic studies of the
 2171 dueling propagating spreading centers at 20°40'S on the East Pacific Rise: Evidence for crustal
 2172 rotations, *Journal of Geophysical Research: Solid Earth*, 98, 13835-13850.
- 2173 Petersen, K., J. Armitage, S. Nielsen, and H. Thybo (2015), Mantle temperature as a control on the
 2174 time scale of thermal evolution of extensional basins. , *Earth planet. Sci. Lett.*, 409, 61–70.
- 2175 Petersen, K. D., and C. Schiffer (2016), Wilson Cycle Passive Margins: Control of orogenic
 2176 inheritance on continental breakup, *Gondwana Research*, 39, 131-144.
- 2177 Petersen, K. D., C. Schiffer, and T. Nagel (2018), LIP formation and protracted lower mantle
 2178 upwelling induced by rifting and delamination, *Scientific Reports*, 8, 16578.
- 2179 Pharaoh, T. C. (1999), Palaeozoic terranes and their lithospheric boundaries within the Trans-
 2180 European Suture Zone (TESZ): a review, *Tectonophysics*, 314, 17-41.
- 2181 Planke, S., P. A. Symonds, E. Alvestad, and J. Skogseid (2000), Seismic volcanostratigraphy of large-
 2182 volume basaltic extrusive complexes on rifted margins, *Journal of Geophysical Research: Solid
 2183 Earth*, 105, 19335-19351.
- 2184 Pollitz, F. F., and I. S. Sacks (1996), Viscosity structure beneath northeast Iceland, *JGR*, 101, 17,771-
 2185 717,793.
- 2186 Presnall, D., and G. Gudfinnsson (2011), Oceanic volcanism from the low-velocity zone – without
 2187 mantle plumes, *J. Pet.*, 52, 1533-1546.
- 2188 Presnall, D. C., and G. Gudfinnsson (2007), Global Na8-Fe8 Systematics of MORBs: Implications for
 2189 Mantle Heterogeneity, Temperature, and Plumes, paper presented at European Geophysical
 2190 Union General Assembly, 15-20 April, 2007.
- 2191 Prestvik, T., S. Goldberg, H. Karlsson, and K. Gronvold (2001), Anomalous strontium and lead
 2192 isotope signatures in the off-rift Oraefajokull central volcano in south-east Iceland. Evidence for
 2193 enriched endmember(s) of the Iceland mantle plume?, *Earth planet. Sci. Lett.*, 190, 211-220.
- 2194 Putirka, K. D. (2008), Excess temperatures at ocean islands: Implications for mantle layering and
 2195 convection, *Geology*, 36, 283-286.
- 2196 Quick, J. E., S. Sinigoi, and A. Mayer (1995), Emplacement of mantle peridotite in the lower
 2197 continental crust, Ivrea-Verbano zone, northwest Italy, *Geology*, 23, 739-742.
- 2198 Ranalli, G. (1995), *Rheology of the Earth*, Springer.
- 2199 Reston, T. J., J. Pennell, A. Stubenrauch, I. Walker, and M. Pérez-Gussinyé (2001), Detachment
 2200 faulting, mantle serpentinitization, and serpentinite- mud volcanism beneath the Porcupine Basin,
 2201 southwest of Ireland, *Geology*, 29, 587-590.
- 2202 Reynisson, R. F., J. Ebbing, E. Lundin, and P. T. Osmundsen (2011), Properties and distribution of
 2203 lower crustal bodies on the mid-Norwegian margin, edited, pp. 843-854, Geological Society,
 2204 London.
- 2205 Ribe, N. M., U. R. Christensen, and J. Theissing (1995), The dynamics of plume-ridge interaction, 1:
 2206 Ridge-centered plumes, *Earth planet. Sci. Lett.*, 134, 155-168.
- 2207 Richard, K. R., R. S. White, R. W. England, and J. Fruehn (1999), Crustal structure east of the Faroe
 2208 Islands; mapping sub-basalt sediments using wide-angle seismic data, *Petroleum Geoscience*, 5,
 2209 161-172.
- 2210 Rickers, F., A. Fichtner, and J. Trampert (2013), The Iceland–Jan Mayen plume system and its impact
 2211 on mantle dynamics in the North Atlantic region: Evidence from full-waveform inversion, *Earth
 2212 planet. Sci. Lett.*, 367, 39-51.
- 2213 Ritchie, J. D., H. D. Johnson, M. F. Quinn, and R. W. Gatliff (2008), Cenozoic compressional
 2214 deformation within the Faroe-Shetland Basin and adjacent areas, *in The Nature and Origin of
 2215 Compression in Passive Margins*, edited by H. D. Johnson, A. G. Doré, R. E. Holdsworth, R. W.
 2216 Gatliff, E. R. Lundin and J. D. Ritchie, pp. 121–136, Geological Society, London, Special
 2217 Publications.
- 2218 Roberts, D. (2003), The Scandinavian Caledonides: event chronology, palaeogeographic settings and
 2219 likely, modern analogues, *Tectonophysics*, 365, 283-299.
- 2220 Roberts, D. G., M. Thompson, B. Mitchener, J. Hossack, S. Carmichael, and H. M. Bjornseth (1999),
 2221 Palaeozoic to Tertiary rift and basin dynamics: mid-Norway to the Bay of Biscay – a new context
 2222 for hydrocarbon prospectivity in the deep water frontier, *Proceedings of the 5th Conference of
 2223 the Petroleum Geology of Northwest Europe*, London, pp. 7-40.

- 2224 Roest, W. R., and S. P. Srivastava (1989), Sea-floor spreading in the Labrador Sea: a new
2225 reconstruction, *Geology*, 17, 1000–1003.
- 2226 Rognvaldsson, S. T., A. Gudmundsson, and R. Slunga (1998), Seismotectonic analysis of the Tjornes
2227 Fracture Zone, an active transform fault in north Iceland, *Journal of Geophysical Research-Solid
2228 Earth*, 103, 30117-30129.
- 2229 Royden, L. (1996), Coupling and decoupling of crust and mantle in convergent orogens: Implications
2230 for strain partitioning in the crust, *Journal of Geophysical Research: Solid Earth*, 101, 17679-
2231 17705.
- 2232 Rudnick, R. L., and D. M. Fountain (1995), Nature and composition of the continental crust: A lower
2233 crustal perspective, *Rev. Geophys.*, 33, 267-309.
- 2234 Rutter, E. H., K. H. Brodie, and P. J. Evans (1993), Structural geometry, lower crustal magmatic
2235 underplating and lithospheric stretching in the Ivrea-Verbano zone, northern Italy, *J. Str. Geol.*,
2236 15, 647-662.
- 2237 Sallares, V., and P. Charvis (2003), Crustal thickness constraints on the geodynamic evolution of the
2238 Galápagos volcanic province, *Earth planet. Sci. Lett.*, 214, 545-559.
- 2239 Sandwell, D. T., R. D. Müller, W. H. F. Smith, E. Garcia, and R. Francis (2014), New global marine
2240 gravity model from CryoSat-2 and Jason-1 reveals buried tectonic structure, *Science*, 346, 65.
- 2241 Santos Ventura, R., C. E. Ganade, C. M. Lacasse, I. S. L. Costa, I. Pessanha, E. P. Frazão, E. L.
2242 Dantas, and J. A. Cavalcante (2019), Dating Gondwanan continental crust at the Rio Grande
2243 Rise, South Atlantic, *Terra Nova*, 0.
- 2244 Sarafian, E., G. A. Gaetani, E. H. Hauri, and A. R. Sarafian (2017), Experimental constraints on the
2245 damp peridotite solidus and oceanic mantle potential temperature, *Science*, 355, 942-945.
- 2246 Sato, H., I. S. Sacks, T. Murase, G. Muncill, and H. Fukuyama (1989), Qp-melting temperature
2247 relation in peridotite at high pressure and temperature: Attenuation mechanism and implications
2248 for the mechanical properties of the upper mantle, *J. Geophys. Res.*, 94, 10647-10661.
- 2249 Schaltegger, U., H. E. F. Amundsen, B. Jamtveit, M. Frank, W. L. Griffin, K. Gronvold, R. G.
2250 Tronnes, and T. Torsvik (2002), Contamination of OIB by underlying ancient continental
2251 lithosphere: U-Pb and Hf isotopes in zircons question EM1 and EM2 mantle components,
2252 *Geochim. Cosmochim. Acta*, 66, A673.
- 2253 Schiffer, C., N. Balling, B. H. Jacobsen, R. A. Stephenson, and S. B. (2014), Seismological evidence
2254 for a fossil subduction zone in the East Greenland Caledonides, *Geology*, 42, 311-314.
- 2255 Schiffer, C., N. Balling, J. Ebbing, B. H. Jacobsen, and S. B. Nielsen (2016), Geophysical-
2256 petrological modelling of the East Greenland Caledonides - Isostatic support from crust and
2257 upper mantle, *Tectonophysics*, 692, 44-57.
- 2258 Schiffer, C., C. Tegner, A. J. Schaeffer, V. Pease, and S. B. Nielsen (2017), High Arctic geopotential
2259 stress field and implications for geodynamic evolution, *Geological Society, London, Special
2260 Publications*, 460.
- 2261 Schiffer, C., R. A. Stephenson, K. D. Petersen, S. B. Nielsen, B. H. Jacobsen, N. Balling, and D. I. M.
2262 Macdonald (2015), A sub-crustal piercing point for North Atlantic reconstructions and tectonic
2263 implications, *Geology*, 43, 1087-1090.
- 2264 Schiffer, C., A. Peace, J. Phethean, K. McCaffrey, L. Gernigon, K. D. Petersen, and G. Foulger
2265 (2018), The Jan Mayen Microplate Complex and the Wilson Cycle, *in Tectonic Evolution: 50
2266 Years of the Wilson Cycle Concept*, edited by G. Houseman, Geological Society of London
- 2267 Schiffer, C., A. G. Doré, G. R. Foulger, D. Franke, L. Geoffroy, L. Gernigon, B. Holdsworth, N.
2268 Kuszniir, E. Lundin, K. McCaffrey, A. Peace, K. D. Petersen, R. Stephenson, M. S. Stoker, and
2269 K. Welford (this volume), The role of tectonic inheritance in the evolution of the North Atlantic,
2270 *Earth-Science Reviews*.
- 2271 Schlindwein, V., and W. Jokat (2000), Post-collisional extension of the East Greenland Caledonides:
2272 a geophysical perspective, *Geophys. J. Int.*, 140, 550-567.
- 2273 Schmidt-Aursch, M. C., and W. Jokat (2005), The crustal structure of central East Greenland—II:
2274 From the Precambrian shield to the recent mid-oceanic ridges, *Geophys. J. Int.*, 160, 753-760.
- 2275 Shen, F., L. H. Royden, and B. C. Burchfiel (2001), Large-scale crustal deformation of the Tibetan
2276 Plateau, *Journal of Geophysical Research: Solid Earth*, 106, 6793-6816.

- 2277 Shih, J., and P. Molnar (1975), Analysis and implications of the sequence of ridge jumps that
2278 eliminated the Surveyor Transform Fault, *J. Geophys. Res.*, 80, 4815-4822.
- 2279 Shorttle, O., J. Maclennan, and A. M. Piotrowski (2013), Geochemical provincialism in the Iceland
2280 plume, *Geochim. Cosmochim. Acta*, 122, 363-397.
- 2281 Sigmundsson, F. (1991), Post-glacial rebound and asthenosphere viscosity in Iceland, *Geophys. Res.*
2282 *Lett.*, 18, 1131-1134.
- 2283 Simon, K., R. S. Huisman, and C. Beaumont (2009), Dynamical modelling of lithospheric extension
2284 and small-scale convection: implications for magmatism during the formation of volcanic rifted
2285 margins, *Geophys. J. Int.*, 176, 327-350.
- 2286 Skogseid, J., S. Planke, J. I. Faleide, T. Pedersen, O. Eldholm, and F. Neverdal (2000), NE Atlantic
2287 continental rifting and volcanic margin formation, *in* *Dynamics of the Norwegian Margin*, edited
2288 by A. Nottvedt, pp. 295-326.
- 2289 Slagstad, T., Y. Maystrenko, V. Maupin, and S. Gradmann (2017), An extinct, Late Mesoproterozoic,
2290 Sveconorwegian mantle wedge beneath SW Fennoscandia, reflected in seismic tomography and
2291 assessed by thermal modelling, *Terra Nova*, 30, 72-77.
- 2292 Smith, W. H. F., and D. T. Sandwell (1997), Global Sea Floor Topography from Satellite Altimetry
2293 and Ship Depth Soundings, *Science*, 277, 1956.
- 2294 Smythe, D. K., A. Dobinson, R. McQuillin, J. A. Brewer, D. H. Matthews, D. J. Blundell, and B.
2295 Kelk (1982), Deep structure of the Scottish Caledonides revealed by the MOIST reflection
2296 profile, *Nature*, 299, 338-340.
- 2297 Soper, N. J., R. A. Strachan, R. E. Holdsworth, R. A. Gayer, and R. O. Greilung (1992), Sinistral
2298 transpression and the Silurian closure of Iapetus, *Journal - Geological Society (London)*, 149,
2299 871-880.
- 2300 Spice, H. E., J. G. Fitton, and L. A. Kirstein (2016), Temperature fluctuation of the Iceland mantle
2301 plume through time, *Geochemistry, Geophysics, Geosystems*, 17, 243-254.
- 2302 Srivastava, S., B. MacLean, R. Macnab, H. Jackson, A. Embry, and H. Balkwill (1982), Davis Strait:
2303 structure and evolution as obtained from a systematic geophysical survey, *Proceedings of the*
2304 *Third International Symposium on Arctic Geology, Calgary, Alberta*, pp. 267-278.
- 2305 Srivastava, S. P. (1978), Evolution of the Labrador Sea and its bearing on the early evolution of the
2306 North Atlantic, *Geophys. J. Int.*, 52, 313-357.
- 2307 St-Onge, M. R., J. A. M. V. Gool, A. A. Garde, and D. J. Scott (2009), Correlation of Archaean and
2308 Palaeoproterozoic units between northeastern Canada and western Greenland: constraining the
2309 pre-collisional upper plate accretionary history of the Trans-Hudson orogen, *in* *Earth*
2310 *Accretionary Systems in Space and Time*, edited by P. A. Cawood and A. Kröner, pp. 193-235,
2311 Geological Society of London.
- 2312 Staples, R. K., R. S. White, B. Brandsdottir, W. Menke, P. K. H. Maguire, and J. H. McBride (1997),
2313 Faeroe-Iceland ridge experiment 1. Crustal structure of northeastern Iceland, *JGR*, 102, 7849-
2314 7866.
- 2315 Starkey, N. A., F. M. Stuart, R. M. Ellam, J. G. Fitton, S. Basu, and L. M. Larsen (2009), Helium
2316 isotopes in early Iceland plume picrites: constraints on the composition of high $^3\text{He}/^4\text{He}$ mantle,
2317 *Earth planet. Sci. Lett.*, 277, 91-100.
- 2318 Steffen, R., G. Strykowski, and B. Lund (2017), High-resolution Moho model for Greenland from
2319 EIGEN-6C4 gravity data, *Tectonophysics*, 706-707, 206-220.
- 2320 Stixrude, L., and C. Lithgow-Bertelloni (2011), Thermodynamics of mantle minerals – II. Phase
2321 equilibria, *Geophys. J. Int.*, 184, 1180-1213.
- 2322 Stoker, M. S., A. B. Leslie, and K. Smith (2013), A record of Eocene (Stronsay Group) sedimentation
2323 in BGS borehole 99/3, offshore NW Britain: implications for early post-rift development of the
2324 Faeroe-Shetland Basin, *Scottish Journal of Geology*, 49, 133-148.
- 2325 Stoker, M. S., S. P. Holford, and R. R. Hillis (2018), A rift-to-drift record of vertical crustal motions
2326 in the Faeroe-Shetland Basin, NW European margin: establishing constraints on NE Atlantic
2327 evolution, *Journal of the Geological Society*, 175, 263-274.
- 2328 Stoker, M. S., G. S. Kimbell, D. B. McInroy, and A. C. Morton (2012), Eocene post-rift
2329 tectonostratigraphy of the Rockall Plateau, Atlantic margin of NW Britain: Linking early
2330 spreading tectonics and passive margin response, *Marine and Petroleum Geology*, 30, 98-125.

- 2331 Stoker, M. S., D. Praeg, J. S. Hjelstuen, J. S. Laberg, T. Nielsen, and P. M. Shannon (2005a),
 2332 Neogene stratigraphy and the sedimentary and oceanographic development of the NW European
 2333 Atlantic margin, *Marine and Petroleum Geology*, 22, 977–1005.
- 2334 Stoker, M. S., D. Praeg, P. M. Shannon, B. O. Hjelstuen, J. S. Laberg, T. Nielsen, T. C. E. van
 2335 Weering, H. P. Sejrup, and D. Evans (2005b), Neogene evolution of the Atlantic continental
 2336 margin of NW Europe (Lofoten Islands to SW Ireland): anything but passive, *in* *Petroleum*
 2337 *Geology: North-West Europe and Global Perspectives—Proceedings of the 6th Petroleum*
 2338 *Geology Conference*, edited by A. G. Doré and B. A. Vining, pp. 1057-1076, Geological Society,
 2339 London.
- 2340 Stoker, M. S., R. J. Hoult, T. Nielsen, J. S. Hjelstuen, J. S. Laberg, P. M. Shannon, D. Praeg, A.
 2341 Mathiesen, T. C. E. van Weering, and A. M. McDonnell (2005c), Sedimentary and
 2342 oceanographic responses to early Neogene compression on the NW European margin, *Marine*
 2343 *and Petroleum Geology*, 22, 1031–1044.
- 2344 Stoker, M. S., M. A. Stewart, P. M. Shannon, M. Bjerager, T. Nielsen, A. Blischke, B. O. Hjelstuen,
 2345 C. Gaina, K. McDermott, and J. Ólavsdóttir (2017), An overview of the Upper Palaeozoic-
 2346 Mesozoic stratigraphy of the NE Atlantic margin, *in* *The NE Atlantic Region: A Reappraisal of*
 2347 *Crustal Structure, Tectonostratigraphy and Magmatic Evolution*, edited by G. Péron-Pinvidic, J.
 2348 R. Hopper, M. S. Stoker, C. Gaina, J. C. Doornenbal, T. Funck and U. E. Ártung, pp. 11-68,
 2349 Geological Society, London, Special Publications.
- 2350 Stuart, F. M., S. Lass-Evans, J. G. Fitton, and R. M. Ellam (2003), High $3\text{He}/4\text{He}$ ratios in picritic
 2351 basalts from Baffin Island and the role of a mixed reservoir in mantle plumes, *Nature*, 424, 57-
 2352 59.
- 2353 Suckro, S. K., K. Gohl, T. Funck, I. Heyde, B. Schreckenberger, J. Gerlings, and V. Damm (2013),
 2354 The Davis Strait crust—a transform margin between two oceanic basins, *Geophys. J. Int.*, 193,
 2355 78-97.
- 2356 Suckro, S. K., K. Gohl, T. Funck, I. Heyde, A. Ehrhardt, B. Schreckenberger, J. Gerlings, V. Damm,
 2357 and W. Jokat (2012), The crustal structure of southern Baffin Bay: implications from a seismic
 2358 refraction experiment, *Geophys. J. Int.*, 190, 37-58.
- 2359 Talwani, M., and O. Eldholm (1977), Evolution of the Norwegian-Greenland Sea, *GSA Bull.*, 88,
 2360 969-999.
- 2361 Tapponnier, P., X. Zhiqin, F. Roger, B. Meyer, N. Arnaud, G. Wittlinger, and Y. Jingsui (2001),
 2362 Oblique Stepwise Rise and Growth of the Tibet Plateau, *Science*, 294, 1671-1677.
- 2363 Taylor, B., K. Crook, and J. Sinton (1994), Extensional transform zones and oblique spreading
 2364 centers, *Journal of Geophysical Research: Solid Earth*, 99, 19707-19718.
- 2365 Theissen-Krah, S., D. Zastrozhnov, M. M. Abdelmalak, D. W. Schmid, J. I. Faleide, and L. Gernigon
 2366 (2017), Tectonic evolution and extension at the Møre Margin – Offshore mid-Norway,
 2367 *Tectonophysics*, 721, 227-238.
- 2368 Thorbergsson, G., I. T. Magnusson, and G. Palmason (1990), Gravity data and gravity map of
 2369 IcelandOS-90001/JHD-01, National Energy Authority Reykjavik.
- 2370 Thybo, H., and I. M. Artemieva (2013), Moho and magmatic underplating in continental lithosphere,
 2371 *Tectonophysics*, 609, 605-619.
- 2372 Trela, J., E. Gazel, A. V. Sobolev, L. Moore, M. Bizimis, B. Jicha, and V. G. Batanova (2017), The
 2373 hottest lavas of the Phanerozoic and the survival of deep Archaean reservoirs, *Nature*
 2374 *Geoscience*, 10, 451.
- 2375 Tryggvason, E. (1962), Crustal structure of the Iceland region from dispersion of surface waves, *Bull.*
 2376 *seismol. Soc. Am.*, 52, 359-388.
- 2377 Tuttle, O. F., and N. L. Bowen (1958), Origin of granite in the light of experimental studies in the
 2378 system $\text{NaAlSi}_3\text{O}_8\text{--KAlSi}_3\text{O}_8\text{--SiO}_2\text{--H}_2\text{O}$, *in* *Origin of Granite in the Light of Experimental*
 2379 *Studies in the System $\text{NaAlSi}_3\text{O}_8\text{--KAlSi}_3\text{O}_8\text{--SiO}_2\text{--H}_2\text{O}$* , edited by O. F. Tuttle and N. L.
 2380 Bowen, Geological Society of America.
- 2381 Ulmer, P., and V. Trommsdorff (1995), Serpentine Stability to Mantle Depths and Subduction-
 2382 Related Magmatism, *Science*, 268, 858.

- 2383 van Gool, J. A. M., J. N. Connelly, M. Marker, and F. C. Mengel (2002), The Nagssugtoqidian
2384 Orogen of West Greenland: tectonic evolution and regional correlations from a West Greenland
2385 perspective, *Canadian Journal of Earth Sciences*, 39, 665-686.
- 2386 Vauchez, A., G. Barruol, and A. Tommasi (1997), Why do continents break-up parallel to ancient
2387 orogenic belts?, *Terra Nova*, 9, 62-66.
- 2388 Vogt, P. R. (1971), Asthenosphere motion recorded by the ocean floor south of Iceland, *Earth planet.*
2389 *Sci. Lett.*, 13, 153-160.
- 2390 Vogt, P. R., G. L. Johnson, and L. Kristjansson (1980), Morphology and magnetic anomalies north of
2391 Iceland, *Journal of Geophysics-Zeitschrift Fur Geophysik*, 47, 67-80.
- 2392 Voppel, D., S. R. Srivastava, and U. Fleischer (1979), Detailed magnetic measurements south of the
2393 Iceland-Faroe Ridge, *Deutsche Hydrographische Zeitschrift*, 32, 154-172.
- 2394 Walker, R. J., R. E. Holdsworth, J. Imber, and D. Ellis (2011), Onshore evidence for progressive
2395 changes in rifting directions during continental break-up in the NE Atlantic, *Journal of the*
2396 *Geological Society*, 168, 27.
- 2397 Wegener, A. (1915), *Die Entstehung der Kontinente und Ozeane*, Friedrich Vieweg und Sohn,
2398 Braunschweig.
- 2399 Welford, J. K., A. L. Peace, M. Geng, S. A. Dehler, and K. Dickie (2018), Crustal structure of Baffin
2400 Bay from constrained 3-D gravity inversion and deformable plate tectonic models, *Geophys. J.*
2401 *Int.*, 214, 1281–1300.
- 2402 Wilkinson, C. M., M. Ganerød, B. W. H. Hendriks, and E. A. Eide (2017), Compilation and appraisal
2403 of geochronological data from the North Atlantic Igneous Province (NAIP), *Geological Society,*
2404 *London, Special Publications*, 447, 69.
- 2405 Zastrozhnov, D., L. Gernigon, I. Gogin, M. M. Abdelmalak, S. Planke, J. I. Faleide, S. Eide, and R.
2406 Myklebust (2018), Cretaceous-Paleocene evolution and crustal structure of the northern Vøring
2407 Margin (offshore Mid-Norway): results from integrated geological and geophysical study,
2408 *Tectonics*, 37.
- 2409 Zhang, J., and H. W. Green (2007), Experimental Investigation of Eclogite Rheology and Its Fabrics
2410 at High Temperature and Pressure, *Journal of Metamorphic Geology*, 25, 97-115.
- 2411 Zhou, H., and H. J. B. Dick (2013), Thin crust as evidence for depleted mantle supporting the Marion
2412 Rise, *Nature*, 494, 195–200.
- 2413